ACCELERATED LIFETIME TESTING OF
CARBON FILLED POLYCARBONATE
UNDER CYCLIC LOADING CONDITIONS

By

GYU-HO   KIM

Bachelor of Science
R.O. Korea Air Force Academy
Seoul, Korea
1986

Master of Science
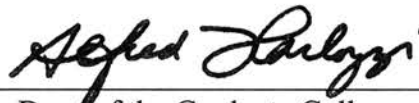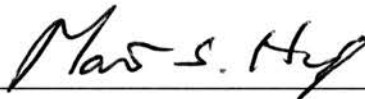Oklahoma State University
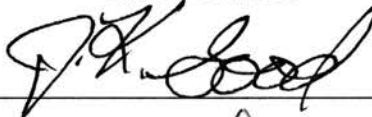Stillwater, Oklahoma
1994

Submitted to the Faculty of the
Graduate College of the
Oklahoma State University
in partial fulfillment of
the requirements for
the Degree of
DOCTOR OF PHILOSOPHY
December, 2003

ACCELERATED LIFETIME TESTING OF CARBON FILLED POLYCARBONATE UNDER CYCLIC LOADING CONDITIONS

Thesis approved

_____
Thesis Adviser

_____

_____

_____

_____
Dean of the Graduate College

ACKNOWLEDGEMENTS

TABLE OF CONTENTS

LIST OF FIGURES

viii

LIST OF TABLES

NOMENCLATURE

T_g	glass transition temperature
T	absolute temperature
D_{ijkl}	component of creep compliance tensor $\boldsymbol{D}$
$\boldsymbol{D}$	creep compliance tensor
D_1	storage compliance
D_2	loss compliance
E_{ijkl}	component relaxation modulus tensor
E_1	storage modulus
E_2	loss modulus
E_d	dynamic modulus
$\boldsymbol{E}$	relaxation modulus tensor
$D(t)$	uniaxial creep compliance
$E(t)$	Young's relaxation modulus
δ	phase angle
ω	angular velocity
t	time
I_1	first stress invariant
$\dot{\Delta}_n^c$	craze widening rate
ΔH	free energy change, activation energy barrier
G	shear modulus
v	Poisson's ratio
r	mean molecular radius
$\tau,\ \sigma_s$	applied shear stress

$\dot{\gamma}^p$	plastic strain
$\dot{\gamma}_,$	pre-exponential fact
R	Boltzmann constant
B_i	back stress
ΔS	entropy change
V_i^p	principle plastic stretch
$v*$	activation volume
$a(\xi)$	shift factor
$K(t)$	bulk modulus
f^v	fractional free volume
N_f	total number of cycles
K_c	fracture toughness
ΔK	stress intensity factor range
σ_{ys}	yield stress
$\dfrac{da}{dN}$	crack growth rate per loading cycle
σ_a	applied peak stress
f	frequency
$\dot{E}_d$	hysteretic heating rate
η	internal viscosity
ε^p	localized plastic strain
$\sigma_{fs,T}$	fatigue endurance limit at given temperature

$\dfrac{d\varepsilon^p}{dN}$ localized plastic strain growth rate per loading cycle

ρ density

c_p specific heat

$a(f)_{f_{ref}}$ time-frequency shift factor

$a\ (T)_{T_{ref}}$ time-temperature shift factor

$a(\sigma_a)_{T_{ref}}$ time-stress shift factor

CHAPTER ONE

INTRODUCTION

Amorphous polymers are often used as structural materials due to their high specific strength, high resistance to corrosion and ease of forming. Examples include various components used in vehicles (bumper, door board, windshield, etc.), aircraft (canopy, cockpit equipment, interior equipment, ventube, etc.), machinery (shaft, bearing, coupling, connecting rod, etc.) and engineering constructions (window, door, roof, pipe, etc.). Some of them are used under fatigue loading conditions. To ensure that they can fulfill their structural integrity over their service life, we need to determine the long-term fatigue life. It is noted that the actual long-term fatigue tests without proper acceleration in testing may not be a method of choice because product design and manufacturing cycle may be sometimes short to meet the demand in high quality by the markets. Consequently, reliable accelerated fatigue tests that can be finished in short duration times must be used. As a result, the development of accelerated fatigue testing method for structural polymers will be the target of this research.

Fatigue is an important aspect of strength analysis since fatigue failure can occur at stress amplitude much lower than the failure stress under monotonic tensile loading condition. Fatigue problem happens in the use of gear teeth, toggle mechanism and many moving or rotating parts of machinery such as shafts, bearings, couplings and connecting rods. Fatigue problem can also happen in the use of non-moving parts such as bumper, door, windshield and interior equipment on vehicles, aircrafts, appliances and many other machines. Therefore, the design and material selection of polymer structural members

1

require the consideration of their fatigue behavior to ensure structural integrity through the service life.

Fatigue behavior of amorphous polymers is different from that of metals. As all amorphous polymers exhibit significant time dependent behavior, their fatigue behavior is inevitably accompanied by creep or relaxation under cyclic stress or cyclic strain loading conditions. A simple increase in the loading frequency as a scheme to accelerate the fatigue test cannot provide reliable fatigue test acceleration to predict long-term fatigue life because viscoelastic effects cannot be scaled in the same way as frequency. In addition, fatigue tests at a high loading frequency can cause viscoelastic hysterises-induced thermal effects. Consequently testing temperature is different from service temperature when the polymer is used at a lower temperature, resulting in underestimation or overestimation of fatigue strength or fatigue life. Because of these distinct features, polymer fatigue life prediction is different from that of time-independent materials such as metals in which a simple increase in loading frequency is sufficient in a wide range of applications. Thus polymer fatigue acceleration needs to be addressed with different approaches.

There are primarily two different approaches in the service life testing of structural components under cyclic loading (Suresh, 1991). They are (1) the total life approach, i.e., the *S-N* curve approach and (2) the defect-tolerant approach. In approach (1), the total service life in terms of number of cycles is represented in terms of the applied cyclic stress level (or cyclic strain level) on standard "perfect" samples. This method primarily determines the number of cycles required to develop critical defects that eventually lead to catastrophic failure. In approach (2) defects such as cracks are introduced into the

samples and the crack growth rate is mainly represented in terms of the applied cyclic stress intensity factor, characterized by the Paris law (Suresh, 1991). This method may be used to determine the service life as well as the residual service life when defects have been detected in the structure. Approach (1) is traditionally and still widely used in automotive, locomotive and other engineering designs targeted toward ground use structural components. Approach (2) is often used in aeronautical engineering where a critical evaluation of the failure behavior is needed to prevent catastrophic failure. This investigation will focus on the accelerated life testing using *S-N* curve approach.

Numerous results on polymer fatigue have been reported using both the *S-N* curve approach (Beardmore and Rabinowitz, 1974; Crawford & Benham, 1975; Bucknall and Stevens, 1980: Sauer and Richardson, 1980; Hertzberg and Manson, 1980; Furue & Shimamura, 1980; Miller & Priest, 1987, Miyano et al., 1999; 2000) and the defect-tolerant approach (Kurube & Wakashima, 1970, 1972; Attermo & Ostberg, 1971; Culver, 1975; Geverich et al., 1976a, 1976b; Martin & Geverich, 1976; Radon, 1980; Takemori, 1984). Various aspects of the physics in polymer fatigue have also been reported. For example, Engel et al. (1981) investigated the fracture surface morphology. McKenna and Penn (1980) as well as Wang, Kim and Lu, (2002) developed cumulative damage models for polymer fatigue. It should be noted that most of these studies for actual fatigue life prediction treated the polymers in the same way as metals and ceramics with fatigue behavior independent of time, frequency, and temperature under specific conditions, except when a high temperature close to, or above the glass transition is involved.

Knauss (1969), Schapery (1975a, 1975b) have established theories for the crack propagation in a linear viscoelastic medium. Knauss (1969) observed the delayed creep

3

failure in several kinds of polymers and developed a temperature-dependent theory for creep-rupture using a cohesive model for the crack process zone for the analysis of an idealized viscoelastic media. He also developed criteria to the crack extension problem in viscoelastic media where energy supplied to the material by external loads is enough to at least equal the energy required for the creation of new surfaces along the lips of the propagating crack. Schapery (1975a, 1975b) developed a theory to predict the size and shape of cracks of time-dependent materials using an energy criterion at the crack tip for continuous crack propagation in linear viscoelastic, isotropic media. Later, Schapery (1984, 1990) proposed a nonlinear correspondence principle and used it to develop a generalized J integral as the crack driving force for quasi-static deformation and fracture analysis in nonlinear viscoelastic media. The studies focused on predicting the mechanical work available at the crack tip for initiation and continuation of crack growth but their approaches are limited to linear viscoelastic media under quasi-static loading conditions and cannot be used for crack propagation analysis in the case where highly nonlinear viscoelastic material and three-dimensional effects are involved in the crack tip deformation. In fact, the fracture and fatigue in nonlinear viscoelastic materials is an area that is still not well understood thus far.

In defect-tolerant approach, a small size of initial defect is normally determined or assumed. The initial size is determined from actual non-destructive evaluation, or is sometimes determined by the limitation, or resolution, of the non-destructive evaluation (NDE) method if NDE cannot detect any initial defects. Under fatigue loading, the defect will grow, until it reaches a critical size that will lead to catastrophic failure of the overall structure. To prevent from failure, the defect has to be controlled to a size smaller than

the critical size during the service life. The major concern using this approach is how long, or how many cycles it takes for the initial defects to grow to a critical size. While defect-tolerant approach is the most reliable method to determine the service life of a structure, it involves efforts such as NDE, and three-dimensional fracture analysis of the structure, which makes this method much more costly than the total life approach (S-N curve approach). As a result, defect-tolerant approach is often limited to extremely critical structures such as nuclear reactors and aerospace structures. The most dominant approach in the design for fatigue service life is still total life approach. This work will focus on the accelerated life testing using S-N curve approach. While there were numerous studies reported on the fatigue and fracture behavior of polymers in the past several decades, there has been few results in open literature to address the prediction of long-term fatigue behavior based on short-term fatigue test data. The development of accelerated life testing for polymer fatigue has its own difficulties. One difficulty is associated with the time-dependent behavior that induces the change in material behavior over the service life. Although acceleration in fatigue testing is accomplished by increasing the frequency so that the total number of loading cycles in high loading frequency test is the same as that during low service frequency, the thermo-mechanical behavior of polymers cannot be accelerated in the same way as frequencies. This will lead to unreliable acceleration of polymer fatigue. This dissertation introduces a testing methodology to predict long-term fatigue life through analysis on properly designed accelerated short-term test.

Accelerated lifetime testing (ALT) for polymer fatigue in this dissertation is intended to process short-term test data obtained from different temperatures and

frequencies to provide reliable (sometimes conservative) prediction of referenced fatigue lifetime at reference state. The development of ALT techniques relies on the understanding of fatigue failure mechanisms. In polymer fatigue, the localized yield-like deformation can normally lead to the initiation of fatigue cracks, leading to final fatigue failure. As a result, attention is focused on developing evolution laws to determine the growth rate of the yield-like deformations. The evolution of the localized yield-like deformation is highly dependent upon the nonlinear viscoplastic behavior, which in turn depends on temperature, stress amplitude and frequency. To account for all the factors, a model based on the consideration of material internal governing time, or reduced time, will be developed to process short-term fatigue data obtained at different temperatures and frequencies to produce realistic long-term fatigue data using time-temperature, time-stress and time-frequency superpositions. The method is expected to be applicable for both isothermal and athermal conditions.

This dissertation consists of five chapters. Chapter 1 is the introduction. A review is given in Chapter 2 on the general microstructure, fatigue and fracture mechanisms and viscoelastic constitutive behavior of polymers for the understanding of the localized yield-like deformation for fatigue crack initiation that dictates the fatigue life in the S-N approach.

In Chapter 3, an accelerated lifetime testing method for fatigue lifetime prediction using the S-N curve approach is developed. A phenomenological approach for the localized yield-like deformation process is considered to account for time, temperature and stress amplitude dependence in fatigue loading. A modified Eyring's activation energy model is applied to describe the localized yield-like deformation process in

fatigue. A reduced time model is proposed to predict long-term fatigue life using short-term data. Chapter 4 deals with experimental setup for accelerated lifetime testing and presents experimental results and discussions under both isothermal/low frequency and athermal/high frequency conditions. Some conclusions and future work are described in Chapter 5.

CHAPTER TWO

BACKGROUND

In this chapter, the general microstructure of glassy polymer as well as physical and mechanical responses under loading conditions are reviewed. A review is provided for fracture and fatigue behavior of polymers. Linear and nonlinear viscoelastic behaviors are reviewed. Nonlinear viscoelastic behavior has been widely studied to characterize thermo-mechanical behavior of realistic materials. These studies are originally focused on creep and/or relaxation phenomena. Some nonlinear viscoelastic models are introduced here to understand and capture the characteristics of localized yield-like deformation, involving highly nonlinear viscoelactic behavior, leading to fatigue crack initiation. Subsequently, the effects of temperature and frequency on the thermo-mechanical behavior of polymers are investigated to understand how they control damage evolution for fatigue lifetime evaluation.

2.1 Microstructure of Glassy Polymers

Amorphous (glassy) thermoplastic polymers are a class of materials made up of covalently bonded long chain (macro) molecules with an amorphous structural state that can be softened and/or melted upon heating. The consequence of linking atoms into a long chain with strong covalent bonds has the relatively high properties for load-bearing applications. Macromolecules of an amorphous polymer generally have long repetitive sequences of a basic chemical structure called the monomer (Painter and Coleman, 1997).

8

The backbone of this long chain is normally composed of carbon atoms linked together by strong covalent bonds. Since a carbon atom has a limited angle to move in the chain, the position of successive atoms is only partially random. The stiffness of the macromolecules results from the stiffness of the monomer itself and from the shape and size of the space on which it occupies or in which it moves.

Several models, as shown in Figure 2.1, have been proposed to represent the structure of amorphous polymers such as coil model (Boyer, 1976), meandering and micellar model (Kausch, 1978), macromolecular entanglement model (Haward, 1993) and cluster model (Kovlov and Novicov, 2001). It can be understood that macromolecules are connected to one another through physical entanglements (reversible knots: typical model for thermoplastics) or irreversible chemical bonds (typical model for thermosets) (Odian, 1991). Kovlov and Novicov (2001) characterized the existence of a cluster or local order that is sensitive to thermal fluctuation in the molecular structure. Local order in an amorphous state is the result of high viscosity in contrast to low viscosity such as in low molecular weight liquids. Kovlov and Novicov (2001) have proposed a local cluster model for physical macromolecular structure that can give a good agreement with macroscopic mechanical behavior: their model is consistent with the free volume theory for viscoelastic materials.

2.2 Response of Molecular Structure upon Loading

The entanglements and/or local clusters are the main anchor points for load carrying. Conformation change, rearrangement, redistribution or occasional loss and
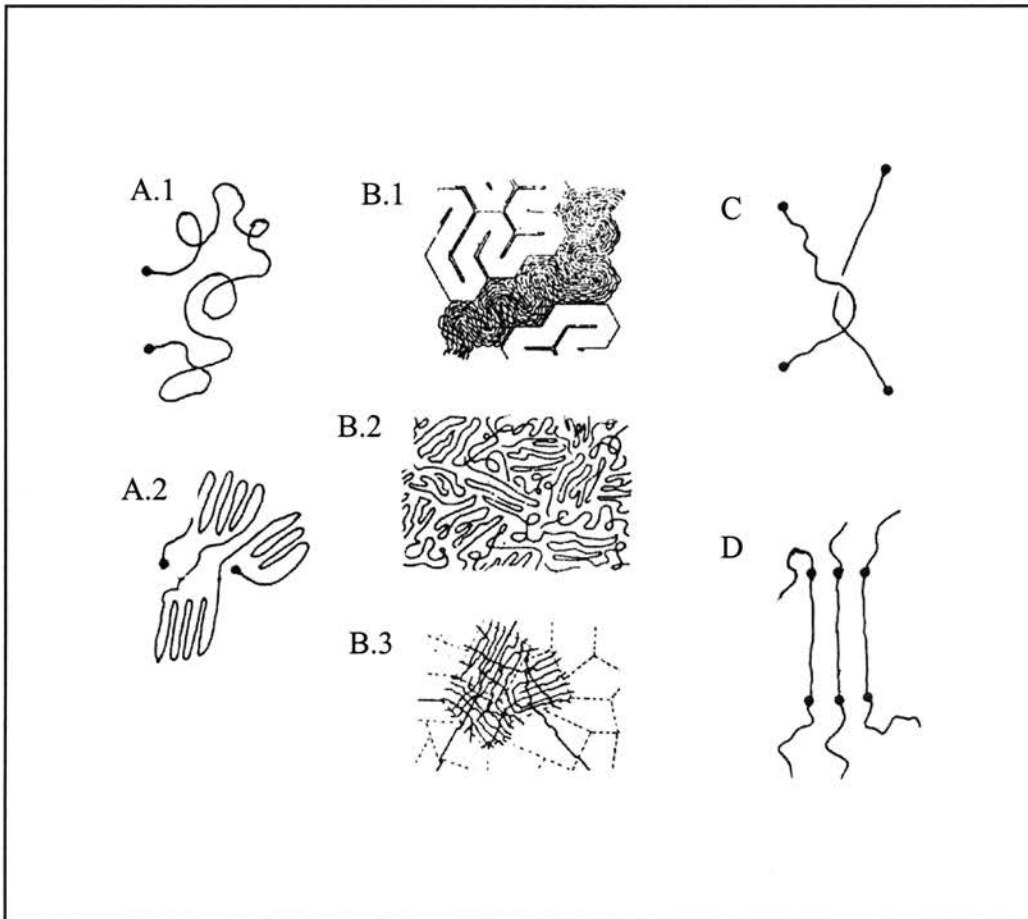
Figure 2.1: Schematic model representations of amorphous polymer structure.

    (A) Coiled molecule (Boyer, 1976),

        A.1-Statistical ball,

        A.2-the same with locally ordered regions

    (B) Amorphous state (Kausch, 1978),

        B.1-Meandering model, B.2-Folded-chain micellar model,

        B.3-Micellar domain structure

    (C) Macromolecular interlacing or entanglement (Haward, 1993)

    (D) Cluster (Kozlov and Novikov, 2001)

breaking of the anchor points and/or backbone chains are primarily responsible for macroscopic thermo-mechanical behavior such as viscoelastic stress-strain response and time-dependent fatigue failure characteristics.

Long chain amorphous polymer molecules below their glass transition temperatures (T_g) are not in a thermodynamic equilibrium state, instead, they are in a 'frozen state' in terms of higher activation energies induced by high viscosities and long relaxation times. When a load is applied to the material, many molecular motions (rotations, vibrations, side groups; β motions) as well as cooperative main chain motions (α motions) can be activated (Quinson et al., 1995; Painter and Coleman, 1997).

Usually, the α motions involve conformational changes of the main chain bonds (for instance, trans-gauche changes). The perturbation induced by the conformational change of a given main chain bond is accommodated by a limited modification (from 10° to 60°) of the torsion angles of about 4~5 bonds on both sides of the jumping bond. The β motions are associated with the rotations of side groups. Under relaxation at a low temperature range, these motions do not induce any modification of the rotation angle of the main chain bond. The α - β coupled motions also occur where side group rotations are shown to be accompanied by simultaneous modifications of the main chain rotation angles. The localized main chain motion can be considered as precursors of the α motions. Figure 2.2 shows the energy damping spectra for semicrystalline and amorphous polymers at various temperatures normalized to T_g. It can be found that there are several damping peaks for each material. At amorphous case, region I and II seem to be related to the β motions and region II and III seem to be relate to α - β coupled motions. Around the peak III, α motions may be dominantly involved.
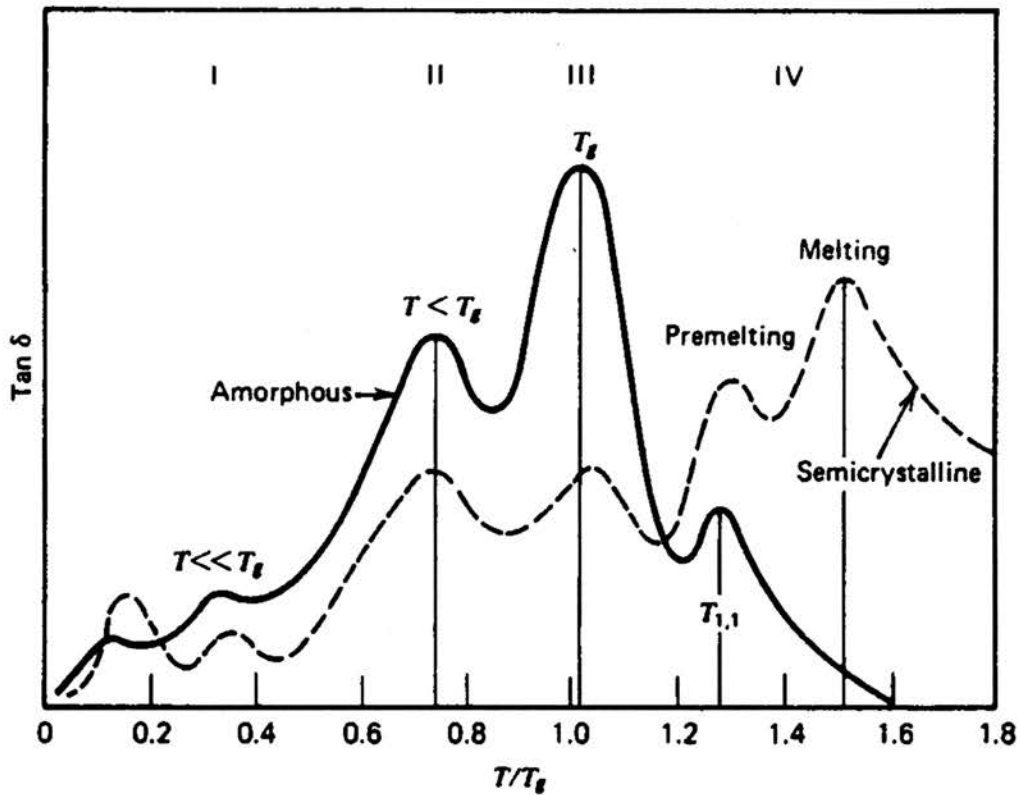
Figure 2.2: Energy damping spectra for semicrystalline and amorphous polymers at various temperatures normalized to T_g. (Polymeric Materials, 1975)

The motions, rearrangement and redistribution of the molecular structure of amorphous polymers may exhibit intrinsic nature of linear and/or nonlinear time-dependent (viscoelastic) material behavior including yield, craze, shear band, fatigue and fracture behavior that will be reviewed in the following sections. The disorder and loose

packing of these long chain molecular structures can be instrumental in promoting high strain deformations. The entanglements or local clusters provided by the entwined long chains ensure strength retention (load carrying anchors) and may be the nests for considerable α motions resulting in localized shear deformation as well as craze formation.

2.3 Linear Viscoelasticity

A distinctive feature of the mechanical behavior of amorphous polymers is the viscoelastic characteristic such that the material response to an applied stress or strain depends on the loading rate or the time period of loading. It is noted that the mechanical behavior of most elastic solids follows the Hooke's law. In these solids, the stress is proportional to strain. On the other hand, the mechanical behavior of some viscous materials tends to follow the Newton's law. In these fluids, the stress is proportional to the strain rate, and is independent of the strain level. The mechanical behavior of many amorphous polymers falls between the behavior of elastic solids and liquids. This behavior is called viscoelastic behavior.

The mechanical behavior of amorphous polymers can be modeled as linear viscoelastic characteristic under small deformation. In analog models, different combinations of elastic springs and viscous dashpots can be used to represent the linear viscoelastic behavior. The basic models include the Maxwell model (spring and dashpot in series) and the Voigt model (spring and dashpot in parallel). More complex combinations of the two basic models are often used to model the linear viscoelastic

behavior more accurately; but they are only analog models and do not have a direct physical relation with molecular mechanisms.

Under arbitrary loading history, the mechanical response of a linear viscoelastic material can be described by the Boltzmann superposition principle (Ward, 1971). The Boltzmann superposition principle is represented by

$$\varepsilon_{ij}(t) = \int_{-\infty}^{t} D_{ijkl}(t-\tau) d\sigma_{kl}, \tag{2.1}$$

$$= \int_{-\infty}^{t} D_{ijkl}(t-\tau) \frac{d\sigma_{kl}}{d\tau} d\tau, \tag{2.2}$$

$$= D_{ijkl}(t)\sigma_{kl}(0^{+}) + \int_{0}^{t} D_{ijkl}(t-\tau) \frac{d\sigma_{kl}}{d\tau} d\tau, \tag{2.3}$$

$$\text{or } \sigma_{ij}(t) = E_{ijkl}(t)\varepsilon_{kl}(0^{+}) + \int_{0}^{t} E_{ijkl}(t-\tau) \frac{d\varepsilon_{kl}}{d\tau} d\tau, \tag{2.4}$$

where ε_{ij} are components of strain tensor $\boldsymbol{\varepsilon}$, σ_{ij} are components of stress tensor $\boldsymbol{\sigma}$, D_{ijkl} and E_{ijkl} are components of creep compliance tensor $\boldsymbol{D}$ and relaxation modulus tensor $\boldsymbol{E}$, respectively. The strain at any time, t, is the result of all changes in the stress that took place until t. Also, initially the material must be in the natural state, i.e., a stress-free state.

In engineering applications, it is sometimes useful to separate the time-independent portion of strain (stress) from the time-dependent portion, for example, under a uniaxial stress state,

$$\varepsilon(t) = \frac{\sigma_{0}}{E_{0}} + \int_{0^{+}}^{t} D(t-\tau) \frac{d\sigma}{d\tau} d\tau, \tag{2.5}$$

14

and
$$\sigma(t) = \varepsilon_0 E_\infty + \int_{0^+}^{t} E(t-\tau) \frac{d\varepsilon}{d\tau} d\tau, \tag{2.6}$$

where $D(t)$ is the uniaxial creep compliance, and $E(t)$ is the Young's relaxation modulus.

2.4 Dynamic Response

The application of a dynamic force to a polymeric material that exhibits linear viscoelastic behavior is considered in this section. A viscoelastic material has non-zero loss modulus or loss compliance that represents the extent of viscous effects. During cycle loading, there is a hysteresis in the stress-strain curve. The hysteresis corresponds to the energy that is mostly dissipated in the form of heat that can sometimes cause a thermal effect.

If a specimen is subjected to a sinusoidal strain, given by

$$\varepsilon = \varepsilon_0 \sin \omega t, \tag{2.7}$$

the steady state stress will be out of phase by a phase angle δ

$$\sigma = \sigma_0 \sin(\omega t + \delta). \tag{2.8}$$

The stress is rewritten as

$$\sigma = \sigma_0 \cos\delta \sin\omega t + \sigma_0 \sin\delta \cos\omega t,$$

$$= \varepsilon_0 (\frac{\sigma_0}{\varepsilon_0}\cos\delta)\sin\omega t + \varepsilon_0 (\frac{\sigma_0}{\varepsilon_0}\sin\delta)\cos\omega t, \tag{2.9}$$

$$= \varepsilon_0 E_1 \sin\omega t + \varepsilon_0 E_2 \cos\omega t, \tag{2.10}$$

where
$$E_1 = (\frac{\sigma_0}{\varepsilon_0})\cos\delta, \quad E_2 = (\frac{\sigma_0}{\varepsilon_0})\sin\delta. \tag{2.11, 12}$$

15

E_1 is defined as storage modulus and E_2 is defined as loss modulus.

The dynamic response to a sinusoidal stress under uniaxial stress conditions using Boltzmann superposition principle is discussed as follows. Let the input stress be

$$\sigma(t) = \sigma_0 \cos \omega t , \qquad (2.13)$$

$$\text{and} \quad \frac{d\sigma}{dt} = -\sigma_0 \omega \sin \omega t , \qquad (2.14)$$

$$\text{thus} \quad \varepsilon(t) = -\sigma_0 \omega \int_{-\infty}^{\infty} D(t-\tau) \sin \omega \tau \, d\tau . \qquad (2.15)$$

Set $t - \tau = s$, then

$$\varepsilon(t) = \sigma_0 \omega \int_{-\infty}^{\infty} D(s) \sin \omega (s-t) \, ds ,$$

$$= \sigma_0 \omega \int_{-\infty}^{\infty} D(s)[\sin \omega s \cos \omega t - \cos \omega s \sin \omega t] \, ds ,$$

$$= \sigma_0 \{ \omega \int_{-\infty}^{\infty} D(s) \sin \omega s \, ds \} \cos \omega t - \sigma_0 \{ \omega \int_{-\infty}^{\infty} D(s) \cos \omega s \, ds \} \sin \omega t . \quad (2.16)$$

Set $f_1(\omega) = \omega \int_{-\infty}^{\infty} D(s) \sin \omega s \, ds$, and $f_2(\omega) = \omega \int_{-\infty}^{\infty} D(s) \cos \omega s \, ds$, then

$$\varepsilon(t) = \sigma_0 [f_1(\omega) \cos \omega t - f_2(\omega) \sin \omega t],$$

$$= \sigma_0 [D_1 \cos \omega t - D_2 \sin \omega t], \qquad (2.17)$$

where D_1 and D_2 are storage compliance and loss compliance, respectively.

The tangent of the phase angle is given by

$$\tan \delta = \frac{D_2}{D_1} = \frac{E_2}{E_1} , \qquad (2.18)$$

In experiments, when a sinusoidal stress wave is applied, the induced strain wave amplitude and phase angle between the stress and strain waves can be recorded. The complex modulus can be computed from these data using Equations (2.11) and (2.12). Loss compliance, D_2, is the one of the important factors for the energy dissipation in fatigue situation leading to temperature rise of polymeric material.

2.5 Fracture Mechanism and Nonlinear Viscoelastic Constitutive Models

Fatigue failure may occur when the amplitude of dynamic load is far less than yield strength. Under fatigue loading localized deformations can occur, resulting in near-yield and/or post yield behavior. In the following sections, yield behavior that leads to plastic deformation and fracture will be reviewed for the purpose of understanding fatigue-induced localized plastic deformation and crack initiation. Some nonlinear viscoelastic models will also be reviewed, as they are candidates that can be used to characterize the localized plastic deformation and to determine some acceleration factors for localized plastic deformation process.

2.5.1 Fracture Mechanism

2.5.1.1 Molecular Chain Breakage during Deformation

The failure mechanism of amorphous polymers can be understood as the process of molecular deformation, fracture and subsequent void growth in bulk polymers. The

detailed analysis of the failure process is highly complex and involves many factors such as molecular structure, environment, loading conditions and time. When an amorphous polymer is deformed, the molecules move, slide on each other, tend to uncoil and break secondary bonds joined by Van der Waals forces. If the molecules' flow is confined by the surrounding molecules, such as physical entanglements and /or local clusters, molecular fracture due to the breaking of primary bonds made of covalent force, will happen. These considerations during the deformation process can allow main chain bond breakage, i.e., molecular fracture, to take place and corresponding free radicals and microvoids to be formed.

Many observations and measurements have captured main-chain bond breakage using ESR (Electron Spin Resonance) spectroscopy (e.g., Kausch, 1978). Even though the free radicals that are formed due to fracture have high reactivity potentials, mobility and change, either by rearrangement along the main chains or reaction with its environment, result in an underestimation of the quantitative measurement; this technique clearly shows that the fracture in molecular structure initiates from main chain bonds breakage resulting in microvoids, rearrangement of molecular structure including irreversible plastic deformation and a corresponding redistribution of the load carrying mechanism. When the load is applied, before fracture, considerable irreversible plastic deformation due to the rearrangement of the molecular structure has been observed (Kitagawa, 1982; Takemori, & Matsumoto, 1982; Nisitani, & Hyakutake, 1985).

2.5.1.2 Localized Yield-like (Plastic) Deformation

An amorphous polymer is understood as that in which the structure can be treated as an ensemble of cooperative rearranging regions including relaxing domains and flow units based upon the Adam-Gibbs theory (1965), where the number of neighboring molecular chains change their position simultaneously. This concept was experimentally observed by measurements of dielectric relaxation and the Kerr effect in glass-forming liquids (Dyre, 1987). The characteristic size of a relaxing region was estimated to be several nanometers (Rizos and Ngai, 1999).

Below the glass transition temperature (T_g), relaxing regions are localized in their cages. These microregions of the materials contain shear microdomains that can be thermo-mechanically activated (Xio et al., 1994). When the expansion of these shear microdomains occurs, correlated molecular movements will follow. In the case of polymers, such movements imply elementary molecular motions corresponding to conformational changes with a characteristic time. It is identified as the β motion. This argument then suggests that, under stress, the shear microdomains, which are bordered by dislocations, can grow by a succession of correlated elementary β motions. This growth corresponds to inelastic strain, since the elastic energy of the borderline forces these sheared regions to return to their initial unstressed states when the stress is removed.

Finally, when the shear microdomains are very close, they 'coalesce', thus annihilating their borderline elastic energy, which leads then to an irreversible shear strain, plastic deformation. Therefore, from the single conformational change, typically β motion, to the more complex molecular movement implying the coalescence of the

19

shear microdomains, maximum α motion, there can be a continuous increasing development of the shear microdomains. Argon et al. (1994, 1996a, 1996b) have studied shear localization especially in polymers and glassy metals. They demonstrated that the nucleation and growth of shear is the prevalent deformation mechanism in glassy media, and that localized regions of intense shear are responsible for yield-like (plastic) deformation of glasses.

The plastic deformation zone in polycarbonate (PC) has been widely observed with circular notched thick specimens (Kitagawa, 1982), blunt notched thin specimens (Nisitani, & Hyakutake, 1985) and unnotched thin specimens (Takemori, & Matsumoto, 1982). In polymer fatigue, the localized plastic deformation process is of special interest because it provides fatigue crack initiation sites. From a mesoscopic point of view, shear yielding and craze formation are two major coupled mechanisms of localized plastic deformation leading to fatigue crack initiation.

2.5.1.2.1 Shear Yielding

Shear yielding is a plastic deformation occurring right after a yield, in the form of a shear band causing the material's softening behavior (Kinloch and Young, 1983). When shear yielding occurs, the material becomes hardened through molecular orientation and leads to coalescence and growth of shear bands. Several studies have considered that fatigue cracks may be initiated from microvoids that are created in the intersection points of shear bands (Wu and Li, 1976; Friedrich & Schafer, 1979; Argon, 1975). It has been observed that some pre-existing defects, such as flaws and molecular inhomogeneities,

20

act as stress concentration points causing a micro-shear band that is initiated by shear yielding (Chau and Li, 1981). Kramer (1975) studied the kinetics of a shear band growth in polystyrene (PS) and the corresponding effects of applied stress and temperature using an Eyring activation model (1958). He found that the propagation of shear band could be controlled by the localized plastic deformation (strain) ahead of the tip of the shear band.

2.5.1.2.2 Craze Formation

Craze formation is the initiation and development of microvoids in the regions of stress concentration on a plane perpendicular to the maximum principle stress (Kinloch and Young, 1983). A craze initiates when the applied tensile stress causes high stress concentrations near flaws, cracks or molecular heterogeneities. These microvoids created by craze formation develop independently and do not coalesce to form cracks. There are highly stretching molecular chains or fibrils stabilizing the craze process. Further deformation, however, makes crazes wide and fibrils break down to form a microcrack. It has been observed that the initiation of craze formation in some polymers does not occur until the crack-tip plastic deformation zone has developed to a critical extent (Yamamoto and Furukawa, 1995; Ishikawa, 1995). It implies that craze formation can also be characterized by the shear yielding mechanism because it creates some amount of localized plastic deformation before it initiates.

Some studies have predicted experimental observations indicating that there exists an incubation time for craze formation at a given stress state and a saturation of the total number of craze nucleation sites (Argon, 1975; Argon and Hannoosh, 1977). However,

when an applied tensile stress amplitude is greater than 40% ~ 50% of the yield stress, repeated void nucleation has been observed (Argon and Salama, 1977). In this case, the incubation time for craze initiation is short enough to be ignored.

In a fatigue problem, craze formation is considered to occur near the localized stress concentration region where the acting stress may be near or above the yield stress. Thus, rapid craze initiation and widening can be of greater consideration rather than a long time incubation condition for craze initiation. Sternstein and Ongchin (1969) have proposed a simple empirical criterion as

$$|\sigma_2 - \sigma_1| \geq -A^0 + \frac{B^0}{I_1}, \quad I_1 \geq 0, \tag{2.19}$$

where I_1 is the first stress invariant, $I_1 = \sigma_1 + \sigma_2$ and A^0 and B^0 are temperature dependent material parameters that define a critical value for craze initiation under pure hydrostatic stress.

Once a craze forms, it widens by further fibrillation. Molecular chain disentanglement can be involved during this widening process (Berger and Saucer, 1991). The craze widening has been considered to show highly nonlinear viscoplastic characteristics in the active zone and have time and temperature dependent behavior in a similar way to that of the homogeneous bulk polymer. A relationship for the craze widening process has been proposed by Estevez et al. (2000) in a similar way to the Argon (1988) expression, as follows:

$$\dot{\Delta}_n^c = \dot{\Delta}^0 \exp\left(\frac{-A^c \sigma^c}{T}\left(1 - \frac{\sigma_n}{\sigma^c}\right)\right), \tag{2.20}$$

where $\dot{\Delta}_n^c$ is the craze widening rate, $\dot{\Delta}^0$, A^c and σ^c are material parameters: $\dot{\Delta}^0$ contains the time dependent characteristics, A^c has temperature dependent part and σ^c represents the athermal stress state. So far, experimentally observed mechanisms for shear yielding, including yield, post-yielding, craze initiation and its widening reveal that the development of localized plastic deformation in a fatigue problem can be characterized using Eyring's activation energy model for the nonlinear viscoplastic flow process that has time-, temperature- and stress-dependence.

Shear yielding and craze formation are considered to be two coupled mechanisms leading to fatigue crack initiation as well as fracture of most glassy polymers. If these two mechanisms are captured within one localized plastic deformation process, the fatigue crack initiation process can be characterized by a localized plastic deformation process. Its behavior may obviously follow yielding and/or post-yielding characteristics associated with highly nonlinear viscoelastic behavior. In next section, some nonlinear viscoelastic constitutive models are given for the purpose of understanding the mechanisms of localized plastic deformation. It is noted that there is no direct relation between constitutive models and localized deformation. Instead, it is expected that some control factors in localized plastic deformation can be determined through investigation of these models.

2.5.1.3 Ductile to Brittle Transition

Some polymeric materials, exhibit a ductile-to-brittle (D-B) transition of the fracture failure mode in static or fatigue loading conditions (Chen, et al., 1993; Min, et

al., 2001). The D-B fracture transition is the change in the mode of failure from ductile fracture with shear yielding to brittle fracture without yielding (Richardson, 1989). Actually, there is no brittle fracture failure in polymers that can be compared with the brittle cleavage fracture failure encountered in metals. Even with low temperature fractures, ductile fibrils can be observed at high magnification (Engel, et al., 1981). However, this deformation is limited to a very thin plane layer and the deformed volume is very small. It can be considered to be a brittle failure from the macroscopic point of view. The D-B fracture transition is understood as the result of competition between yield stress and brittle (craze) stress (Vincent, 1960; Donald and Kramer, 1982; Kramer, 1990). It is obviously dependent on applied stress amplitude and temperature as well (Haward, 1972). This implies that fracture mode transition from ductile to brittle can occur as temperature and/or alternating stress amplitude decrease.

2.5.2 Nonlinear Viscoelasticity

Realistic analysis of mechanical behavior of viscoelastic materials reveals that they exhibit considerable nonlinear viscoelastic behavior under thermo-mechanical loading conditions. Plastics and rubber (Lai and Bakker, 1995; Tuttle et al., 1995; Ha and Schapery, 1998), asphalt concrete (Uzan, 1996), polycrystalline ice (Schapery, 1997) and biological materials (Fung, 1993) are some of the materials exhibiting nonlinear viscoelastic behavior.

Nonlinearities in polymers may come from intrinsic and/or localized nonlinear stress-strain responses that can be as small as atomic or molecular structures or the

combined effect on macroscale stress-strain responses of many defects or inhomogeneities that can be characterized using local continuum mechanics on the analysis of distributed microcracks (Lemaitre, 1990; Wang, Lu and Kim, 2002). There are a number of nonlinear viscoelastic constitutive for polymeric materials. The nonlinear viscoelastic constitutive models can be classified into four major groups and are reviewed herein.

2.5.2.1 Empirical Model

Empirical models do not have a physical basis and are usually used to characterize and explain experimental results. They are limited to certain conditions of the experiments and cannot be applied to other deformation and temperature conditions. A widely used empirical model may be the power law representation of the viscoelastic behavior. The model was initiated from linear viscoelastic constitutive model and was revised to account for nonlinearity. The linear viscoelastic constitutive behavior can be modeled using the Boltzmann superposition principle. Under uniaxial conditions, the superposition implies that incremental changes in strain can be linearly accumulated in incremental relaxation behavior. This gives rise to the representation of strain as shown in Equation (2.1) or (2.5).

Nonlinear viscoelastic behavior has been modeled using the modified Boltzmann superposition principle. Leaderman (1943) first proposed a modified Boltzmann superposition as follows:

$$\varepsilon(t) = D_0 \sigma(t) + \int_{0^+}^{t} D(t-\tau) \frac{d\vartheta(\sigma(\tau))}{d\tau} d\tau , \qquad (2.21)$$

25

where $D(t)$ is the linear viscoelastic creep compliance and $\vartheta(\sigma)$ is the nonlinear function of the stress history. A simple representation using the power law form of the above modified superposition gives following form

$$\varepsilon(t) = \varepsilon_0 + C_1 t^n,\tag{2.22}$$

where ε_0, C_1 and n are stress dependent functions. It, however, can be a challenging work to computer $\vartheta(\sigma)$. Findley and Adams (1948) represented these functions by

$$\varepsilon(t) = \varepsilon_0' \sinh(\sigma / \sigma_e),\tag{2.23}$$

$$C_1 = C_1' \sinh(\sigma / \sigma_m),\tag{2.24}$$

where ε_0', C_1', σ_e and σ_m may be functions of the temperature or concentration/solvent effect, but not of the time or applied stress. Findley and Lai (1966) later proposed another form of the Boltzmann superposition

$$\varepsilon(t) = D_0 \sigma(t) + \int_{0^+}^{t} D(t - \tau; \sigma) \frac{d\sigma(\tau)}{d\tau} d\tau,\tag{2.25}$$

where the creep compliance has a nonlinear function of stress. Using Equation (2.25), Findley (1981) predicted long-term (over 26 years) nonlinear creep behavior and recovery characteristics of polyvinyl chloride (PVC) and polyethylene (PE). These models have been used and have had some success in modeling the nonlinear deformation response well below glass transition temperatures (T_g) under ambient conditions.

A drawback of these models is that there is no explicit incorporation of the thermal history. The parameters are only valid at the same temperature as in the experiment. Thus these model parameters cannot be used for other cases where temperatures are different.

Under fatigue conditions, temperature change induced by dissipated heat prevents the modified Boltzmann superposition principle from being used to characterize the fatigue behavior for fatigue life prediction.

2.5.2.2 Energy Activation Models

The Eyring energy activation models (1958) were developed based upon the assumption that plastic flow will occur if the energy barrier is overcome by the applied work. Argon (1973) considered that specific molecular movements contribute to the plastic flow and suggested that the plastic resistance to flow is made up of both intermolecular and intra-molecular processes. Initially, randomly oriented molecular segments may become partially aligned when a deformation is imposed. Argon considered this process as adding an initially 'kinked' segment to a group aligned initially. Opposition to this alignment originates from both the chain itself and the surrounding neighbors with a characteristic free energy that is required for alignment. During deformation, this configuration keeps stable but upon cessation of the deformation, the segment may return to its original configuration or could be permanently changed according to the condition as to whether the surrounding molecules follow similar processes. In this section, several nonlinear constitutive models originated from the consideration of Eyring activation energy are summarized. Review of nonlinear viscoelastic constitutive model may gives a possible way to characterize the localized yield-like deformation around fatigue crack initiation zone leading to fatigue failure.

2.5.2.2.1 Boyce Formulation for Post-Yield Behavior

Boyce et al., (1988) proposed a constitutive model using the framework proposed by Argon (1973), in which the plastic resistance to flow is assumed to come from (i) the intermolecular resistance to segment rotation, and (ii) the entropic resistance to molecular alignment.

Plastic Resistance Concept

This model characterizes the change of activation energy barrier of free energy by applied stress causing rate change of plastic flow. Plastic flow is considered to occur when the intermolecular resistance to the segment is overcome and the intermolecular motion and rotation is possible. Argon (1973) derived a formula for the free energy change needed to cause the segment rotation for a shear deformation as follows:

$$\Delta H = \frac{3\pi G\omega^2 r^3}{16(1-v)}\left(1-\left(\frac{\tau}{0.0077G(1-v)}\right)^{5/6}\right),$$ (2.26)

and the plastic deformation rate is given by

$$\dot{\gamma}^p = \dot{\gamma}\exp\left(-\frac{\Delta H}{RT}\right),$$ (2.27)

where $\Delta H, G, v, \omega, r, \tau$ are the free energy change, the shear modulus, Poisson's ratio, the net angle of rotation of the molecular segment, the mean molecular radius and applied shear stress and $\dot{\gamma}^p$, $\dot{\gamma}, R, T$ are corresponding plastic strain, the pre-exponential fact, Boltzmann constant and the absolute temperature, respectively.

Later, Boyce et al., (1988) simplified Argon (1973) model to

$$\dot{\gamma}^p = \dot{\gamma}_0 \exp\left(-\frac{AS_0}{T}\left(1-\left(\frac{\tau}{S_0}\right)^{5/6}\right)\right),$$ (2.28)

or in terms of the shear stress such as

$$\tau = S_0\left(1-\frac{T}{AS_0}\ln\left(\frac{\dot{\gamma}}{\dot{\gamma}^p}\right)\right)^{6/5}.$$ (2.29)

where S_0 and A are defined as

$$S_0 = \frac{0.077G}{(1-\nu)},$$ (2.30)

$$A = \frac{39\pi G\omega^2 a^3}{16R}.$$ (2.31)

Boyce et al. (1988) noticed that when the absolute temperature approaches zero and a considerable plastic strain rate remains, the shear stress approaches S_0. Thus, S_0 can be defined as the isothermal shear yield strength of the material.

Entropic Resistance Concept

Employing the entropy concept of thermodynamics is another way to characterize nonlinear viscoelastic behavior. Park et al., (1984) characterized the behavior of the plastic flow using the entropic resistance concept. They assumed that the structure of isotropic amorphous polymers consists of randomly oriented molecular chains connected

by physical entanglements. A large deformation occurs when the stretching of these chains starts, followed by subsequent orientation. If an imposed deformation is large enough, the corresponding external stress state remains even though the deformation stops.

Physically, when the material is stressed enough for the intermolecular chain to move, the molecules can align along the direction of the stress. The internal stress, called the back stress, B_i, is related to the derivative of the entropy change, ΔS, with respect to the principle plastic stretch, V_i^p, through

$$B_i = -TV_i^p \frac{\partial \Delta S}{\partial V_i^p} . \qquad (2.32)$$

In order to calculate the back stress, Boyce et al., (1988) used the statistical rubber elasticity theory of Wang and Guth (1952) to model the plastic deformation and found:

$$B_i = C^R \frac{\sqrt{N}}{3} \left(V_i^p \zeta^{-1} \left(\frac{V_i^p}{\sqrt{N}} \right) - \frac{1}{3} \sum_{j=1}^{3} V_i^p \zeta^{-1} \left(\frac{V_i^p}{\sqrt{N}} \right) \right), \qquad (2.33)$$

where C^R is the rubber modulus that is equal to nRT where n, R and T are the number of chains per unit volume, the Boltzmann constant and absolute temperature and N, ζ are the number of rigid chain links between entanglements and the Langevin function, respectively. The Langevin function and its inverse function are given by

$$\zeta(\alpha_i) = \coth(\alpha_i) - \frac{1}{\alpha_i} = \left(\frac{V_i^p}{\sqrt{N}} \right), \qquad (2.34)$$

and
$$\zeta^{-1} \left(\frac{V_i^p}{\sqrt{N}} \right) = \alpha_i . \qquad (2.35)$$

Boyce et al., (1988) applied Equations (2.33 ~ 2.35) to model the relation between true stress and true strain for PMMA using the experimental data from Hope et al.,

30

(1980a, 1980b). Boyce and Arruda (1987) also characterized the plastic flow behavior of polycarbonate (PC) under uniaxial extension and compression conditions up to strains of 125%. Under both extension and compression, strain hardening was observed. The same model parameters were then used for a finite element analysis of the tensile stress-strain response of polycarbonates (PC). There was good agreement between modeling and experimental results in the small strain range but a considerable discrepancy was observed at larger strains. The study has elicited an interest in more accurate modeling for the effect of molecular structure change during the deformation such as the orientation and strain hardening of the material.

The models driving from the concepts of plastic resistance and/or entropic resistance focused on describing the qualitative post-yield behavior and can not be used for the nonlinear viscoelastic response prior to yielding. The theory of barrier activation energy, however, has been used extensively to characterize nonlinear relaxation behavior.

2.5.2.2.2 Hassan and Boyce Model

Hasan and Boyce (1995) modified the previous theory to characterize and account for a distribution of activation energy barriers to model nonlinear viscoelastic behavior involving elastic-viscoplastic transition. In a typical monotonic test, there are various stages in deformation history and the corresponding distribution of localized free volume may change significantly, and these changes can be related to different activation energy barriers corresponding to different possible local shear transformations. A shear

31

transformation may result from the rearrangement of the molecular structure that can occur during deformation and/or relaxation.

When a material is in its stress free state, it is assumed that there exist a number of sites that can be transformed potentially. When a relatively small stress is applied, the regions of localized and high free volume can be transformed or relaxed causing linear deformation. When the number of deformation sites increases, there will be a deviation from linear viscoelastic behavior.

The strain energy for transformation is stored elastically in the relatively rigid surrounding material, where the localized free volume is much lower. This rigid region may create a back stress on the transformed regions that prevents multiple shear transformations by increasing the activation energy needed for transformation. When the stress is removed, a rapid deformation recovery back to its initial state can occur.

As the deformation increases, more regions possessing higher activation energies and lower localized free volume can undergo shear transformations, resulting in a change in mechanical behavior towards high nonlinearity. At the same time, the back stress effects start to dissipate and some inelastic strain becomes irrecoverable within the transformed regions undergoing continuous shearing. The plastic flow is the result of this continuous shearing process.

Through the entire deformation process, the localized free volume may increase continuously. The increased localized free volume may contribute to higher inelastic (viscoplastic) deformation. Finally, strain softening can occur after yield as the material contains a large number of liquid-like regions that make continuous plastic flow possible.

The mathematical representation of the physical deformation process will be given here. The fraction of localized molecular structure rearrangements can be related with the first order rate kinetics. The corresponding fraction change can be expressed in terms of the activation energy between the forward transition and the reverse transition as

$$\dot{\psi}_f(\Delta H_f, \Delta H_r) = -\psi_f(\Delta H_f, \Delta H_r)\omega_0\left(\exp\left(\frac{-\Delta H_f}{RT}\right) - \exp\left(\frac{-\Delta H_r}{RT}\right)\right), \qquad (2.36)$$

where ψ_f is the fraction of materials that have undergone localized structure rearrangements and $\Delta H_f, \Delta H_r$ are the magnitude of activation energy for forward transition and reverse transition, respectively, and ω_0 is the attempt frequency. Each fraction of regions is assumed to contain a distribution of possible energy barriers that can be represented by a probability density function

$$\psi_f = \int_0^\infty \int_0^\infty \psi_f(\Delta H_f, \Delta H_r) d\Delta H_f d\Delta H_r . \qquad (2.37)$$

The plastic strain rate can be characterized using the probability distribution function as

$$\dot{\gamma}^p = \dot{\gamma}_0 \int_0^\infty \int_0^\infty \psi_f(\Delta H_f, \Delta H_r)\left(\exp\left(\frac{-\Delta H_f}{RT}\right) - \exp\left(\frac{-\Delta H_r}{RT}\right)\right) d\Delta H_f d\Delta H_r, \qquad (2.38)$$

and

$$\dot{\gamma} = \omega_0 D_f \Delta\gamma \sim \omega_0 \frac{V}{v^k}\frac{2\gamma^T v^k}{V} = 2\omega_0\gamma^T, \qquad (2.39)$$

where D_f is the total number of available processes, v^k, is the activation volume, γ^T, is the local transformation on the berries configuration and V is the total volume. It is assumed that the strain increment per transformation shown in Equation (2.38) is independent of the activation of the transformation.

The plastic strain rate equation is given by

$$\dot{\gamma}^P = \dot{\gamma} \int_0^\infty \psi_f(\Delta H) \left(\exp\left(\frac{-(\Delta H - \tau v^k)}{RT} \right) - \exp\left(\frac{S}{RT} \right) \exp\left(\frac{-(\Delta H - \tau v^k)}{RT} \right) \right) d\Delta H, \quad (2.40)$$

where τ is the equivalent shear stress, v^k is the activation volume and S is the local transformation strain energy, respectively. The first term in equation (2.39) accounts for the probability of the forward transformation and the second term accounts for the reverse transformation that opposes the deformation.

Using a pseudo-Gaussian distribution of activation energies, the overall inelastic (plastic) strain rate can be expressed by the sum of the two components of the rate equation such as

$$\dot{\gamma}^P = (\dot{\gamma}_1^P + \dot{\gamma}_2^P) \left(\exp\left(\frac{\tau v^k}{RT} \right) - \exp\left(\frac{-\tau v^k + S}{RT} \right) \right). \quad (2.41)$$

Thus, the constitutive model for the overall strain rate can be defined as the sum of the elastic and inelastic parts such as

$$\dot{\gamma} = \frac{\dot{\tau}}{G} + \dot{\gamma}^P, \quad (2.42)$$

and

$$\dot{\gamma}_1^P = \dot{\gamma}_0 e^{-a\eta} \left(\frac{(\sqrt{2} + (2 - \eta)e^{3\pi(1-\eta)/4})}{(1 + (1-\eta)^2)(\sqrt{2} + 2e^{3\pi/4})} \right), \quad (2.43)$$

$$\dot{\gamma}_2^P = \dot{\gamma}_0 e^{-a\eta} \left(\frac{(\sqrt{2}e^{\pi(1/4-\eta)} + (2+\eta)e^{\pi(1-\eta/4)})}{(1 + (1+\eta)^2)(\sqrt{2}e^{\pi/4} + 2e^{3\pi})} \right), \quad (2.44)$$

where $\eta = \dfrac{1}{RT}$.

The elastic part can be modeled by the Maxwell type model and the inelastic part can be modeled by the form of nonlinear dashpot. The internal variables such as a, α

34

and S are assumed to change via the first order kinetic process. The model contains eleven adjustable material parameters that need to be determined from nonlinear stress-strain data.

Hassan and Boyce (1995) demonstrated the application of their theory to model the mechanical behavior of PMMA. They determined eleven material parameters from compressive stress-strain data, and predicted uniaxial creep during compression. Figure 2.3 shows the comparison of experimental results and model predictions for quenched PMMA at 296K and 323K using a distribution of activation energies. It showed that the prediction was good in the post yield region less but the model was not able to predict the nonlinear behavior prior to yield even though the model could represent the curvature derivation from linear viscoelastic behavior. The Hassan and Boyce model (1995) can predict the change in creep response from small stresses to large stresses including plastic flow. The prediction, however, indicated a more pronounced nonlinear behavior than was observed in experiments using PMMA material. The same trend was also observed in the compressive stress-strain prediction of thermoset material (Lu et al., 2001).

2.5.2.3 Reduced Time Models

These models incorporate a reduced time that characterizes the nonlinear deformation phenomenon. It is assumed that the time scale of relaxation depends on the thermodynamic state during the deformation process. Hopkins (1958) first introduced the reduced time concept to describe non-isothermal behavior. It can be used to characterize

35
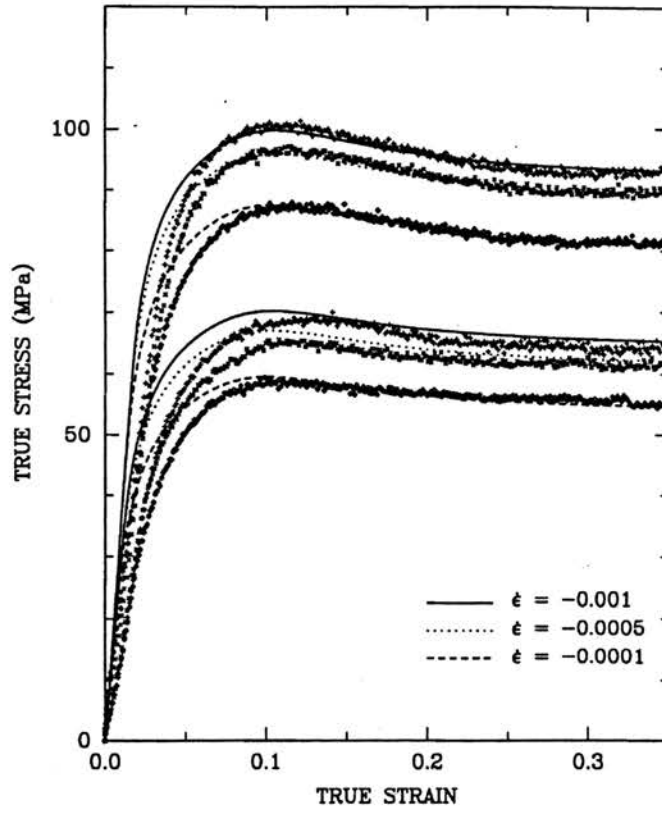
Figure 2.3: Experimental results and model predictions for quenched PMMA at 296K and

323K using a distribution of activation energies (Hassan and Boyce, 1995)

nonlinear behavior. The reduced time, $\varphi(t)$, or material internal governing time is

determined by

$$\varphi(t) = \int_0^t \frac{d\xi}{a(\xi)}, \tag{2.45}$$

where $a(\xi)$ is the shift factor that accounts for an acceleration or deceleration of the time scale of relaxation resulting from a large deformation. Two main frameworks using the reduced time concept will be reviewed herein: (1) the Schapery model (1969) that accounts for nonlinear creep and relaxation by a shift factor that is an implicit function of stress and strain, and (2) the Knauss and Emri formulation (1981) that uses a free volume concept as the controlling factor in the changes in relaxation behavior.

<u>2.5.2.3.1 Schapery Model</u>

Schapery (1969) developed a reduced time constitutive model based on irreversible thermodynamics. This model uses a shift factor dependent on both temperature and stress to characterize the nonlinear deformation. Strain response under a given stress history expressed as

$$\varepsilon(t) = g_0 D_0 \sigma + g_1 \int_0^0 \Delta\sigma(t-\xi)\frac{dg_2\sigma}{d\xi}d\xi,$$ (2.46)

and
$$t - \xi = \int_\xi^t \frac{d\xi'}{a_\sigma[\sigma(\xi')]},$$ (2.47)

where g_0, g_1, g_2 and a_σ are the stress dependent material functions, D_0 and $D(t)$ are the initial and transient creep compliance. Any functional form can be used to represent the linear viscoelastic creep compliance for $D(t)$. A power law form has been used for many applications based upon experimental results.

37

Schapery (1969) applied the theory to characterize the creep and creep recovery behavior of semi-crystalline nitrocellulose film and a glass reinforced phenolic resin. Nitrocellulose film was considered to be a low strength material, in which both g_2 and a_σ material functions were used to account for nonlinearity. The prediction was good for long-term behavior. Glass reinforced phenolic resin was considered to be a high strength material, and the nonlinearity could be characterized through the shift factor a_σ determined by graphically shifting single step nonlinear creep data using time-stress superposition. The prediction for creep and creep recovery was in good agreement with both long-term and short-term data. Schapery performed multiple step relaxation studies to verify a one-dimensional constitutive relation using polyisobutylene (PIB), an uncrosslinked amorphous polymer and demonstrated that the theory could predict three-step stress relaxation behavior very well.

2.5.2.3.2 Knauss and Emri Model

Knauss and Emri (1981) developed a different constituve model using reduced time based on free volume considerations. This model considers that the localized free volume controls the deformation rate, and the free volume depends on temperature, deformation and solvent concentration. The constitutive model is represented in terms of

$$S_{ij} = 2\int_0^t G(t-\xi)\frac{\partial e_{ij}}{\partial \xi}d\xi = \sigma_{ij} - \frac{1}{3}\sigma_{kk}\delta_{ij} \, , \qquad (2.48)$$

$$\sigma_{kk} = 3\int_0^t K(t'-\xi')\frac{\partial[\Re + \alpha_T * \Delta T + \gamma * C]}{\partial \xi}d\xi \, , \qquad (2.49)$$

38

where e_{ij} is the deviatoric component of the infinitesimal strain tensor i,e.,

$e_{ij} = \varepsilon_{ij} - \frac{1}{3}\varepsilon_{kk}$, G is the linear viscoelastic shear modulus, $K(t)$ is the bulk modulus,

$\Re$ is the dilatation due to deformation which is the isotropic part of the total strain i,e.,

$\Re = \varepsilon_{kk}$. The contribution $\alpha_T * \Delta T$ accounts for the change in the stress due to

temperature change and $\gamma * C$ from solvent swelling, and $\Re$ from dilatation that can

occur during mechanical deformation. The symbol * indicates a Stieltjes convolution

integral, for example, $\alpha_T * \Delta T = \int_{-\infty}^{\infty} \alpha_T(\tau)\Delta T(t-\tau)d\tau$. Equation (2.47) represents the

deviatoric part and the equation (2.48) represents the isotropic part. Both equations are

coupled through the reduced time.

The material internal governing time t'

$$t' = \int_0^t \frac{d\xi}{a[\Re(\xi), T(\xi), C(\xi)]},$$ (2.50)

and the shift factor is given by the Doolittle (1951) expression in the form of

$$\log a = \frac{B}{2.303}\left(\frac{1}{f^v} - \frac{1}{f_0^v}\right),$$ (2.51)

where f^v is the fractional free volume and B is a material constant. Under uniaxial

stress state, stress-strain relation is represented by

$$\sigma_{11} = \int_0^t E(t' - \xi')\frac{\partial e_{11}}{\partial \xi}d\xi.$$ (2.52)

This equation is reduced to the Boltzmann superposition for small deformations where

the reduced time t' is approximately t.

39

Knauss and Emri (1981) applied the theory to characterize the uniaxial stress strain response at a strain rate of 0.01 and 0.1 min^{-1} at temperatures of 24.3 and 26.5 ^{0}C using polyvinyl-acetate (PVAc) specimens, and with very good agreement. The governing equations under a single strain rate ramp loading are as follows:

$$\sigma_{11} = \overset{\bullet}{\varepsilon} \int_{0}^{t'} E(t' - \xi') d\xi , \tag{2.53}$$

$$\Re(t) = \frac{1}{3} \int_{0}^{t'} M_g \frac{\partial \sigma_{11}}{\partial \xi} d\xi , \tag{2.54}$$

$$t' = \int_{0}^{t} \frac{d\xi}{a[\Re(\xi), \alpha_T \Delta T]} , \tag{2.55}$$

$$\log a = \frac{-B}{2.303 f_0} \left(\frac{\alpha_T \Delta T + \Re(t)}{f_0 + \alpha_T \Delta T + \Re(t)} \right) . \tag{2.56}$$

And the stress for a ramp loading followed by a ramp unloading deformation hysteresis is given by

$$\sigma_{11} = \overset{\bullet}{\varepsilon} \int_{0}^{t'} E(t' - \xi') d\xi - 2 \overset{\bullet}{\varepsilon} H(t - t_1) \int_{t_1}^{t'} E(t' - \xi') d\xi . \tag{2.57}$$

If the duration time for experiments with a constant strain rate is relatively short, the relaxation behavior of the bulk modulus is not significant as compared with that of shear modulus, so that it can be considered to be a constant, M_0. It is also noted that temperature may have a significant effect on the shift behavior through a temperature induced volume change, $\alpha_T * \Delta T$. In the case where α_T is assumed to be a constant, the volumetric strain is $\alpha_T T$ and is independent of thermal history.

2.5.2.4 Summary on the Nonlinear Viscoelastic Constitutive Models

Some leading nonlinear viscoelastic constitutive models have been represented to help understand the thermo-mechanical behavior of localized yield and post-yield situation in fatigue. The Eyring activation model can characterize macroscopic nonlinear viscoplastic flow rate. This perhaps implies that the localized plastic deformation can also be characterized to include the effects of temperature and applied stress amplitude on plastic flow rate. If the stress amplitude and temperature can control the internal governing time in the reduce time model, it can predict long-term characteristics of the localized plastic deformation through the characterization of its short-term behavior. In next section, the general behavior of polymer fatigue on localized plastic deformation will be reviewed because it is related to the fatigue damage evolution for characterization of long-term fatigue behavior.

2.6 Fatigue Behavior

Polymers, like metals, are subject to fatigue failure. The fatigue behavior in polymers can be different from that of metals because of the different nature of the molecular structure. Polymers have a long backbone type main chain, side groups and their packing patterns. These are different from metals. Cyclic loading in polymer molecular structures can activate main chain motions corresponding to sub-molecular motions and often gives rise to sizeable relaxation peaks in the glassy state. These peaks, broadened considerably by the disorder and loose packing of these long chain molecules,

are instrumental in promoting a high strain deformation (beyond general yield), local damage formation and final fatigue failure.

The entanglements provided by the entwined long-chains ensure strength retention at these high strains, thus enabling polymers to undergo considerable highly localized plastic flow such as shear deformation in polymers (Adam and Gibbs, 1965; Xio et al., 1994; Dyre, 1987, 1999; Rizos and Ngai, 1999). This potential for extensive molecular rearrangement with retention becomes especially manifest under the cyclic loading of fatigue (Takemori, 1984). Because of the sub-critical nature, fatigue loads can produce highly localized deformation zones (Chen et al., 1993; Chen et al., 1994; Tsuji et al., 1999). Thus, small cracks initiated at defects can evolve further into cumulative damage, resulting in fatigue failure.

2.6.1 Fatigue Endurance Limit and Fatigue Crack Initiation

In this section, phenomenological theory in fatigue strength and fatigue crack initiation are reviewed; emphasis is placed on the evolution of the localized plastic deformation leading to a finite fatigue life. The localized yield-like deformation of time-dependent (viscoelastic) materials also exhibits time-dependent (viscoplastic) behavior because highly nonlinear viscoelastic behavior is involved in shear yield and craze formation.

The fatigue endurance limit is generally understood as a limit stress below which fatigue failure never occurs and the S-N curve becomes horizontal. In most materials, including metals and polymers, the fatigue endurance limit is usually associated with a

fatigue life of 10^6~10^7 cycles or higher. More brittle material shows clearer fatigue endurance limit than that of more ductile material. Above fatigue endurance limit, inhomogeneous and localized yield-like deformation, that exhibits highly nonlinear viscoelastic behavior, may occur in a polymer to induce fatigue-damage accumulation sites through which fatigue cracks initiate and propagate.

A macroscopic fatigue crack initiation process in amorphous polymers was observed as the coalescence of many microcracks that have developed during a long period of time of cycle loading. Many thermoplastics (Engel et al., 1981) and rubber (Wang, Lu and Kim, 2002) can be examples. In glassy polymers, fatigue-induced microcracks are followed by the development of localized plastic deformation zones and they are combined together to form a 'fatigue initiation site' that is optically measurable (Engel et al., 1981). In most cases, the polymer fatigue mechanism consists of localized plastic deformation, microcrack growth, microcrack coalescence, fatigue crack initiation, fatigue crack propagation and final fatigue fracture.

When a microcrack is formed in a particular localized plastic deformation zone, crazing and shear yielding are usually thought to be a coupled mechanism prior to further fatigue crack growth. It has been reported that craze initiation does not occur until the crack-tip plastic zone has evolved to a critical extent (Yamamoto and Furukawa, 1995; Ishikawa, 1995). It, therefore, implies that the life of fatigue crack initiation can be characterized by the continuous damage mechanism that describes the growth of plastic deformation under fatigue loading.

2.6.2 Fatigue Life Prediction

Prediction of fatigue lifetime is one of the major concerns in polymer fatigue for engineering applications. Total fatigue lifetime of a material is considered to consist of two parts: one is the fatigue crack initiation life and the other is the fatigue crack propagation life. For small, smooth and initially flawless specimens, the time for the fatigue crack nucleation phase is considered as the fatigue crack initiation life. Fatigue crack propagation life accounts for the fatigue crack propagation phase from an initially sizable fatigue crack to its critical size that may cause a catastrophic and/or total failure of the structures. Taking into account the large statistical scatter of the fatigue life, fatigue crack initiation life (fatigue crack nucleation phase) in high cycle fatigue is understood to contribute to most of the total fatigue life. And the fatigue crack propagation life (fatigue crack propagation phase) is considered nonsignificant compared with that of the first phase. One approach in fatigue life investigation is to determine the relationship between the amplitudes of cyclic stress and the total number of cycles (N_f) of loading applied prior to failure. This approach is called S-N (curve) approach. The S-N approach considers the fatigue crack initiation life to be dominant in total fatigue lifetime.

Recently, there have been many applications of polymer structure and components such as gears, shafts, bearings, couplings and so on that would be subjected to considerable fatigue situation. Polymer structure design procedures must take into account the reliable fatigue data to assure targeted service life. Consequently, there is a great demand in the development of laboratory-level fatigue test technique that can produce reliable fatigue data to predict actual long-term service life. However, it is a

challenging work because of intrinsic nature of viscoelastic behavior in polymers so that the fatigue behavior depends on test conditions, sample pre-history and/or manufacturing process. Among them, different test conditions may cause the most considerable variation in fatigue data. If the test conditions are different from actual service temperatures and/or loading frequencies test data may not provide reliable fatigue life prediction. In this section, the effects of stress amplitude, temperature and frequency on the fatigue life are discussed in detail.

2.6.2.1 Functional Dependence of Polymer Fatigue

The fatigue lifetime of all polymeric materials has a considerable functional dependence on a host of variables listed below (Takemori, 1984).

- Test parameters – temperature, stress amplitude, mean stress level, frequency, loading waveform, etc.

- Sample prehistories – annealing, heat treatments, and presence of weld planes, surface coatings, irradiation, exposure to solvent, etc.

- Compositional variables – molecular weight, molecular weight distribution, percent crystallinity, crystallite morphology, the presence of impact modifiers, reinforcing fibers, fillers, etc.

Test parameters or test environments may have a special interest to the practical engineer because their effects are most. Among the test parameters, temperature and frequency effects at a given stress amplitude need to be considered carefully.

45

2.6.2.1.1 Temperature Dependence

In what follows, a review is given for polymer fatigue involving temperature dependence.

Notched Specimens

In the past several decades, numerous studies have focused on finding the temperature dependence of fatigue crack growth rates. Kurobe and Wakashima (1970, 1972) observed that fatigue crack growth rate in PMMA increased with decreasing temperature over a testing temperature range between $-10^{\circ}C$ and $50^{\circ}C$ under a displacement controlled condition. Conversely, Radon and Culver (1975) found that fatigue crack growth rate decreased gradually with decreasing temperature from $-60^{\circ}C$ to $60^{\circ}C$ in Polystyrene under a load controlled condition at a frequency of 0.15Hz. Gerverich and his coworkers (1976a, 1976b) observed the temperature dependence of fatigue crack growth in polycarbonate and polysulfone specimens. They found that the fatigue crack growth rate at 1Hz increased with decreasing temperatures until $-50^{\circ}C$ and then decreased with a further temperature decrease. Martin and Gerberich (1976) have attempted to explain these phenomena using an adiabatic assumption near the fatigue crack tip; they predicted a local temperature rise of up to $100^{\circ}C$. However, Attermo and Ostberg (1971) observed that the temperature increase at the fatigue crack tip in Polycarbonate was less than $30^{\circ}C$, even at 11Hz. Thus, it is expected that a much smaller temperature increase would occur at 1Hz.

Generally, the observations have indicated that if the materials with initial cracks are under isothermal and displacement controlled cyclic loading conditions, the fatigue

crack growth rate will decrease as temperature increases. This is because a temperature increase will tend to soften the material, causing a reduction in modulus and the corresponding stress intensity factors, resulting in more ductile behavior in the material, and thus leading to slower growth of the fatigue crack. It is noted that studies on temperature effects were mostly limited to experimental observations; successful modeling was not available.

Unnotched Specimens

For metallic materials, numerous studies have been conducted to determine thermo-mechanical fatigue behavior. Some models for fatigue life prediction have been proposed for materials used in jet engines that are subjected to combination of cyclic load and cyclic temperature history (Miller and Priest, 1987; Sehitoglu and Maier, 2001). In polymeric materials, however, only a few studies have been conducted to characterize the fatigue behavior using the S-N approach at various temperatures. No results have been reported on the fatigue behavior using the S-N curve approach when a temperature variation, induced by hysteretic heating, is involved.

Furue and Shimamura (1980) made an effort to correlate the characteristic fatigue behavior of several polymers to their fundamental mechanical properties, such as flexural strength and Young's modulus, through extensive fatigue tests on fifteen different materials including plastics and composites. They showed that at a given alternating stress amplitude, fatigue life at elevated temperatures is shorter than that at room temperature. The experiments, however, were accomplished under only two different

temperature conditions ($20^{\circ}C$ and $50^{\circ}C$). Thus, temperature-dependent fatigue behavior was not examined over a wide range of temperatures.

Miyano et al. (1999, 2000) also observed the temperature-dependent fatigue life behavior of Carbon Fiber Reinforced Plastics (CFRP) using S-N curve approach. They demonstrated that 'temperature' could be one of fatigue acceleration factors if its effect is quantitatively characterized using a nonlinear viscoelastic model based on reduced time concept. They also proposed a methodology for fatigue lifetime prediction at different frequencies using time-temperature and time-frequency superposition. However, their methodology was not based upon fatigue mechanisms, instead it was based on the correlation between static loading response and fatigue behavior. The contribution of their work lies on the first application of time reduce model to predict long-term tensile failure stress and S-N curve at different frequency. Their work was the first attempt. A detailed discussion about their work is given in Section 2.6.2.2.

2.6.2.1.2 Frequency Dependence

All viscoelastic materials exhibit a considerable time-dependent relationship between stress and strain. In the case where different strain rates are used as input, there exist different responses in stress in viscoelastic media. Different loading frequencies in fatigue situations can also cause different effect on the corresponding fatigue life values. In notched specimens, two major different theories have been proposed to describe the effect of frequency on fatigue crack growth rate. Both theories focused on the fatigue crack process zone where viscoelastic deformation such as yield-like deformation in

shear and localized heterogeneous deformation such as crazing are all present, causing the fatigue crack growth process to be highly nonlinear.

One theory is that an increase of the loading frequency causes a considerable decrease in the fatigue crack growth rate, resulting in an increase of fatigue life (Chou and Sun, 1982; Ramsteiner and Armbrust, 2001). In this case, only the mechanical fatigue process can be considered. Wnuk(1971) proposed that the fatigue crack growth rate in a polymer could be represented by superposition of elastic and viscoelastic components in the form of

$$\frac{da}{dN} = \frac{l^*}{12}\left[4\left(\frac{\Delta K}{K_c}\right)^4 + \frac{C}{f}\left(\frac{\Delta K}{K_c}\right)^2\right],$$ (2.58)

where l^* is $\pi K_c^2 / 8\sigma_{ys}^2$, K_c, fracture toughness, ΔK, the stress intensity factor range, σ_{ys}, yield stress and C is a function of the time rate of change of the normalized creep, $D(t)/D(t_0)$, for the material. This relationship can describe the observed decrease in fatigue crack growth rate with increasing loading frequency found in PVC, PMMA, PS, PPO and Noryl.

A simple modification of the Paris law has been proposed by Yokobori and Sato (1976) in the form of

$$\frac{da}{dN} = Cf^{-\lambda}(\Delta K)^n,$$ (2.59)

where C, λ and n are constants.

Mukherjee and Burns (1971) proposed a frequency-dependent fatigue crack growth rate based on statistical analysis for PMMA

$$\frac{da}{dN} = 10^{-16.25} f^{-0.43} K_{mean}^{2.13} (\Delta K)^{2.39} \text{ } in/cycle \cdot \qquad (2.60)$$

Based upon this empirical formula, the fatigue crack growth rate at the frequency of 0.1Hz is approximately 7 times higher than that of 10Hz, assuming that other conditions are identical.

Attermo and Ostberg (1971) proposed another theory based on the consideration that a thermal fatigue is induced by a high loading frequency assuming adiabatic heating hypothesis concerning the effect of localized heating at the advancing crack tip. A temperature increase was observed at the crack tips up to $20\,^{0}C$ in PVC, PMMA and PC. This thermal effect was postulated that highly localized hysteretic heating causes a thermal fatigue problem and a higher loading frequency creates a higher fatigue crack growth rate.

In unnotched specimens, it was also observed that loading frequency is an important test parameter because the hysteretic heating rate is linked, based on linear viscoelastic analysis, to frequency through (Ferry, 1974)

$$\dot{E}_d = \pi f D_2(f,T)\sigma_a^2, \qquad (2.61)$$

where $\dot{E}_d$ is the hysteretic heating rate during each cycle, σ_a is the applied maximum stress, f is frequency, and D_2 is loss compliance. Equation (2.61) indicates that the rate of hysteretic heating rate is linearly proportional to loss compliance, loading frequency and the square of the stress amplitude. Heat transfer characteristics of the materials need fatigue, when the specimen is thick. This implies that the geometry of the
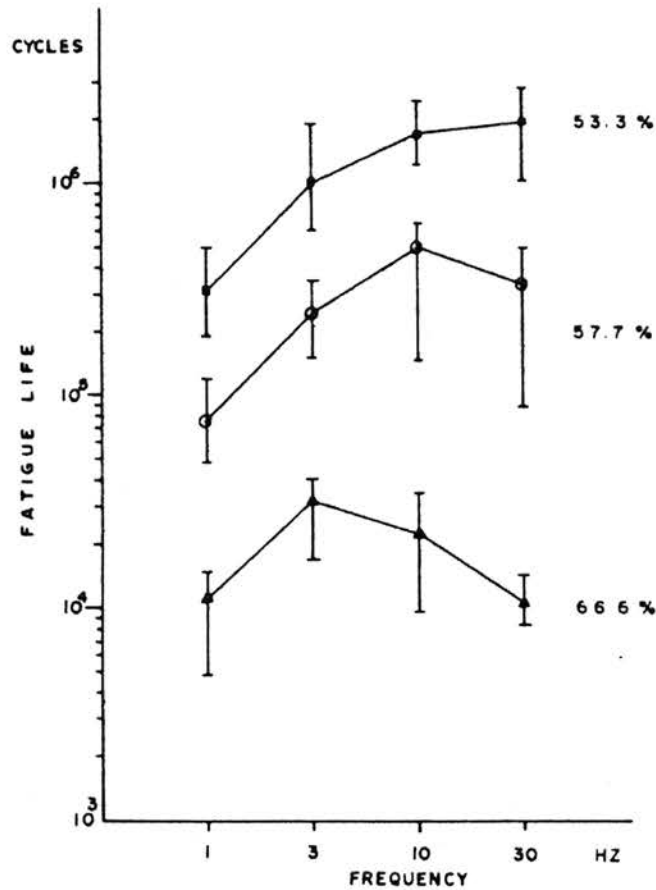
Figure 2.4: Fatigue life test with different frequencies and loading ratios
of laminated composite specimen (Sun and Chan, 1979).

specimen has strong effects on the fatigue process involving athermal conditions.

Sun and Chan (1979) observed a frequency effect on the fatigue life of a laminated
composite specimen with a center hole. Figure 2.4 shows that at low frequencies the
fatigue life increases as frequency increases. But the fatigue life declines as frequency
increases even higher at 57.7% and 66.6% load level (not in the case of 53.3%). Figure

(A)
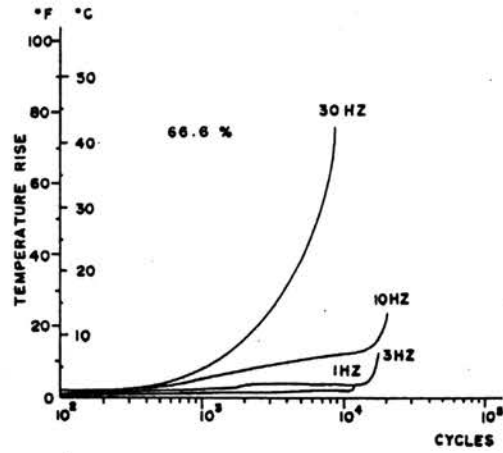
(B)
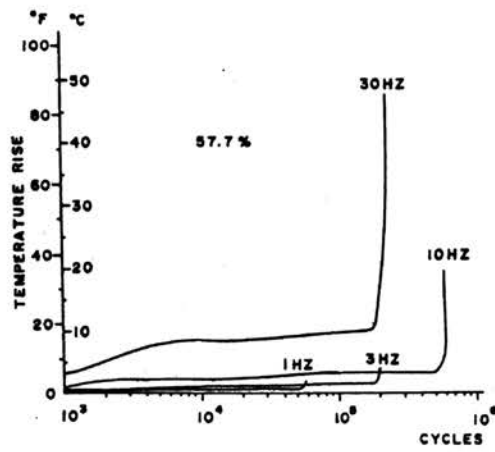
(C)
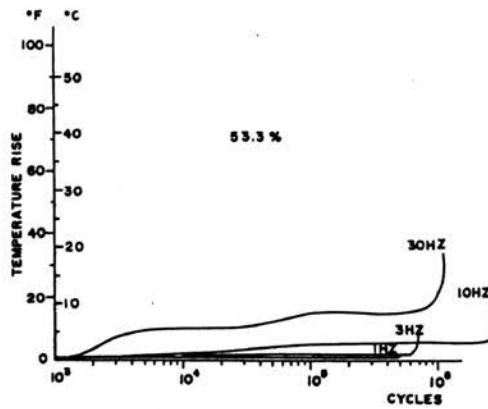
Figure 2.5: Temperature rise near the hole at (A) 66.6%, (B) 57.7%, (C) 53.3% load level.
(Sun and Chan, 1979)

52

2.5 shows the corresponding temperature history at different frequencies. It can be observed that at the 53.3% load level, fatigue life increases as the load frequency increases; it tends to level off at higher frequencies. But at the 66.6% load level a substantial temperature increase occurs and fatigue life decreases at this load level due to deteriorated material behavior at a higher temperature induced by thermal fatigue.

From the literature review on the frequency effect on fatigue behavior of viscoelastic materials, the following summary is given:

1) Under isothermal conditions with stress or strain control, notched or unnotched specimens under high loading frequency conditions cause high strain rate, high yield strength, high modulus and low plastic deformation per loading cycle. The corresponding fatigue life increases in terms of the number of cycles.

2) Under an athermal conditions where both thermal fatigue as well as mechanical fatigue are involved, there is a competition between two different fatigue processes. Whether thermal fatigue or mechanical fatigue prevails depends on the viscoelastic behavior of the materials and the deformation localization such as shear yielding and crazing associated with the thermo-mechanical behavior.

2.6.2.1.3 Thermal Energy Dissipation under Dynamic Loading Conditions

In viscoelastic media, stress and strain responses are not in phase during cyclic loading. Strain is always behind stress by a phase angle between 0 and $\pi/2$ radians.

Equation (2.61) has shown the relation between hysteretic heating rate, $\dot{E}_d$, and the applied peak stress, σ_a, frequency, f, and loss compliance, D_2. As polymers are

thermal insulators compared with metals, with much lower thermal conductivity, the temperature can increase in polymers under fatigue loading. The temperature increases with frequency and loading amplitude.

Ezrin (1996) categorized thermal fatigue phenomenon of polymers into three groups based on the magnitude of loss compliance even though this property is not a constant rather it changes with frequency and temperature as shown in the equation (2.61).

- Group 1 – Materials with low ambient loss compliance, less than $0.1 \times 10^{-11} \, cm^2/dyne$. They fail primarily by crack propagation because the generated heat is little and can be readily transferred to the surrounding environment. This group includes Polyvinyl Chloride (PVC), Polyphenylene Oxide (PPO), Polysulfone, Urea, Diphenylamine (DAP), Phenolic and Epoxy.

- Group 2 – Materials with intermediate loss compliance, 0.1 to $0.5 \times 10^{-11} \, cm^2/dyne$. They tend to fail by simultaneous thermal fatigue and mechanical fatigue. Thermal energy due to viscoelastic hysteresis can accelerate or decelerate the mechanical fatigue process. This group of materials includes Polymethyl Methacrylate (PMMA), Acetal, Polyethylene Terephthalate (PET), Alkyd and Polycarbonate (PC).

- Group 3 – Materials with high loss compliance, 0.5 to $5 \times 10^{-11} \, cm^2/dyne$. They tend to fail exclusively by thermal failure because the amount of heat generated in hysteresis is so high such that material tends to soften, leading to thermal failure. This group of materials includes Fluoroplastics, Polypropylene (PP), Polyethylene (PE) and Nylon.

For the materials in groups 2 and 3, the temperature has to be controlled very well during fatigue tests not to have effect by thermal fatigue.

2.6.2.2 Accelerated Lifetime Testing

Many polymeric structural components are used under low frequency cyclic loading conditions for a lifetime on the order of decades. To ensure these components to carry the loads safely over the service life, accelerated lifetime testing, i.e., short-term testing for prediction of long-term service life, must be considered, especially for critical parts where failure can cause catastrophe. Conventionally, an increase in the loading frequency is used for accelerating fatigue tests for time-independent materials such as metals under moderate temperatures. A change in the loading frequency is not considered to cause significant effect on the linear and/or cumulative fatigue processes and the corresponding fatigue life prediction for time-independent materials.

However, polymer fatigue has distinct features. As it has been reviewed, polymer fatigue behavior exhibits considerable temperature- and/or frequency- dependence. Different temperature and loading frequency from actual service conditions would give different experimental results that cannot be used for reliable prediction of actual service life. Another issue in fatigue life prediction is that a reliable fatigue lifetime cannot be predicted from the fatigue experiment under a high loading frequency because thermal effects induced by viscoelastic hysteresis can accelerate or decelerate the fatigue process in different test conditions. Because of these distinct features, there exist a great need for

the development of an accelerated fatigue life testing methodology of polymers for engineering applications.

To develop an accelerated lifetime testing methodology, thermo-mechanical behavior of viscoelastic material under fatigue should be understood so that appropriate accelerated factors such as frequency, temperature and higher stress can be used effectively. However, it is noted that a constitutive law capable of modeling the general thermo-mechanical behavior under arbitrary loading and environmental conditions does not exist. We need, therefore, some proven methods, such as the reduced time concept in viscoelasticity to accelerate the fatigue tests. The only published work using this method is the work by Miyano et al. (1999, 2000). Their work deals with prediction of long-term static strength as well as fatigue strength. Even though there are some limited assumptions, an accelerated fatigue life testing method has been proposed. A detailed review of their work is given here.

Miyano et al. (1999, 2000) investigated the fatigue behavior of CFRP under different temperatures and frequencies and proposed a methodology to predict fatigue behavior at different temperatures and frequencies. They used a model based on a reduced time to account for time-temperature superposition and time-frequency superposition associated with fatigue behavior. They however, did not propose an accelerated lifetime test technique; instead they demonstrated a continuous dependence of temperature and frequency in polymer fatigue. The hypotheses used for their work are:

1) The failure process is the same under constant strain rate flexural, creep, and fatigue loading.

2) The linear cumulative damage law is applicable for a non-decreasing stress

56

process.

3) Fatigue strength has a linear dependence upon stress ratio.

Under these hypotheses, they showed that the fatigue life could be predicted using the master curve of tensile strength at different loading rates. However, fatigue failure can occur at much lower stress amplitude than tensile failure stress and/or at much shorter time than that under static loading having same stress level. The dynamic fatigue process is quite different from monotonic loading condition in that highly nonlinear plastic deformation around localized damage sites under dynamic loading is a unique phenomenon. The fatigue life cannot be necessarily predicted by the monotonic loading until failure, so that a different approach is needed in the development of a more reliable accelerated testing technique.

Figure 2.6 shows the tensile strength as a function of temperature at different loading rates obtained by Miyano and his coworkers. The results indicate that the strength decreases as temperature increases at all strain rates. A master tensile strength curve was generated in Figure 2.7 by shifting short-term data on the tensile strengths as a function of creep rupture time. It was found that the tensile failure stress in tensile tests obeys the time-temperature superposition principle. They defined the time-temperature shift factor as

$$a(T)_{T_0} = \frac{t_s}{t_s'} = \frac{(t_s)_T}{(t_s)_{T_0}},$$
(2.62)

where t_s, t_s' are the time to failure at a given loading rate and temperatures T and T_0, respectively. Theoretical treatment of shift behavior needs to be considered herein. The time-temperature shift factor defined in Equation (2.62) can be computed in terms of the

57
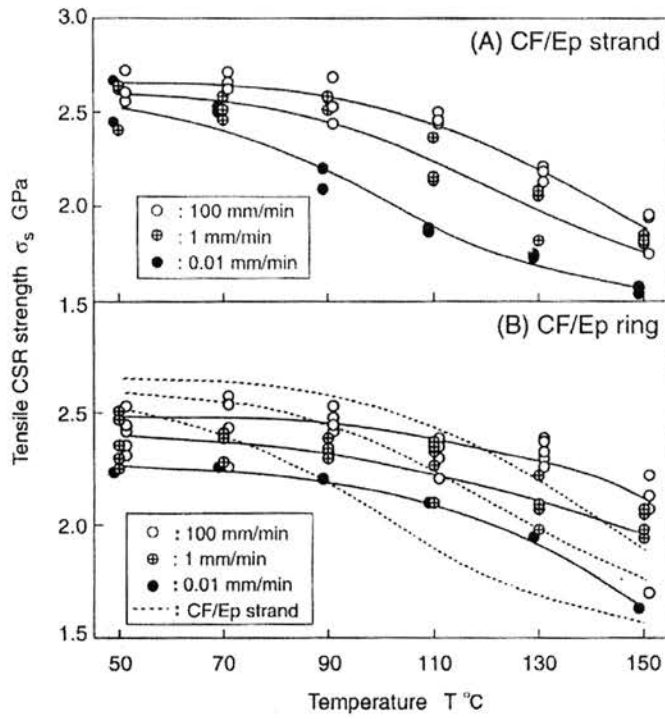
Figure 2.6: Tensile strength vs temperature at various loading rates. (Miyano et al., 2000)
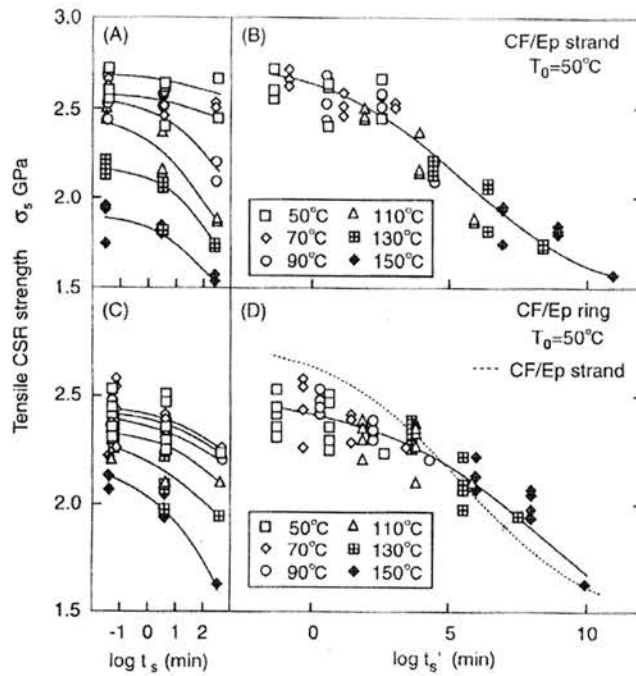
Figure 2.7: Master curve of tensile strength. (Miyano et al., 2000)

change of the material's internal viscosity (Doolittle, 1951) as

$$a(T)_{T_0} = \frac{\eta_T}{\eta_{T_0}}.$$ (2.63)

The material's internal viscosity used in Equation (2.63) is inversely proportional to the strain rate under a constant stress rate. It is noted that strain rate, $\frac{d\varepsilon}{dt}$, depends on the stress rate and stress amplitude and can be estimated using the global yield strain, ε_y and the time to reach yielding, t_s, these give

$$\eta = \left(\frac{d\varepsilon}{dt}\right)^{-1}, \text{ and } \frac{d\varepsilon}{dt} = \frac{\varepsilon_y}{t_s}.$$ (2.64)

Therefore,

$$a(T)_{T_0} = \frac{\eta_T}{\eta_{T_0}} = \frac{\left(\frac{d\varepsilon}{dt}\right)_{T_0}}{\left(\frac{d\varepsilon}{dt}\right)_T} = \frac{\varepsilon_y'/t_s'}{\varepsilon_y/t_s} = \left(\frac{\varepsilon_y'}{\varepsilon_y}\right)\left(\frac{t_s}{t_s'}\right),$$ (2.65)

where $\left(\varepsilon_y'/\varepsilon_y\right)$ is the ratio of yield strain magnitudes at temperatures T and T_0.

Equation (2.65) shows that the ratio of the global yield strain needs to be included to characterize the time-temperature shifting behavior in Equation (2.62). Miyano and his coworkers did not take into account the effect of temperature on yielding strain. In fact, the yield behavior of many thermoplastic materials depends on temperature and time (Figure 2.8). Consequently, the methodology proposed by Miyano et al. can be revised to account for this effect through the time-temperature superposition principle for polymer fatigue. They also applied the time-frequency superposition principle using time-frequency shift behavior as
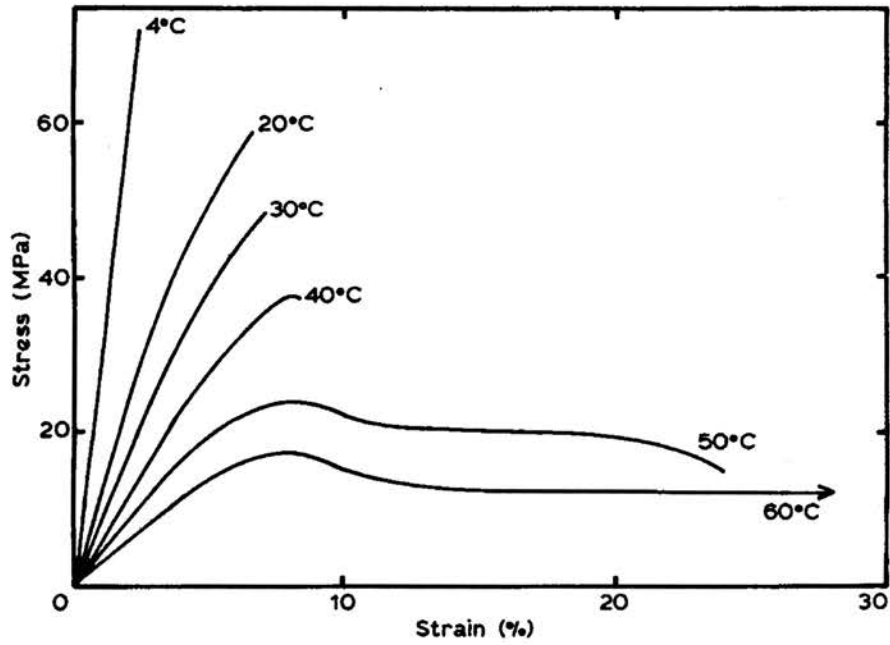
Figure 2.8: Variation of stress-strain behavior of PMMA with different

temperature conditions. (Kinloch and Young, 1983)

$$a_{T_0}(T) = \frac{f'}{f}, \qquad (2.66)$$

$$a_{T_0}(T) = \frac{t_f}{t'_f}, \qquad (2.67)$$

where f is frequency and t_f is time for failure.

Equations (2.66) and (2.67) imply that the frequency ratio is equal to the inverse of the ratio of the time for failure. This relationship was obtained from monotonic tensile tests where the time to failure is considered to be the half period of the loading frequency. The failure mechanisms for rupture failure and fatigue failure is quite different because the fatigue failure may occur even when the applied stress is far below the yielding stress. Furthermore, many polymers exhibit a failure mode transition from ductile failure to brittle failure under different loading conditions. Therefore, time-frequency shifting behavior cannot be generalized from a simple monotonic tensile behavior.

Using the assumption that the failure process is the same under the constant strain rate flexural, creep, and fatigue loading, Miyano et al. combined the master tensile curve shown in Figure 2.7 and S-N curves at different temperatures to generate the master curve of tensile failure stress in the S-N curve as shown in Figure 2.9 through horizontal shifting behavior based on time-temperature superposition. Then, they predicted the S-N curve at different temperatures and frequencies using the master curve of tensile failure stress in the S-N curve and time-frequency shift factor as shown in Equations (2.66) and (2.67), based on the time-frequency superposition. Figure 2.10 shows the S-N curve prediction for $f = 0.02$ Hz and had comparison with experimental results. Their results have an agreement with actual data.

2.7 Closure

In this chapter, the thermo-mechanical behavior of polymers under various loading and environmental conditions and corresponding mechanisms for fatigue and fracture
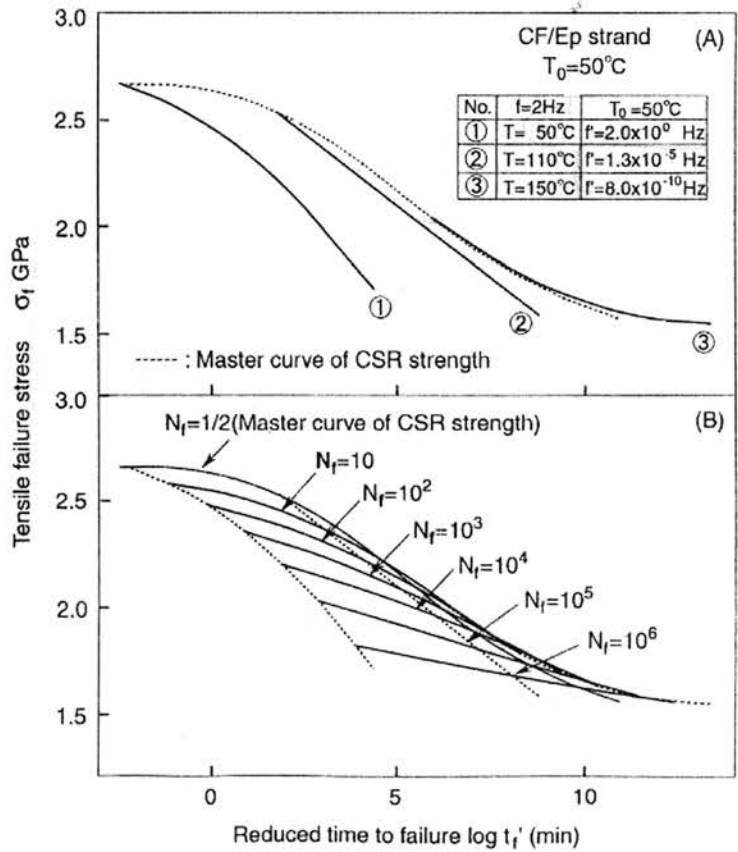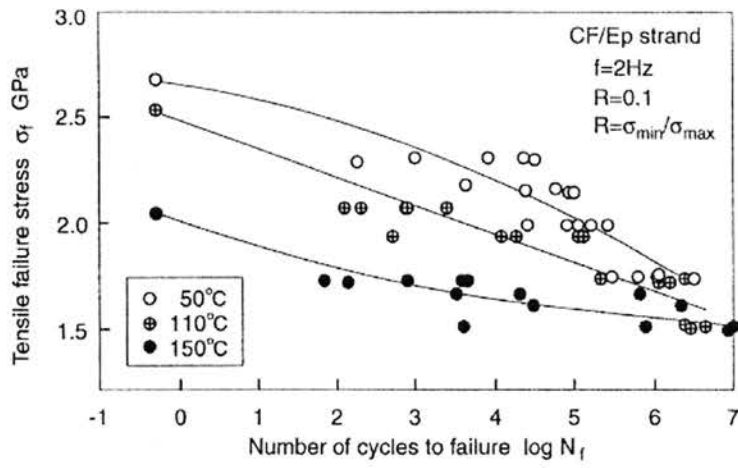
Figure 2.9: (A) Tensile failure stresses in fatigue vs number of cycles to failure,

(B) Master curve of tensile failure stress in fatigue.(Miyano et al., 2000)
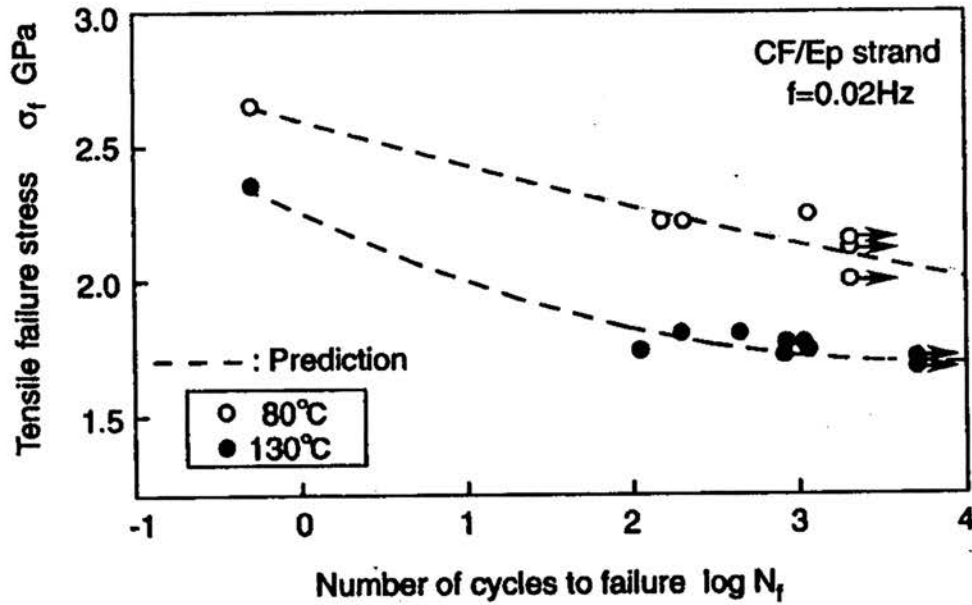
Figure 2.10: Predicted S-N curves for $f = 0.02$ Hz based on the data for 2 Hz

and test data for $f = 0.02$ Hz. (Miyano et al., 2000)

have been reviewed. It is expected that a suitable nonlinear viscoelastic model, that is capable of describing the yield-like deformation in time-dependent materials such as polymers in fatigue, needs to be identified for quantifying fatigue acceleration factors that include temperature, moisture, frequency, stress amplitude. While several leading nonlinear viscoelastic models exist, most of them deal with both linear viscoelastic and

nonlinear viscoelastic behavior. Eyring's energy activation model is one that is established based on consideration of the distribution of local energy barriers in yield-like deformation, and is capable of capturing such effects as temperature and stress amplitude, and is represented in relatively simple form. This model has been used as the basis for the successful models such as Argon (1973) and Boyce (1988) models. The use of this model does not require lengthy experiments to determine the material functions; rather, some simple tension or compression experiments suffice to determine the model parameters. Consequently, this model is identified as a nonlinear viscoelastic constitutive model for the consideration of nonlinear viscoelatic behavior accounting for the dependence of yield-like deformation on environmental and loading conditions.

Fatigue behavior of polymers has been reviewed in the second part of this chapter. In fatigue acceleration, it is noted that a simple increase in frequency will not necessarily accelerate the viscoelastic behavior of polymers, and a frequency over a certain limit will result in self-heating in polymers, leading to athermal condition. Most work on polymer fatigue did not focus on the acceleration of viscoelatic behavior of polymers. While there are some limited pieces of work on the effects of frequency, temperature on fatigue using either total life approach or defect tolerant approach, they were not intended for the development of accelerated fatigue testing techniques. The most relevant work in the past was the work conducted by Miyano and his group (1999, 2000) on fatigue acceleration on composites with thermoset materix, but not on polymers. Because it is the matrix material (i.e., polymer) that contributes to the viscoelastic behavior in composite, it is anticipated that the approach used by Miyano and his group (Miyano, et al, 1999 and 2000) might not be necessarily applicable to polymers due to the fact that (1) one

assumption in the work by Miyano and his co-workers might not be able to be generalized from composites to polymers. The assumption states that failure process is the same under constant strain rate flexural, creep, and fatigue loading, so that fatigue data can be analyzed based on quasi-static strength data to generate a fatigue strength master curve through time-temperature superposition with the consideration that static failure is a special case of fatigue failure with $N_f = 0.5$ cycles (2) the yield strain in the work by Miyano and his co-workers is considered independent of frequency and temperature. While this is the case for the composite CFRP they used in their study, this is not necessarily the case with polymers. As a result, their approach cannot be directly applied to polymer fatigue acceleration; and (3) self-heating induced by viscoelastic hysteresis was not encountered in their work, but is a problem associated with fatigue acceleration at a higher frequency than a low service frequency. Consequently the work by Miyano and his co-workers needs to be extended to address these issues and needs to be applied directly to polymers if a fatigue acceleration approach is to be established. In summary, there are some work accomplished in fatigue of time-dependent materials, a systematic approach for fatigue acceleration specifically developed and validated for polymers does not exist, and has become the research topic of this dissertation.

2.8 Research Objective

The objective of this research is to develop an accelerated lifetime testing (ALT) methodology utilizing temperature, stress and frequency as fatigue acceleration factors. This ALT technique will enable realistic long-term and high cycle fatigue life to be

predicted from the fatigue data obtained from short-term accelerated fatigue, instead of from combined monotonic tensile tests and fatigue tests as implemented by Miyano et al (1999, 2000).

Quantitative effects of these factors on fatigue will be characterized based on the consideration of dependence of yield-like deformation on these factors through some appropriate nonlinear viscoelastic models. The ALT for polymer fatigue in this dissertation is intended to process short-term fatigue test data obtained from different temperatures and frequencies to provide reliable prediction of realistic long-term fatigue lifetime at a low service frequency (e.g., 1 Hz).

CHAPTER THREE

DEVELOPMENT OF LIFETIME TESTING TECHNIQUES

3.1 Introduction

This chapter will describe a technique for accelerated lifetime testing (ALT) based on the consideration of dependence of localized nonlinear viscoelastic deformation in the fatigue crack initiation process. Temperature, stress and frequency dependent evolution of the localized plastic deformation leading to fatigue failure will be characterized to determine a finite fatigue life using the S-N curve approach. Localized nonlinear viscoelastic deformation processes may be described by a modified energy activation model. The model identifies the dependence of fatigue life on temperature, stress amplitude and frequency. This model uses the reduced time concept to allow short-term accelerated fatigue data at elevated temperatures and/or higher loading frequencies to be processed for the prediction of relatively long-term fatigue behavior under service conditions at lower temperatures and frequencies.

3.2 Time-Temperature Superposition for Fatigue Life Prediction

Fatigue loads produce a highly localized plastic deformation zone where creep, shear yielding, craze and microcracks occur. Localized plastic deformation during a

loading cycle may exhibit time dependent characteristics because of the viscoelastic nature of polymer material. The activation model for nonlinear viscoplastic behavior of plastic flow in viscoelastic material (Erying and Ree, 1958; Argon, 1973; Hussan and Boyce, 1995) can also be employed for characterization of fatigue-induced localized plastic deformation.

If sinusoidal loading input is considered, the activation energy barrier will be its minimum value when the maximum load is applied to the material. Therefore, it is likely that most of plastic deformation flow during a loading cycle may occur when the applied stress amplitude reaches its maximum (peak) load such as

$$\left(\int_0^{1/f} \varepsilon^p(t)dt \right)_T = \left(\frac{d\varepsilon^p}{dN} \right)_T \approx \left(\frac{d\varepsilon^p}{dN} \right)_{T,\sigma_a} \tag{3.1}$$

where f is frequency, σ, ε are applied stress and strain, σ_a is maximum stress amplitude, ε^p is localized plastic strain and T is absolute temperature.

For a fatigue loading cycle, the magnitude of localized plastic deformation flow in a viscoelastic material under constant amplitude and constant frequency that is low enough not to cause a thermal effect, can be expressed by the portion of the internal viscosity from an Arrhenius-type relation as a function of temperature. This can be envisioned by the following equation:

$$\left(\frac{d\varepsilon^p}{dN} \right)_{T,\sigma_a} \propto A'\eta_{T,\sigma_a}^{-1} = A\exp\left(-\frac{\Delta H_{\sigma_a}}{RT} \right), \tag{3.2}$$

where $\left(\dfrac{d\varepsilon^p}{dN}\right)_T$, η_{T,σ_a}, ΔH_{σ_a}, R, σ_a and T are plastic deformation flow per loading cycle

at a given temperature, T, internal viscosity at T and σ_a, activation energy barrier for

molecular structure movement at σ_a, gas constant, applied maximum stress amplitude

and absolute temperature, respectively. A' and A are arbitrary constants. At a certain

reference temperature, T_{ref}, it will be rewritten as

$$\left(\frac{d\varepsilon^p}{dN}\right)_{T_{ref},\sigma_a} \propto A'\eta_{T_{ref},\sigma_a}^{-1} = A\exp\left(-\frac{\Delta H_{\sigma_a}}{RT_{ref}}\right). \qquad (3.3)$$

Accelerated lifetime testing means a laboratory-level and short-term testing in

which data can be produced and processed to predict actual long-term fatigue behavior in

service condition. It is possible that the accelerated lifetime testing methodology can be

developed with the consideration of the reduced time model to predict fatigue lifetime.

Reduced time models incorporate a reduced time concept that characterizes the

nonlinear deformation phenomenon. It is assumed that the time scale of relaxation

depends on the thermodynamic state during the deformation process. The reduced time

models characterize nonlinear deformation behavior that can be captured by time-

temperature superposition (Williams et al., 1955; Hopkins, 1958; Schapery, 1969; Knauss

and Emri, 1981).

The internal governing time denoted by $\varphi(t)$, which is the material time scale

related to the experimental scale shown as a factor called the time shift factor, $a(T)_{T_{ref}}$,

can be given by

$$\varphi(t) = \int_0^t \frac{d\tau}{a_{T_{ref}}} = \int_0^t \frac{d\tau}{\eta_T / \eta_{T_{ref}}}, \tag{3.4}$$

$$\log\left(a(T)_{T_{ref}}\right) = \log\left(\frac{\eta_T}{\eta_{T_{ref}}}\right) = \frac{\Delta H_{\sigma_a}}{R}\left(\frac{1}{T} - \frac{1}{T_{ref}}\right). \tag{3.5}$$

Plotting the $\log(a(T)_{T_{ref}})$ against $\left(1/T - 1/T_{ref}\right)$ will give the calculation of the activation energy ΔH_{σ_a} from the slope.

Localized plastic deformation during one loading cycle with constant stress amplitude can be predicted based upon the reference temperature by employing the time-temperature superposition principle as follows:

$$\left(\frac{d\varepsilon^p}{dN}\right)_T \propto A'\eta_T^{-1} = A'a(T)_{T_{ref}}\eta_{T_{ref}}^{-1} \propto a(T)_{T_{ref}}\left(\frac{d\varepsilon^p}{dN}\right)_T. \tag{3.6}$$

There is no clear mechanism yet to explain that localized plastic deformation on the unnotched specimen due to fatigue loading initiates and develops continuously under continuous fatigue loading conditions to increase its deformation zone before the actual macroscale fatigue crack initiation. Many studies, however, have observed that there are considerable plastic deformation zones created at the crack tip before fatigue crack initiation in glassy polymer with various notch conditions (Kitagawa, 1982; Nisitani and Hyakutake, 1985; Takemori, & Matsumoto, 1982).

If it is assumed that fatigue damage accumulates linearly in the form of localized plastic deformation under the cyclic loading conditions, and a macro fatigue crack occurs when the magnitude of the accumulated plastic deformation reaches a critical or threshold value, then fatigue lifetime in S-N curve can be estimated as follows:

70

$$\left(\frac{d\varepsilon^p}{dN}\right)_T = \left(\frac{\varepsilon_c^p}{N_f}\right)_T, \tag{3.7}$$

$$\left(\frac{N_f}{\varepsilon_c^p}\right)_T \propto A'\eta_T = A'a(T)_{T_{ref}}\eta_{T_{ref}} \propto a(T)_{T_{ref}}\left(\frac{N_f}{\varepsilon_c^p}\right)_{T_{ref}}, \tag{3.8}$$

where ε_c^p is the critical value of plastic strain and $N_{f,T}$ is the failure number of cycles at temperature, T. Therefore,

$$\left(N_f\right)_T = a(T)_{T_{ref}} \cdot \left(N_f\right)_{T_{ref}}, \tag{3.9}$$

$$\text{or} \quad \log\!\left(N_f\right)_{T_{ref}} = \log\!\left(N_f\right)_T - \log\!\left(a(T)_{T_{ref}}\right). \tag{3.10}$$

Equation (3.10) reveals that at a given stress amplitude the fatigue lifetime in terms of the number of cycle before failure can be estimated by a different fatigue lifetime at a different temperature using time-temperature superposition. It also means that the short-term fatigue data at higher temperatures can be shifted along the logarithmic time scale until a smooth overlapping reaches to construct a master fatigue data that can be used to predict the relatively long-term fatigue lifetime. The fatigue failure mode does not change with temperature in the equation (3.10).

3.3 Time-Stress Superposition for Fatigue Life Prediction

To apply the time-temperature superposition for an accelerated fatigue test of polymer, the fatigue fracture mode at elevated temperature needs to be kept same as that at reference temperature because it is assumed that the magnitude of the accumulated plastic deformation (critical value) is a constant that does not change with temperature.

71

Thermoplastic glassy polymers become ductile when the temperature is high. Corresponding fatigue-induced fracture will have a ductile fracture mode at a high temperature even though the applied stress amplitude is relatively small. Many glassy polymers exhibit the brittle fracture mode at low temperatures and low stress amplitudes (Chen, et al., 1993; Min, et al., 2001). D-B transition changes critical size of localized plastic deformation before fatigue crack initiation.

When fracture modes become different at a given alternating stress amplitude, the corresponding fatigue lifetime may be considerably different: fatigue lifetime for the brittle fracture mode is much longer than that for the ductile fracture mode. The tendency of D-B fracture transition in fatigue may be closely related with the effective stress amplitude that is the stress difference between the applied stress amplitude and the fatigue endurance limit, because a material that undergoes a more brittle fracture in fatigue may have a higher and clearer fatigue endurance limit in its S-N curve. It can be said that below the fatigue endurance limit the localized plastic deformation process hardly occurs and it may take more than 10^8 or 10^9 cycles to reach the critical size of the localized plastic deformation. No fatigue failure is considered to occur below the fatigue endurance limit.

Under a cyclic loading condition at a given temperature, the magnitude of localized plastic deformation will be a function of the effective stress amplitude such as

$$\left(\frac{d\varepsilon^p}{dN}\right) = \Theta\big(eff(\sigma)_T\big), \tag{3.11}$$

72

$$\text{and} \quad eff(\sigma)_T = \sigma_{a,T} - \sigma_{fs,T}, \quad (3.12)$$

where Θ, $\sigma_{a,T}$ and $\sigma_{fs,T}$ are a function, the applied stress amplitude and the fatigue endurance limit at a given temperature, T, respectively. Fatigue strength is also assumed to have the same magnitude as the probable microvoid nucleation stress. At a given temperature, T, the relation can be expressed as

$$\left(\frac{d\varepsilon^p}{dN}\right)_{\sigma_a,T} \propto A'\eta_{\sigma_a}^{-1} = A\exp\left(-\frac{\Delta H_{\sigma_a}}{v_{fs}^*(\sigma_a - \sigma_{fs})}\right)_T, \quad (3.13)$$

where v_{fs}^* and σ_{fs} are the activation volume for deformation or the volume of the jumping segment for plastic deformation and the fatigue strength, respectively. The dimension of $(v_{fs}^* \cdot \sigma)$ is energy or work done by applied stress for plastic deformation, and no plastic deformation is assumed to occur when the applied stress amplitude reaches the fatigue endurance limit, σ_{fs}, of the material.

The total amount of the localized plastic deformation at each loading cycle will be a combination of contributions from temperature and applied stress amplitude. It is assumed that the contribution of those factors for plastic deformation can be linearly decomposed into two parts. It can be represented by the following relation at a given temperature, T, and a reference temperature, T_{ref} :

$$\left(\frac{d\varepsilon^p}{dN}\right)_{T,\sigma_a} \propto A'\eta_{T,\sigma_a}^{-1} = A\exp\left(-\frac{\Delta H_{\sigma_a}}{RT}\right)\exp\left(-\frac{\Delta H_{\sigma_a}}{v_{fs}^*(\sigma_a - \sigma_{fs})}\right)_T, \quad (3.14)$$

$$\left(\frac{d\varepsilon^p}{dN}\right)_{T_{ref},\sigma_a} \propto A'\eta_{T_{ref},\sigma_a}^{-1} = A\exp\left(-\frac{\Delta H_{\sigma_a}}{RT_{ref}}\right)\exp\left(-\frac{\Delta H_{\sigma_a}}{v_{fs}^*(\sigma_a - \sigma_{fs})}\right)_{T_{ref}}. \quad (3.15)$$

The corresponding time shift factor can be obtained as

$$\log\left(a(T,\sigma_a)_{T_{ref}}\right) = \log\left(\frac{\eta_{T,\sigma_a}}{\eta_{T_{ref},\sigma_a}}\right) = \log\left(a(T)_{T_{ref}}\right) + \log\left(a(\sigma_a)_{T_{ref}}\right) \qquad (3.16)$$

$$= \frac{\Delta H_{\sigma_a}}{R}\left(\frac{1}{T} - \frac{1}{T_{ref}}\right) + \frac{\Delta H_{\sigma_a}}{v_{fs}^*}\left(\left(\frac{1}{\sigma_a - \sigma_{fs}}\right)_T - \left(\frac{1}{\sigma_a - \sigma_{fs}}\right)_{T_{ref}}\right).$$

Time-temperature shift factor, $\log\left(a(T)_{T_{ref}}\right)$ can be determined empirically by plotting the $\log(a(T)_{T_{ref}})$ against $\left(1/T - 1/T_{ref}\right)$ and it allows calculation of the activation energy ΔH_{σ_a} from the slope. Activation volume v_{fs}^* is a pre-determined value. ΔH_{σ_a} and v_{fs}^* are temperature and stress dependent value. However, in fatigue situation, testing temperature is well below glass transition temperature (T_g) and stress amplitude is well below the global yield strength. Thus, it is assumed that ΔH_{σ_a} and v_{fs}^* are constant values.

Using Equation (3.16), the fatigue life at the reference temperature can be predicted at different temperatures employing time-temperature and time-stress superpositions. The short-term fatigue data (S-N curves) at higher temperatures can be shifted along the logarithmic time scale to construct a master fatigue data that can predict the realistic long-term fatigue life (S-N curve) for practical applications. Therefore, the formulation of the equation using time-temperature-stress superposition for ALT of amorphous polymers under isothermal condition may be

$$\left(N_f\right)_{T,\sigma_a} = a(T,\sigma_a)_{T_{ref}} \cdot \left(N_f\right)_{T_{ref},\sigma_a}, \qquad (3.17)$$

or $\log\left(N_f\right)_{T_{ref},\sigma_a} = \log\left(N_f\right)_{T,\sigma_a} - \log\left(a(T,\sigma_a)_{T_{ref}}\right).$ \qquad (3.18)

3.4 Time-Frequency Superposition for Fatigue Life Prediction

In this section, the frequency effect on fatigue life in the S-N curve will be considered. Due to the viscoelastic nature of glassy polymers below their glass transition temperature, a lower frequency during a fatigue loading cycle causes a lower Young's modulus and a lower magnitude of yield stress, resulting in a higher strain energy release, a bigger irreversible localized plastic deformation zone and a shorter fatigue lifetime in terms of the number of cycles in the S-N curve.

The frequency effect on fatigue in an unnotched sample can be considered in two ways. First, it may cause a change in the stress-strain response and the corresponding magnitude of the yield stress during the fatigue cycle under isothermal conditions, where no hysteric-heating-induced thermal fatigue occurs. Second, it may cause a contribution of thermal fatigue due to viscoelastic hysteresis that causes an obviously athermal condition. In general, thermal fatigue may occur at a high loading frequency and/or high strain conditions.

The frequency-dependent fatigue crack growth (Mukherjee and Burns, 1971; Yokobori and Sato, 1973) can be represented in the general form of Equation (2.59,60). A similar approach to the frequency effect on the fatigue lifetime in the S-N curve for accelerated lifetime testing can be proposed. An increase in the localized plastic deformation zone during fatigue at given temperature and stress amplitude under

isothermal conditions may be a function of strain energy density and frequency f as follows:

$$\frac{d\varepsilon^p}{dN} = \Theta\left(\int_0^{1/f} \sigma d\varepsilon, f\right).$$

(3.19)

The corresponding localized plastic flow can be proposed as follows:

$$\left(\frac{d\varepsilon^p}{dN}\right)_f \propto A'\eta_f^{-1} = A\exp\left(-\frac{\Delta H_{\sigma_a}}{\int_0^{1/f} \sigma d\varepsilon \Big/ \log(f)}\right).$$

(3.20)

At a certain reference frequency f_{ref}, it will be rewritten as:

$$\left(\frac{d\varepsilon^p}{dN}\right)_{f_{ref}} \propto A'\eta_{f_{ref}}^{-1} = A\exp\left(-\frac{\Delta H_{\sigma_a}}{\int_0^{1/f} \sigma d\varepsilon \Big/ \log(f_{ref})}\right).$$

(3.21)

It has been observed that Young's modulus of some glassy polymers changes little during fatigue loading (Wang et al., 2000). This implies that the strain energy density also changes little when the stress amplitude is constant. If the strain energy density is assumed to be constant, corresponding time-frequency shift factor will be as follows:

$$\log\left(a(f)_{f_{ref}}\right) = \log\left(\frac{\eta_f}{\eta_{f_{ref}}}\right) = m_f \log(f) - m_{f_{ref}} \log(f_{ref})$$

(3.22)

$$\text{where } m_f = \frac{\Delta H}{\int_0^{1/f} \sigma d\varepsilon} \text{ and } m_{f_{ref}} = \frac{\Delta H}{\int_0^{1/f_{ref}} \sigma d\varepsilon}.$$

(3.23)

m_f and $m_{f_{ref}}$ are frequency dependent material parameters at a given temperature. If m_f and $m_{f_{ref}}$ are considered to be a little difference, for the simplest form, within a moderate range of frequency and temperature, then the above time-frequency shift factor can be rearranged and simplified as:

$$\log\left(a(f)_{f_{ref}}\right) = m\log\left(\frac{f}{f_{ref}}\right), \tag{3.24}$$

where m is a constant. Again, the above time-frequency shifting behavior is possible only under isothermal conditions.

Two considerations, however, may be needed to quantify the hysteretic heat effect on fatigue lifetime. 1) The surface temperature is assumed to be the same as that inside the body when the specimen is thin enough. Furthermore, temperature measurement from the surface is considered to give a similar temperature state on the localized plastic deformation zone for the fatigue crack initiation site because, fatigue crack initiation, in general, is considered to occur from the surface. 2) Pseudo isothermal condition (thermal equilibrium state) can be considered if the surface temperature becomes stabilized at a certain elevated temperature above the ambient temperature. Then time-temperature superposition can be employed to capture the hysteretic-heating effect quantitatively on the fatigue lifetime in the S-N curve.

Therefore, an accelerated fatigue life testing methodology can be envisioned by employing time-temperature, time-stress, and/or time-frequency superposition as follows:

$$\left(N_f\right)_{T,f} = a(T, \sigma_a, f)_{T_{ref}, f_{ref}} \cdot \left(N_f\right)_{T_{ref}, f_{ref}}, \tag{3.25}$$

$$\text{or} \quad \log\left(N_f\right)_{T_{ref}, f_{ref}} = \log\left(N_f\right)_{T,f} - \log\left(a(T, \sigma_a, f)_{T_{ref}, f_{ref}}\right), \tag{3.26}$$

$$\text{where} \quad \log\left(a(T, \sigma_a, f)_{T_{ref}, f_{ref}}\right) = \log\left(a(T, \sigma_a)_{T_{ref}}\right) + \log\left(a(f)_{f_{ref}}\right), \tag{3.27}$$

77

$$\log\bigl(a(T,\sigma_a)_{T_{ref}}\bigr)=\frac{\Delta H_{\sigma_a}}{R}\left(\frac{1}{T}-\frac{1}{T_{ref}}\right)+\frac{\Delta H_{\sigma_a}}{v_{fs}^{*}}\left(\left(\frac{1}{\sigma_a-\sigma_{fs}}\right)_{T}-\left(\frac{1}{\sigma_a-\sigma_{fs}}\right)_{T_{ref}}\right),$$

$$\text{and}\qquad \log\bigl(a(f)_{f_{ref}}\bigr)=m\log\left(\frac{f}{f_{ref}}\right).$$

3.5 Closure

Accelerated fatigue characteristics of glassy polymers have been investigated based upon the consideration of the localized plastic deformation process. The localized plastic deformation process represents the evolution of fatigue crack initiation and controls the fatigue lifetime in the S-N curve. The fatigue lifetime is represented in terms of the number of cycles when a linearly developing localized plastic deformation zone becomes a critical value in size before macrocrack initiates. Highly nonlinear viscoelastic behavior of creep, yield, post-yield and craze formation has been captured using modified energy activation model that exhibits temperature, stress and rate (frequency) dependence under fatigue loading conditions. A reduced time model in polymer fatigue has been developed through the use of time-temperature, time-stress and/or time-frequency superposition. Using this model and corresponding shift factors, short-term accelerated fatigue test data at elevated temperatures and/or higher loading frequencies can be shifted to generate a

master S-N curve that allows the prediction of relatively long-term fatigue behavior under service conditions with relatively low temperatures and frequencies.

For practical application of the developed ALT method, three different types of test technique can be available: 1) isothermal/ low and constant loading frequency conditions 2) isothermal/ low and different frequency conditions 3) athermal/ high loading frequency conditions. Three different reduced models such as time-temperature, time-stress and/or time-frequency superposition can be used according to the test conditions. In next chapter, the validity of the proposed ALT method will be demonstrated through the experiments.

CHAPTER FOUR

EXPERIMENTAL RESULTS AND DISCUSSION

4.1 Experimental Setup

4.1.1 Material Preparation

Among the commonly used structural polymers, two kinds of carbon particle filled polycarbonate specimens were used in the accelerated life testing because the plain and molded carbonate generally has high strength with 58.6 ~ 70 MPa of yield strength and 1.6 ~ 2.4 GPa of Young's modulus. The material has relatively high thermal and chemical resistance. One material for the test is Lexan ML 6339R filled by carbon black made by GE Plastics, The other one is Lexan C1200 filled by carbon black, also made by GE Plastics. The carbon particle Lexan ML 6339R specimens were used for the tests under isothermal conditions typically attained at a 0.5Hz frequency. The carbon filled Lexan C1200 specimens were used for the tests under athermal conditions associated with 10Hz frequency. While it may be ideal to use one material in all these tests, the specimens were consumed faster than expected due to additional consumption in specimens for producing good alignment, for testing at different strain rates at quasi-static loading and so on. However, the use of the two materials should not be considered as a major drawback, as the theory for accelerated life testing is now examined

individually by one of the two materials under one given condition. The theory for accelerated life testing is going to be validated individually by two separate experiments. The two carbon filled polycarbonate materials have the same glass transition temperature, T_g, of 143-150$^{\circ}C$. As this work has been intended to investigate the ALT using the S-N curve approach, only dog bone shaped, unnotched test specimens complying with ASTM standard 638D were used. All specimens were made by injection-molding. Figure 4.1 shows the geometry of the test specimen. Each specimen has a width of 6.4 mm, a thickness of 1.5 mm and a gauge length of 25.4 mm.

To remove the unknown effects of previous thermal and loading histories on these specimens, all specimens were treated using the same thermal history. They were first heated to 100$^{\circ}C$ and then kept for three hours to minimize possible free volume expansion due to sudden moisture evaporation inside specimen body; they were then annealed at 140$^{\circ}C$ for six hours. Annealed specimens were then cooled down gradually in the temperature chamber by simply switching the power of the chamber. The average cooling rate was 0.5$^{\circ}C/\min$. After annealing, all specimens were stored in a bell jar with a constant humidity of 53$\pm$1% for 12$\pm$2 days (Lexan ML 6339R) and 70$\pm$7 days (Lexan C1200) before being tested. Specimens were protected from the exposure by ultra violet (UV) light in the desiccators. In each of the two groups of fatigue testing (low and high frequencies), all specimens had the same thermal and loading history. It should be noted that physical aging times are identical for specimens in each group, so that the effects of physical aging will not affect the S-N curve. This research was not intended to

81

6.4 mm

12.7 mm

25.4 mm
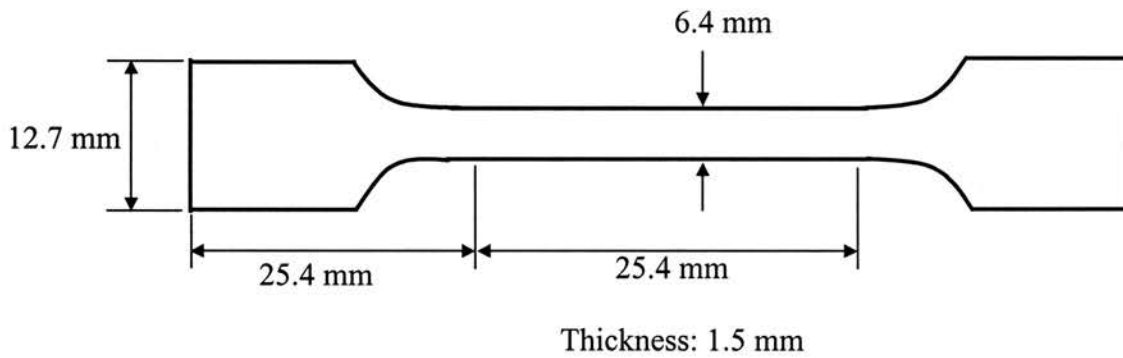
25.4 mm

Thickness: 1.5 mm
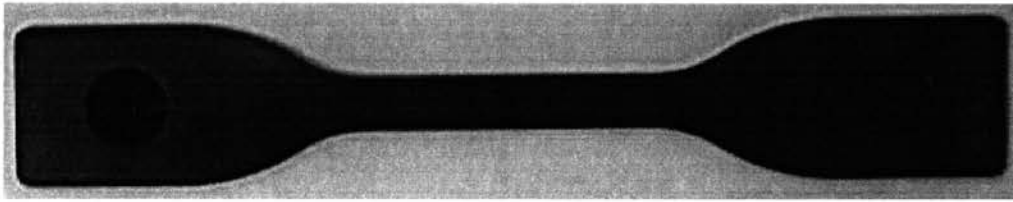
Figure 4.1: Geometry of Specimen: before and after annealing.
(There is no change in dimensions)

investigate the effects of physical aging; additional experiments are needed if the effects

of physical aging are a major concern.

4.1.2 Experimental Setup

Figure 4.2 shows the experimental setup used in fatigue testing. An MTS servo

hydraulic load frame is used to apply loads on specimens. The load frame is controlled by
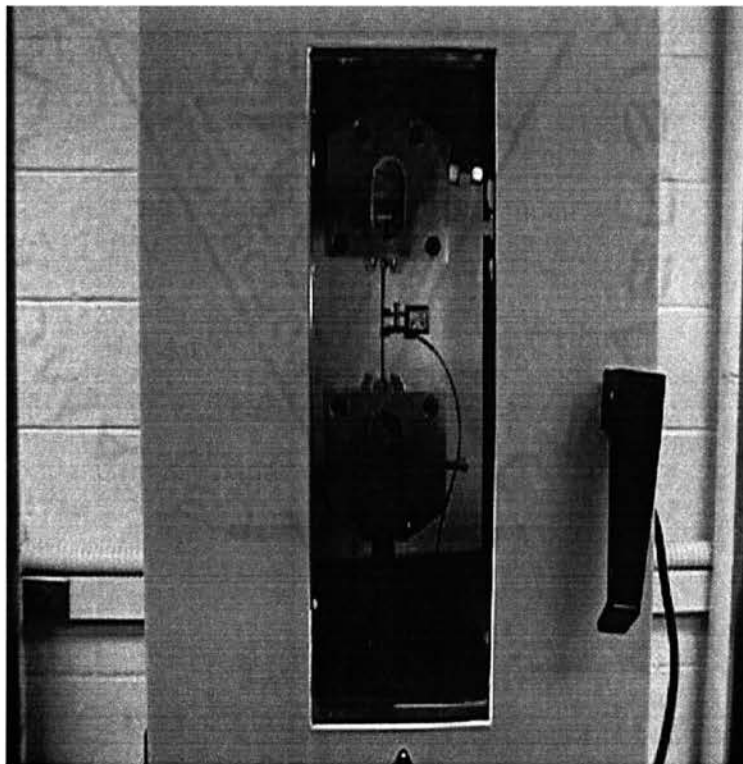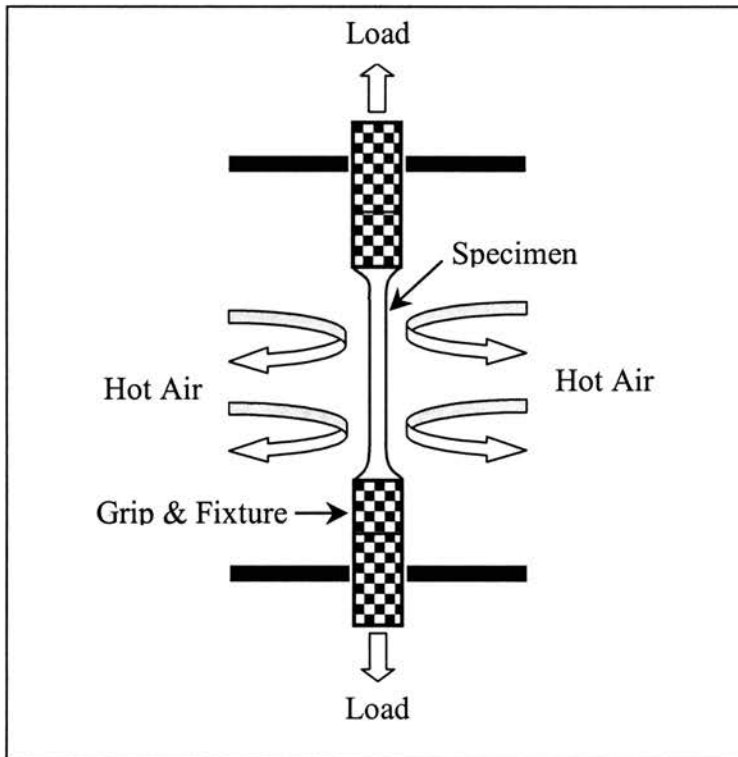
Figure 4.2: Experimental setup.

an Instron digital controller (Fastrack 8800). An Instron temperature chamber fitted into the MTS frame is used to control a constant temperature surrounding a test specimen. A data acquisition system using LabView software was used for data acquisition at different temperatures. The temperature in the temperature chamber was found to be within $\pm 1\,^{o}C$ of the set temperature.

Fatigue tests were conducted with different loading frequencies ranging from 0.1Hz to 10Hz (0.1, 0.3, 0.5, 1.0, 10 Hz). The stress ratio, i.e., the ratio of minimum stress to the maximum stress in fatigue loading cycle, had a range between 0.05~0.2, giving a tension-tension fatigue loading condition. A zero or negative stress ratio causing buckling is not possible even though a stress close to the minimum stress is reached after a certain number of cyclic loading. It is expected that the minimum stress in each loading cycle does not have much effect on the fatigue strength represented by the maximum stress in cyclic loading because the minimum stress is always set to be very small, much smaller than the fatigue endurance limit of the materials in all accelerated fatigue testing. Prior to fatigue loading, each specimen was preheated for two hours at elevated temperatures to allow the loading fixture and specimen to reach a thermal equilibrium state.

4.1.3 Calibration

Fatigue experiments are very sensitive to the alignment of the specimen with respect to the loading axis of the load frame. Longitudinal marked centerline of the specimen was

84

aligned with a plumb line that passes the center of the top and bottom grips. In addition to this method to adjust the alignment, an alignment check was made in each time when the fixture is set up on the load frame. The alignment evaluation was made through the full-field deformation measurements in the region of uniform deformation in a specimen using Digital Image Correlation (DIC), a non-contact surface deformation. DIC was first proposed by a group of researchers at University of South Carolina (Peters and Ranson, 1982; Sutton, Wolters, Peters, Ranson and McNeil, 1983). Lu and Cary (2000) refined the technique to allow for the measurements when second order nonlinear deformation is involved in the deformation process. In this work, a code, namely WinDIC2.0, developed by Lu and Cary (2000) is used. A detailed discussion of the DIC method can be found in Handbook on Experimental Mechanics (Kobayashi, 1993). DIC compares a deformed image with a reference image to find the deformation by tracking the motion of a distinct grayscale pattern. white silicone paste was randomly painted on the specimen to generate a gray scale pattern on the polycarbonate specimen. The speckle pattern would follow the movements of the material points on the surface of a specimen.

After careful alignment has been made, images of a specimen surface were acquired by a digital image acquisition system that consists of a Kodak ES1.0 digital camera, a frame grabber installed on a PC and controlling software. Figure 4.3 shows the surface images of the specimen with speckle patterns. The deformation was computed from the reference image and deformed image using WinDIC2.0. The displacement field was
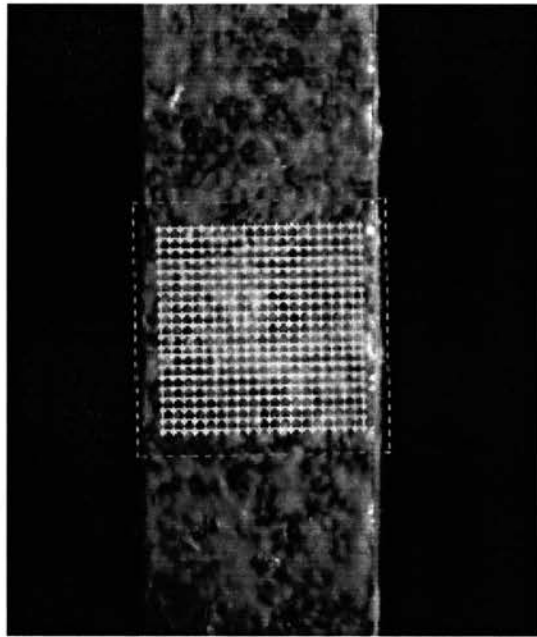
(A)
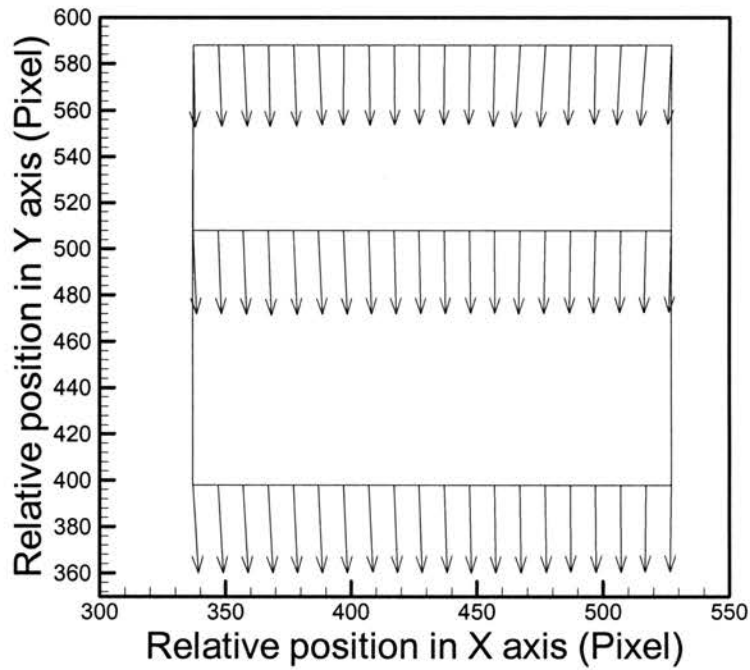
(B)

Figure 4.3: Alignment check for experiment (A) Speckle pattern of the specimen surface (specimen size in the image: 20mm × 6.4mm) (B) Deformation fields calculation after deformation in arbitrary scale (top, center and bottom line speckles of observation box).

shown in Figure 4.3(B). Strain computation indicated that the average axial strain is 0.0094 and the standard deviation is 0.000558. The standard deviation is only 5.93% of the average strain, indicating that all axial strain values are very close, so that very good alignment has been achieved. After fatigue tests, the fracture surfaces of some specimens were observed using a JEOL Scanning Electron Microscope (SEM) at an magnification of 18 times to get information of fracture process.

To achieve higher frequencies above 1Hz for a more effective acceleration in fatigue, displacement controlled fatigue tests were simply employed without consideration of PID (the Proportional, the Integral and the Derivative) control. All displacement controlled fatigue test data were converted into load-controlled S-N data using the average amplitude of the recorded load data prior to fatigue failure in displacement-controlled fatigue loading condition. Others had used this approach. For example, Beardmore and Rabinowitz (1974) observed the cyclic softening behavior on several ductile thermoplastics including Polycarbonate (PC) and found that a cyclic steady state region, in which the softened strain relation is maintained constant, was the greatest part in the regimes of the fatigue life. Therefore, the stabilized stress amplitude has been recommended as the converted value to convert displacement controlled test data into stress controlled test data (Rabinowitz et al., 1973; Crawford and Benham, 1974).
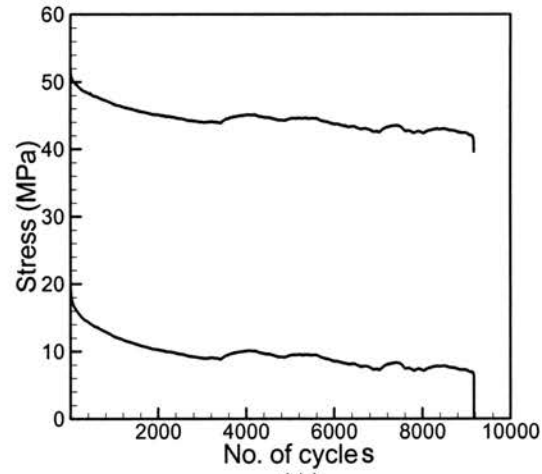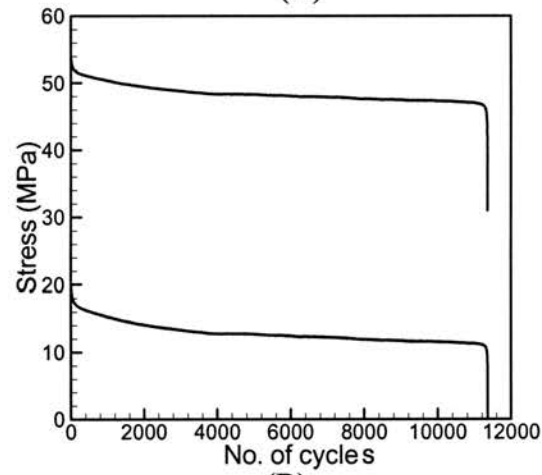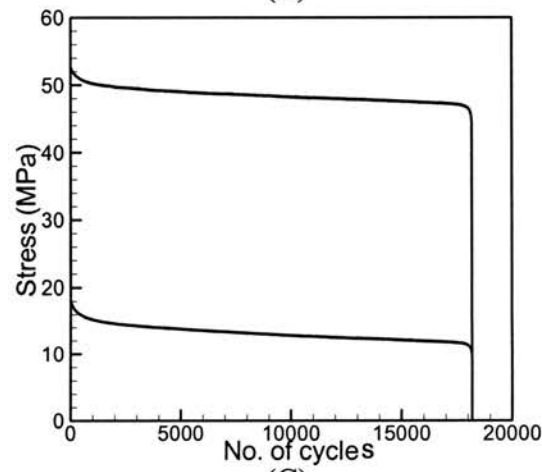
Figure 4.4: Stress response ($\Delta\sigma$) of displacement controlled fatigue tests at different loading frequencies; (A) f = 0.1 Hz, (B) f = 1.0 Hz, (C) f = 10 Hz.
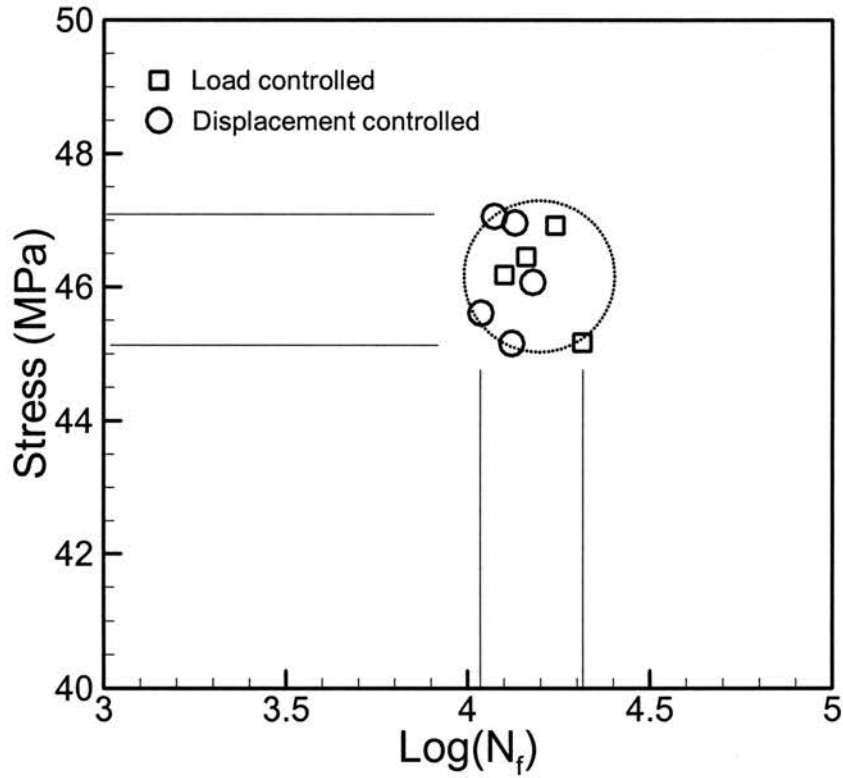
Figure 4.5: Validity check for mean stress amplitude to convert displacement-controlled data into stress-controlled data with 1.0 Hz loading frequency.

However, it is found that sometimes a stabilized stress region does not exist. Figure 4.4 shows some stress responses from the displacement controlled fatigue tests at different frequencies. At a low frequency (such as 0.1Hz), stress amplitude is not stable throughout the fatigue life. At a high frequency (above 1Hz), regions for incubation and

transition before the stabilized stress region are relatively small and the overall stress response is quite smooth and stabilized throughout the fatigue life.

It should be noted that the objective of this study is to find the fatigue service life at a low frequency from accelerated testing, sometimes at a much higher frequency than service frequency. Consequently, a method has to be developed to convert the S-N curve at a high frequency to the S-N curve at service frequency. To this end, a frequency dependent load-displacement conversion factor is needed for conversion of S-N curves at different frequencies. To do this, an average stress amplitude rather than stabilized stress amplitude was used to find the stress amplitude from displacement controlled fatigue tests. Figure 4.5 shows the validity of the averaged stress amplitude by comparing the converted stress amplitude with actual stress controlled fatigue data at a loading frequency of 1Hz. It demonstrates that the average stress amplitude value can be a possible choice for use in computing the stress amplitude. As the loading frequency increases, the average stress amplitude may become more reliable because there is less change in the stress-strain response at higher loading frequencies. In the experimental investigation, all fatigue test data above 1Hz were obtained from displacement controlled tests.

During each test temperature on the specimen surface was continuously monitored by a T-type copper-constantan thermocouple (Omega, TT-T-36-SLE) attached to the surface of each specimen. The thermocouple output was recorded by a digital data acquisition system. A high temperature, high thermal conductivity paste

(OMEGATHERM 201) was used as heat conduction agent between the thermocouple and the specimen surface. This gray, smooth paste does not become hard and is expected to maintain a continuous insulation resistance. Based on the manufacturer's specification, the paste is not expected to have an effect on temperature variation on either the (slow) moving surface or the thermocouple even when the paste is exposed to temperatures from $-38\,^{0}C\sim200\,^{0}C$ for along time.

The thermocouple was calibrated carefully for temperature measurement. Distilled water with ice cubes in a container under the ambient condition of 760 *mbar* of air pressure was stirred for more than five minutes to reach the thermally equilibrated zero $0\,^{0}C$ iced water. Distilled water was also boiled more than two minutes to achieve a thermally equilibrated $100\,^{0}C$. Two different output voltages from the thermocouple under icy water and boiled water conditions were used for reference temperature calibration. Transient temperature was recorded with $\pm0.1\,^{0}C$ of accuracy, which is the default value of the thermocouple. The surface temperature provided the actual temperature on the specimen surface, and was used in the analysis to determine the accelerated fatigue life.

4.2 Results and Discussion

4.2.1 Accelerated Fatigue Life Testing under Isothermal Conditions

In this section, results on short-term fatigue testing under isothermal conditions are presented and processed to determine the long-term fatigue behavior. Based on the time-temperature superposition, the long-term viscoelastic behavior corresponds to the behavior at an elevated temperature. Consequently, fatigue testing at higher temperature would facilitate the acceleration in viscoelastic behavior of polymers. Shifting and processing the short-term fatigue data would result in a master curve for fatigue life applicable for long-term fatigue life prediction.

To apply the developed accelerated lifetime testing (ALT) technique, it is necessary to determine whether the material used in this test exhibits viscoelastic behavior at room temperature so it can be appropriate for this experiment. It can be determined by rate-dependent stress-strain response of the material. The tensile test will also give the appropriate ranges of stress amplitude for the fatigue tests, that is less than the yield stress. Tensile tests to determine the stress-strain responses at different displacement rates (crosshead rates) were conducted first. Average strain rate was then computed using the test results. Figure 4.6 shows the tensile stress-strain responses at room temperature ($27^{0}C$) under different strain rates. Under all these rates, the initial Young's modulus is essentially unchanged. At low strain rate, the magnitude of yield stress is relatively low. As the strain rate increases, the magnitude of yield stress increase.

When the stress amplitude is below ~20MPa, stress-strain response does not change significantly with the strain rate. When the stress amplitude is above ~20MPa, the rate
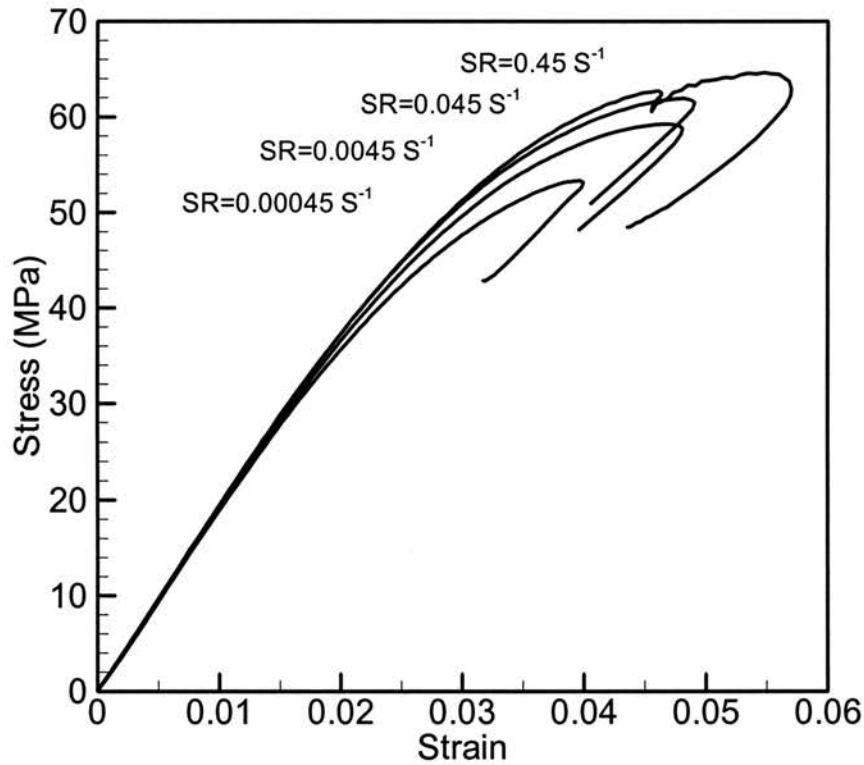
Figure 4.6: Tensile stress-strain responses at room temperature

(27^0C) with different strain rates.

dependence begins to appear. When the strain rate is below 0.045 S^{-1}, there is clear rate

dependence in yield stress. When the strain rate is above 0.045 S^{-1}, the rate dependent

tendency decreases but the magnitude of yield stress and corresponding yield strain

continue to increase. Rate-dependent temperature rise was considered by measuring

surface temperature during the tensile test because thin specimen makes temperature . Temperature rise at all these rates was less than $0.2\,^0C$. When the thickness of the specimen (1.5mm) is considered to be thin enough and no temperature difference on the surface and inside of the specimen is assumed, it can be said that there is little thermal effect on the monotonic stress-strain response under different strain rates.

Based on the stress-strain response, as shown in Figure 4.6, appropriate stress magnitudes lower than yield stress can be selected for fatigue tests. Using appropriate stress amplitude, fatigue tests were conducted first at a frequency 0.1Hz under which no temperature change was observed so that the isothermal condition is justified throughout the fatigue. It is noted that an extensometer was used in this fatigue test to measure exact strain. The sharp knife-edges of the extensometer caused critical initial defects on the specimen surface before actual fatigue test. Thus, the corresponding total fatigue life may be shorter than that of unnotched specimen.

Figure 4.7 shows the dynamic stress-strain response during fatigue tests at a frequency 0.1Hz under stress control. In Figure 4.7(A) shows the stress-strain relation in selected cycles and Figure 4.7(B) shows a continuously measured strain with respect to the number of cycles until final fatigue failure. There is no considerable change in the stress-strain response during fatigue. When it is considered that tensile stress-strain response is the same as the response of first cycle in fatigue, the stress-strain response obtained at tensile tests may be very close to those obtained in the stress-controlled fatigue condition when the temperature and frequency are constant.

Figure 4.7(A) indicates loop in stress-strain relation in a cycle. The released strain energy may be dissipated or contribute to build fatigue damage to the material. However,
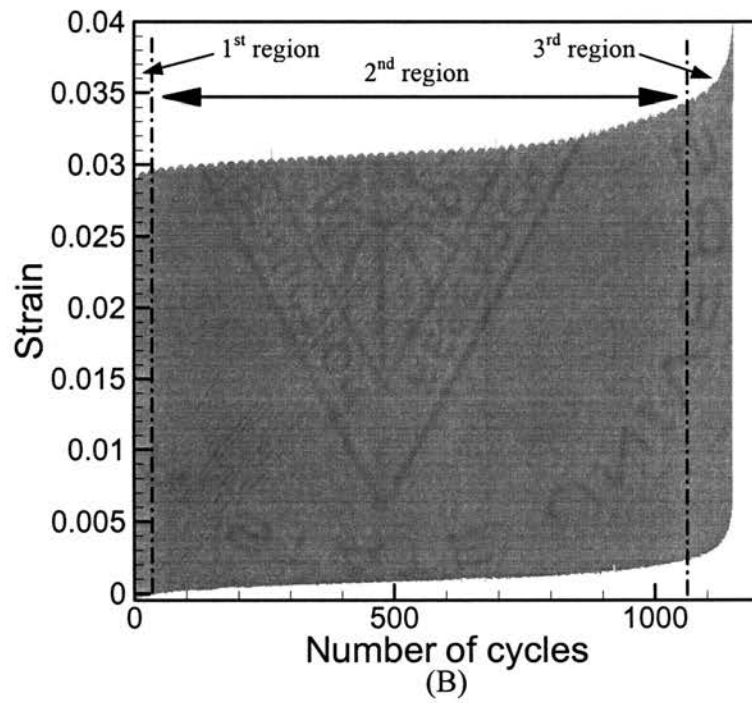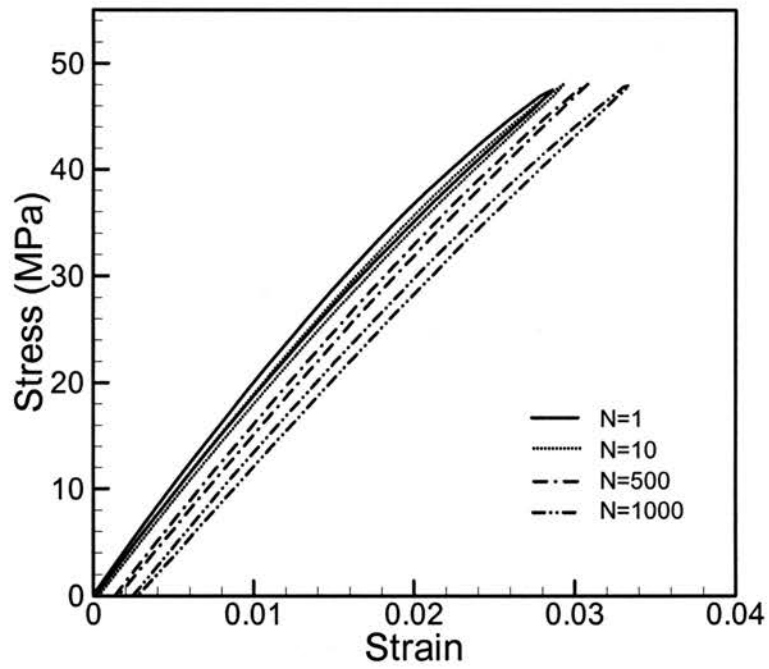
Figure 4.7: Dynamic responses at frequency of 0.1Hz under room temperature ($27\,^0C$)

(A) Stress-strain response at selected cycle,

(B) Strain history during fatigue.

the hysteresis is small and has not caused measurable temperature variation on the specimen. It can be observed from both Figures 4.7(A) and 4.7(B) that there is a continuous accumulation of irreversible deformation. Irreversible deformation is usually understood as plastic deformation or yield-like deformation in the viscoelastic material. Irreversible deformation can be induced by any possible fatigue damage and will eventually lead to fatigue failure

The strain history in Figure 4.7(B) can be divided into three different regions. The initial region (1st region) is associated with sharp increase in irreversible strain or plastic deformation. This sharp increase of residual (plastic) strain in the initial region can be associated with cycle softening behavior in viscoelastic material under strain-controlled conditions that is observed by Beardmore and Rabinowitz (1974). After the first stage, the plastic strain accumulation rate seems to be stable during most of the fatigue lifetime. This stable region is called the 2nd region. The last (unstable) region (3rd region) involves a rapid increase of plastic deformation. This unstable region was the result of the propagation of a fatigue crack after its initiation. The second stage gives most of the fatigue lifetime. The stable yield-like (plastic) strain accumulation in the 2nd stage can be approximated as the linear accumulation of plastic deformation with respect to number of cycles. As a result, cumulative plastic deformation can be used to characterize fatigue behavior for fatigue lifetime prediction.

In what follows, the long-term fatigue data are first presented. Short-term accelerated data are then presented and processed to determine a master curve for prediction of long-term fatigue behavior. The master curve is then compared with long-term data to examine the accelerated fatigue life testing methodology. We proceed first
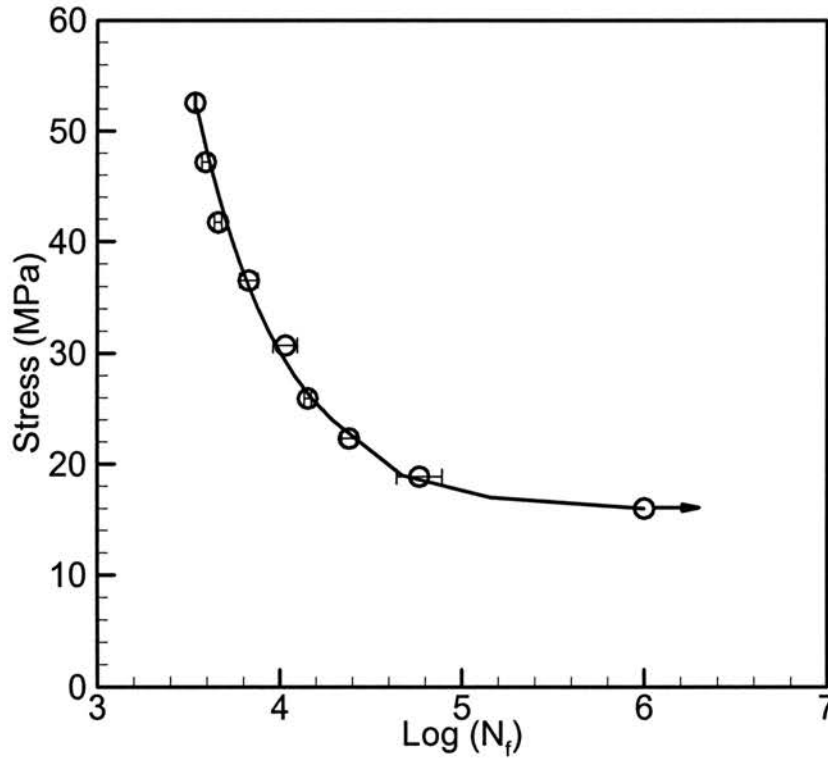
Figure 4.8: Long-term S-N data with frequency 0.5Hz at room temperature ($27^\circ C$).

with the presentation of long-term data. Relatively long-term fatigue tests at room temperature ($27^\circ C$) were conducted at a frequency 0.5Hz and the results were plotted as the stress-lifetime (S-N) curve as shown in Figure 4.8. At the stress amplitude reached 16MPa, fatigue life exceeded 10^6 cycles and the stress amplitude is considered to be close to fatigue endurance limit. Further fatigue tests beyond 10^6 cycles were stopped. The

fatigue endurance limit or fatigue strength was considered to exist around but less than 16MPa for this experiment. Three tests at the same stress amplitude were performed to determine the mean fatigue life and the corresponding error range. There is a sharp decrease of the curve at the low cycle (high stress amplitude) range when compared with elastic material such as metals. This reveals that the material exhibits ductile rather than brittle characteristics.

Short-term fatigue tests at temperatures $27°C$, $60°C$, $80°C$ and $100°C$ were conducted. S-N curves at these temperatures are depicted in Figure 4.9. The figure shows that at a given stress amplitude the fatigue life decreases with temperature. And it was observed that the short-term S-N curve at the low temperature ($27°C$) is relatively steep and flattens as the temperature increases. Furthermore, between two neighboring curves, it can be found that there is a portion for smooth overlapping each other. This allows the horizontal shifting of these curves to form a smooth master curve as shown in Figure 4.10. The corresponding shift factors are shown in Figure 4.11 and tabulated in Table 1.

$$\log(N_f)_{T_{ref}} = \log(N_f)_T - \log(a(T)_{T_{ref}}), \tag{4.1}$$

The shift factor in logarithmic scale, $\log(a(T)_{T_{ref}})$, is an empirically determined numerical value by which a short-term S-N curve must shifted to make it smoothly overlap the reference S-N curve. In Figure 4.9, the maximum fatigue life in each short-term S-N curve is around 10^4 cycles but, in the master S-N curve, in Figure 4.10, the maximum fatigue life has been extended up to $10^{5.9}$ cycles.

98
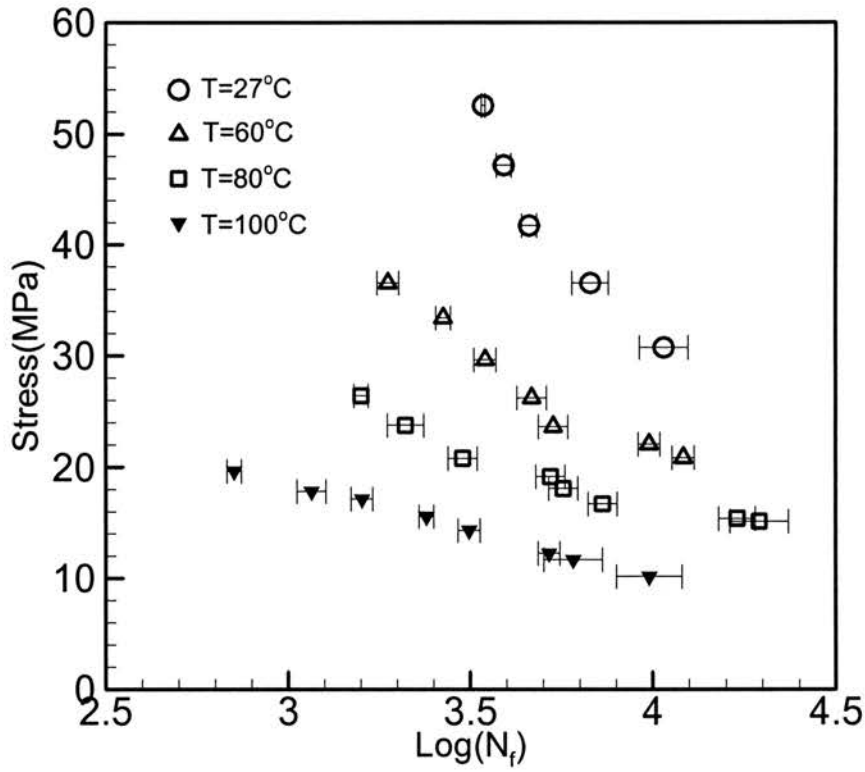
Figure 4.9: Short-term S-N data at different temperatures.
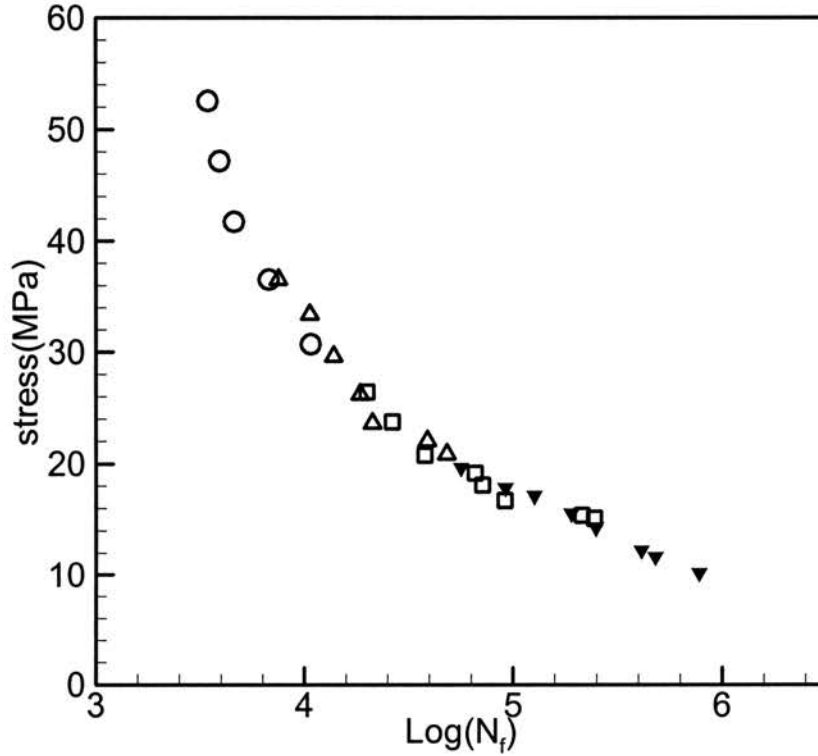
Figure 4.10: Generation of a master S-N curve at 0.5Hz using

the time-temperature superposition principle.

99
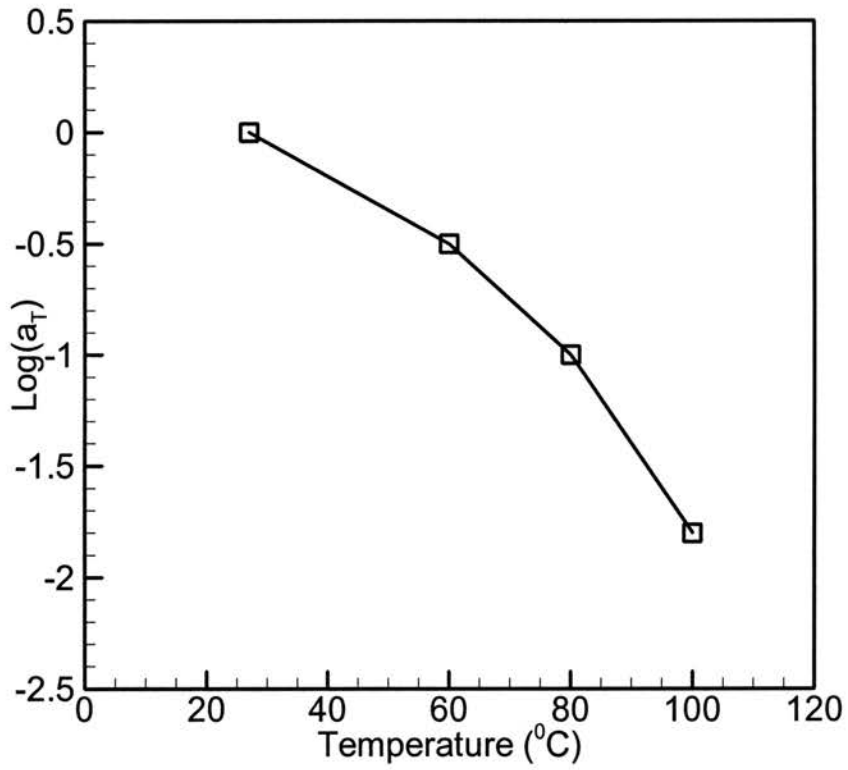
Figure 4.11: Shift factors for the master S-N curve using the

time-temperature superposition principle.

Table 1: Time-temperature shift factor.

Temperature (^{o}C)	27	60	80	100
$\log(a(T)_{T=27^{0}C})$	0.0	-0.5	-1.0	-1.8
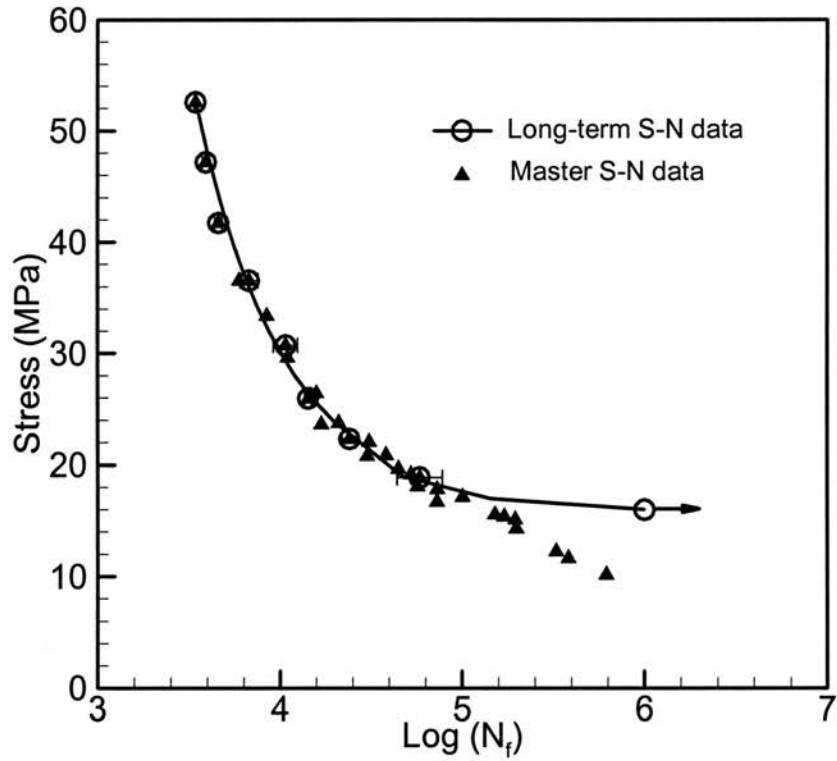
Figure 4.12: Comparison of actual long-term S-N data and master S-N data

generated by time-temperature superposition.

Figure 4.12 shows the comparison of the actual long-term S-N data and the master

S-N data generated by time-temperature superposition alone. When the stress level is

high, there is a good agreement between master S-N data and the actual long-term data.

But when the stress level decreases, there are some differences between prediction and

actual data. In this experiment, the fatigue life up to 10^5 cycles can be well predicted from the consideration of time-temperature superposition but the fatigue life prediction above 10^5 cycles cannot match the actual long-term data using time-temperature superposition only. It indicates that the use of time-temperature superposition alone may not be sufficient for accelerated fatigue lifetime prediction. A natural question is why such a shortcoming in the prediction exists. To answer this question, fracture surfaces of fatigue-failed specimen were examined.

Fracture surfaces of some specimens failed in fatigue were examined using an SEM. A magnification of 18 times was used. At room temperature ($27^\circ C$), the ductile fatigue fracture mode appears dominant at high stress amplitude (Figure 4.13). But as stress amplitude decreases the fracture mode tends to become more brittle. When the stress amplitude is 53MPa, after a certain number of cycles just prior to failure, a rapid and global plastic deformation over the entire gauge length occurred suddenly and an obvious necking process was observed during the test so that the size of the cross sectional area reduced significantly, causing catastrophic fracture (Figure 4.13(A)). Its fracture surface looks fairly smooth without localized flap-like irregularity because entire surface area already had severe plastic deformation (necking) before failure. As the stress amplitude decreases, typical ductile fatigue failure is observed, but the depth of the plastic deformation field decreases continuously from high stress to low stress (Figures 4.13(B)~(F)).

At high stress amplitude, as in the case of stress amplitude above 36MPa, polymers are relatively easy to deform and produce crease-like, and/or flap-like fractures. There are multiple localized plastic deformation zones that have developed individually. These
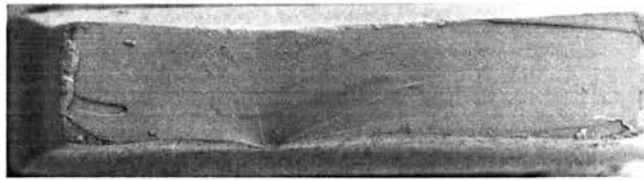
(A) $\sigma_a = 53$Mpa, $\log(N_f) = 3.45$
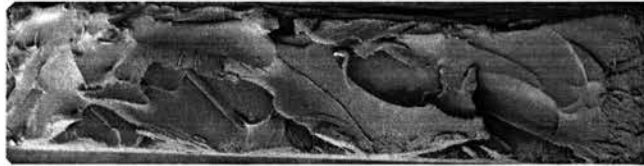
(B) $\sigma_a = 47$Mpa, $\log(N_f) = 3.6$
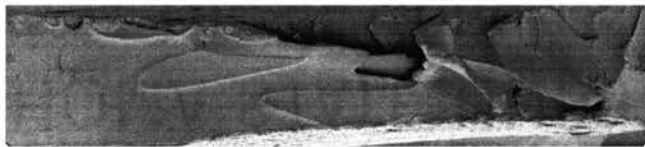
(C) $\sigma_a = 42.5$Mpa, $\log(N_f) = 3.65$

(D) $\sigma_a = 36.5$Mpa, $\log(N_f) = 3.85$

(E) $\sigma_a = 31$Mpa, $\log(N_f) = 4.0$

(F) $\sigma_a = 26$Mpa, $\log(N_f) = 4.5$
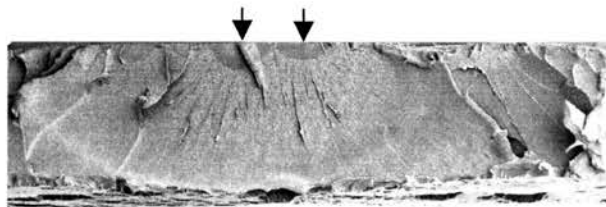
(G) $\sigma_a = 19$Mpa, $\log(N_f) = 4.8$

Figure 4.13: Fracture surfaces at room temperature ($27\,^\circ C$).

(Arrows indicate locations of craze zones)

103

plastic zones meet each other and create three-dimensional fatigue fracture surfaces as number of cycles increases. As the stress amplitude decreased, the size of the plastically deformed zone also decreased and its depth became smaller. In Figures 4.13(C) and (F), a smooth fracture surface can be observed and the brittle fracture mode appears on the fractograph. As the stress amplitude reached 19MPa, the craze zone can be seen clearly.

It is noted that the craze formation is generally understood as the precursor of brittle fractures even though craze itself exhibits ductile behavior (Kinloch and Young, 1983). The fracture surface (e.g. Figure 4.13 (G)) shows clear a crack initiation point and many parallel fracture paths that combine in the direction of crack propagation. Concentric beach marks appear around fatigue crack initiation points. These phenomena are typical features of macroscopic brittle fractures of polymers (Engel, et al., 1981). As shown in the Figure 4.13 (G), brittle fracture failure involves more highly localized but smaller plastic deformation during fatigue, especially in depth (refer Figures 4.13(B) and 4.13 (G)). It typically shows one or two fatigue damage initiation sites, different from the ductile fracture failure in which multiple damage sites are developed. From the observation of fracture surfaces from fatigue-failed specimens tested at room temperature ($27^{\circ}C$), it can be seen that ductile fatigue fracture is dominant at high stress amplitudes (Figure 4.13 (A),(B) and (C)) and brittle fracture failure is dominant at low stress amplitudes(Figure 4.13 (E),(F) and (G)).

Figure 4.14 shows the fracture surfaces for the specimens tested at $60^{\circ}C$. These fractograph also reveal that a higher stress amplitude leads to more ductile fracture (Figures 4.14 (A) and (B)) and a lower stress amplitude induces more brittle fracture

(A) σ_a = 36.5 Mpa, log(N_f) = 3.25

(B) σ_a = 30Mpa, log(N_f) = 3.5

(C) σ_a =23.5Mpa, log(N_f) = 3.7
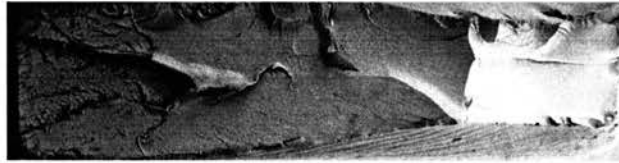
(D) σ_a = 21Mpa, log(N_f) = 4.1

Figure 4.14: Fracture surfaces at $60\,^{o}C$.

(Figures 4.14 (C) and (D)). When the stress amplitude is 21MPa, the brittle fracture failures appear to be very similar to those below 31 MPa at $27\,^{o}C$ (Figures 4.13 (E) and (F)). When the fracture surfaces are compared with those at $27\,^{o}C$, it is noted that specimens tested under relatively low stress at a high temperature. This observation

105

provides a phenomenological support to fatigue process acceleration due to the effect of temperature. At a given stress amplitude, the fatigue damage process can be accelerated with the help of elevated temperatures. In other words, actual fatigue lifetime at a reference stress amplitude and temperature can be estimated by the fatigue life at the same stress amplitude and an elevated temperature, i.e., using the temperature-induced acceleration factors, i.e., shift factors.

Fatigue failed fractographs at $80^\circ C$ are shown in Figure 4.15. At a high stress amplitude higher than 21MPa (Figures 4.15 (A) and (B)), highly ductile fracture is observed. At stress amplitude lower than 18MPa (Figures 4.15 (C) and (D)), ductile fracture is still dominant and the typical brittle fracture mode does not appear although the direction of the fatigue damage growth can be recognized. Some crazes are observed but they do not indicate the existence of major fatigue damage initiation sites as observed in the brittle fracture failure mode (Figure 4.13(G)). Instead, all the crazes were trapped by some other plastic deformation zones and they did not develop further to produce subsequent plastic deformation from those crazed zones. The plastic deformation zones that have developed without any connection with craze sites seem to be the major damage sites leading to fatigue failure.

Figure 4.16 shows the fractographs for specimens tested at $100^\circ C$. A feature of these fracture surfaces is that they reveal highly ductile fractures at all stress amplitudes. Typical brittle fracture failure is hardly observed even at low stress amplitude, e.g. σ_a=18MPa, (Figure 4.16 (C)) even though some crazes were observed. Ductile-to-brittle (D-B) fracture made transition is observed when the testing temperatures were $27^\circ C$ and $60^\circ C$ (Figures 4.13 and 4.14). However, any clear D-B transition and/or brittle fracture

(A) $\sigma_a = 26.5 Mpa$, $\log(N_f) = 3.2$

(B) $\sigma_a = 21 Mpa$, $\log(N_f) = 3.5$

(C) $\sigma_a = 18 Mpa$, $\log(N_f) = 3.75$

(D) $\sigma_a = 15 Mpa$, $\log(N_f) = 4.3$
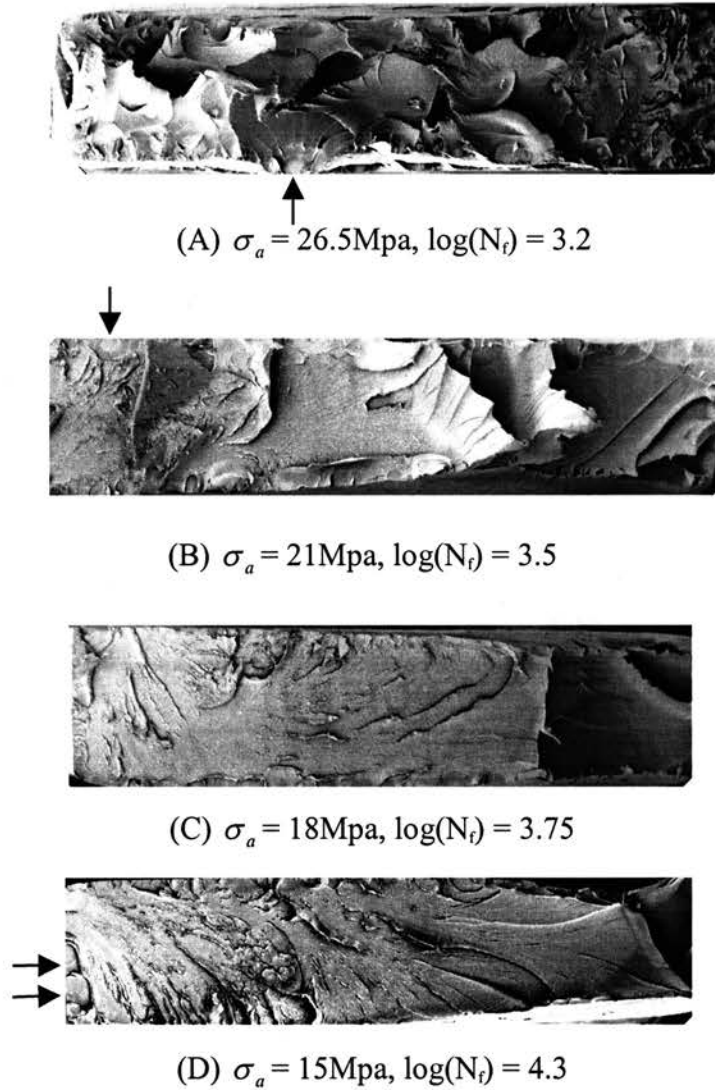
Figure 4.15: Fracture surfaces at $80^o C$.

(Arrows indicate locations of craze zones)

(A) σ_n = 19.5Mpa, $\log(N_f)$ = 2.85

(B) σ_a = 17.5Mpa, $\log(N_f)$ = 3.1

(C) σ_a = 14Mpa, $\log(N_f)$ = 3.5

Figure 4.16: Fracture surfaces at $100\,^{o}C$.

(Arrow indicates location of craze zone)

are hardly seen when the testing temperatures were $80\,^{o}C$ and $100\,^{o}C$ (Figures 4.15 and 4.16).

From the SEM observation, similar ductile fracture surfaces were obtained at both high-stress/low-temperature and low-stress/high-temperature. It is also observed that the plastic deformation process during the fatigue loading is superimposable by increasing

the temperature as well as by increasing the stress amplitude. When the temperature was $60^{\circ}C$, D-B fracture transition continued and could be examined using the time-temperature superposition principle. When the temperature was above $80^{\circ}C$, D-B fracture transition could not be maintained and ductile fracture was dominant at all stress amplitudes. The observation of fracture surfaces implies that accelerated fatigue life tests must include the consideration of D-B fracture transition. In the Chapter 3, D-B fracture transition behavior in polymer fatigue has been characterized and considered by the time-stress superposition and can be used to include the effect of D-B transition of fatigue acceleration. Using Equation (3.15), time-stress superposition will be used to process each short-term S-N data through a shift factor given by

$$\log\left(a(\sigma_a)_{Tref}\right) = \frac{\Delta H_{\sigma_a}}{v_{fs}^*}\left(\left(\frac{1}{\sigma_a - \sigma_{fs}}\right)_T - \left(\frac{1}{\sigma_a - \sigma_{fs}}\right)_{T_{ref}}\right). \tag{4.2}$$

The equation shows that the time-stress shift factor is a function of applied stress and fatigue endurance limit at given temperature. At the fatigue endurance limit, σ_{fs}, the localized plastic deformation process hardly occurs and it may take more than 10^8 cycles before fatigue failure.

To compute time-stress shift factor, activation energy barrier ΔH_{σ_a}, activation volume v_{fs}^* and fatigue endurance limit σ_{fs} need to be determined. ΔH_{σ_a} can be computed using Equation (3.5) as

$$\log\left(a(T)_{Tref}\right) = \frac{\Delta H_{\sigma_a}}{R}\left(\frac{1}{T} - \frac{1}{T_{ref}}\right) \tag{4.3}$$

Using the empirically determined time-temperature shift factor shown in Table (1) and Equation (4.4), the ΔH_{σ_a} values at $60\,^{\circ}C$, $80\,^{\circ}C$ and $100\,^{\circ}C$ can be computed as 12.58kJ/mol, 16.61kJ/mol and 22.94kJ/mol, respectively. The average value of ΔH_{σ_a} is 17.76kJ/mol. Activation volume v^*, 6.4 nm^3 per molecule for PC (Ward, 1983) can be converted into 0.003854 m^3/mol by multiplying Avogadro's number (6.022×10^{23}mole^{-1}). this value of activation volume was computed using yield stress. Activation volume decreases as applied strain or stress increases (Jeong et al, 1999). In fatigue situation, the activation volume will be onset value for fatigue process. If the activation volume is assumed to be inversely proportional to stress, activation volume for fatigue can be determined as

$$v_{fs}^* = \frac{\sigma_y}{\sigma_{fs}} v^* \tag{4.4}$$

Table 5.1 shows the fatigue endurance limit for a few thermoplastics. For most thermoplastics, the fatigue endurance limit, σ_{fs}, is between $0.2\sigma_y$ and $0.3\sigma_y$ at room temperature. As a result, σ_{fs} is assumed to be $0.24\sigma_y$, i.e., $\sigma_{fs} = 0.24\sigma_y$. Furthermore, this relation is assumed to be true at elevated temperatures as well, i.e.,

$$\left(\sigma_{fs}\right)_T = 0.24\left(\sigma_y\right)_T. \tag{4.5}$$

Using the Equations (4.3), (4.4) and (4.5) and empirically determined time-temperature shift factor, $\log\left(a(T)_{T_{ref}}\right)$, time-stress shift factor can be computed through following equation

$$\log\left(a(\sigma_a)_{T_{ref}}\right) = (1.1MPa)\left(\left(\frac{1}{\sigma_a - \sigma_{fs}}\right)_T - \left(\frac{1}{\sigma_a - \sigma_{fs}}\right)_{T_{ref}}\right). \tag{4.6}$$

110

Table 2: Fatigue endurance limit (σ_{fs}) and yielding stress (σ_y) of some polymers.

(Riddell, 1974; Trantina and Ysseldyke, 1987)

Material	σ_{fs} (MPa)	σ_y (MPa)	σ_{fs} / σ_y
ABS	10	30 ~ 65 (48)	0.15 ~ 0.33 (0.21)
PET	11	50 ~ 57 (53)	0.19 ~ 0.22 (0.21)
Polystyrene	10.5	25 ~ 69 (45)	0.42 ~ 0.15 (0.23)
PMMA	10	40 ~ 45 (43)	0.25 ~ 0.22(0.23)
PTFE	2.4	9 ~ 30 (11)	0.1 ~ 0.27 (0.22)
PC	15	58 ~ 70 (64)	0.21 ~ 0.25(0.23)
PEI	17.5	95 ~ 105 (100)	0.17 ~ 0.18 (0.175)

( ): average value

In equation (4.6), the applied stress amplitude at elevated temperatures must be greater than fatigue endurance limit at the reference temperature. When the stress amplitude at an elevated temperature is below the fatigue endurance limit at the reference temperature, those data are neglected, as the proposed ALT technique is only applicable to predict service life above endurance limit using horizontal shifting.
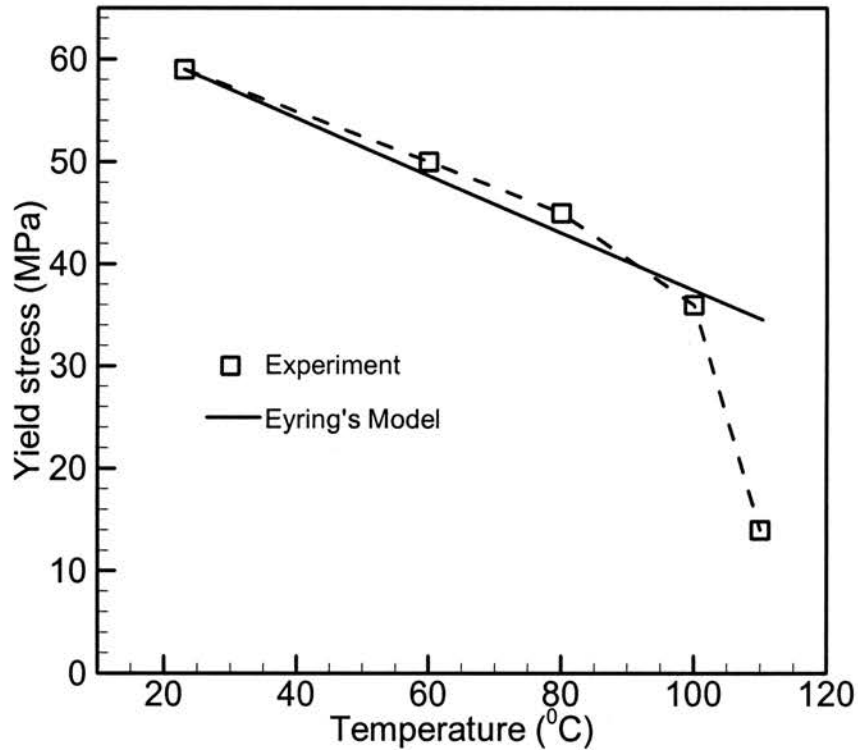
Figure 4.17: Change of the global yield stress at different temperatures

at a strain rate of 0.0225 s^{-1}.

Global yield stress at different temperatures can be obtained in tension experiments. Figure 4.17 shows the change of global yield defined as the stress at the onset of necking under a constant strain rate of 0.045s^{-1} at different temperatures. As the temperature increases, global yield stress decreases. The solid line is the prediction of yield stress by Eyring's model which predicts a linear dependence of yield stress as

$$\frac{\sigma_y}{T} = \frac{2}{v^*}\left[\frac{\Delta H}{T} + \log\left(\frac{d\varepsilon/dt}{\alpha}\right)\right], \qquad (4.7)$$

where σ_y, T, α are yield stress, absolute temperature, and a constant; ΔH, v^* and $d\varepsilon/dt$ are activation energy barrier (free energy change), activation volume and strain rate, respectively. If ΔH and v^* are assumed to be constants and the strain rate, $d\varepsilon/dt$, is a fixed value, then the yield stress can be a linear function of temperature only. When the temperature is less than $100^\circ C$, the temperature dependence on global yielding follows an Arrhenius type linear temperature-dependent behavior.

At $110^\circ C$, the global yielding initiates immediately after the load is applied. It indicates that at $110^\circ C$, the molecular activation energy barrier cannot maintain its prior value and reduces significantly. It is understood that the relaxation process at this temperature is triggered by main chain movement in the molecular structure i.e., α motion (Painter and Coleman, 1997) causing deformation instability under external loads. Characteristic internal viscous flow and/or reduced internal material governing time may also cause divergence from the Arrhenius type linear temperature-dependent behavior. This result implies that there is a temperature limitation for the application of the time-temperature superposition. For polycarbonate, the temperature limit is $100^\circ C$ as observed in the Figure 4.17. In the accelerated fatigue tests in this study, temperatures were controlled up to $100^\circ C$ (including $100^\circ C$) below its glass transition temperature (T_g: $145^\circ C$) so that Arrhenius type relation still holds.

Using the time-stress shift factor determined by Equation (4.2) short-term S-N curves at different temperatures shown in Figures 4.9 and 4.17 are processed. Figure 4.18

113
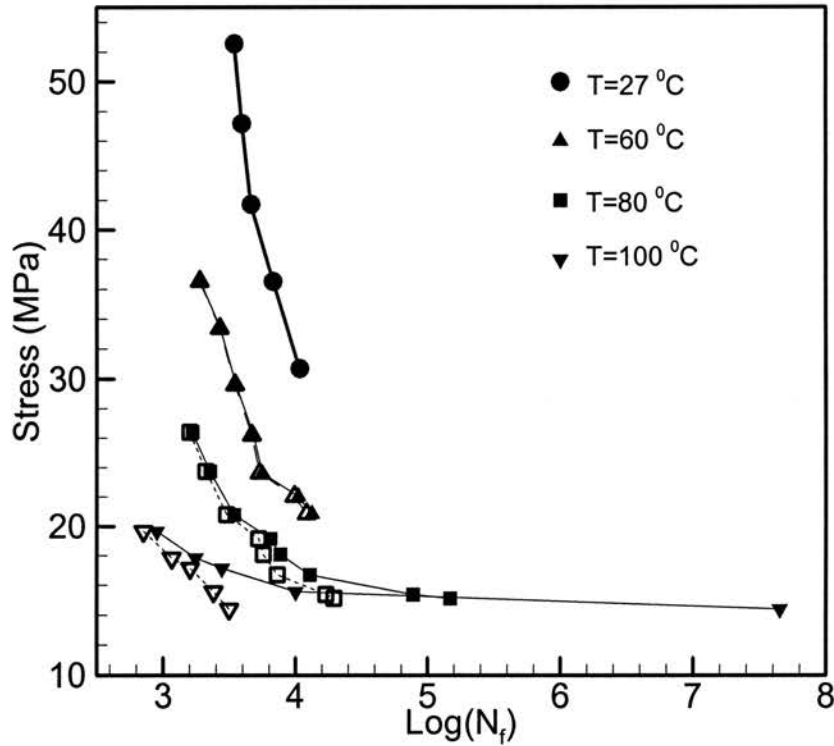
Figure 4.18: Shifting behaviors of short-term S-N curves

using time-stress superposition.

shows the S-N curves after the application of time-stress superposition using data shown in Table 3. When the temperature is low, time-stress shift factors are small and they do not cause considerable shifting in raw data. When the temperature is high, however, there is considerable shifting in the short-term S-N curve.

From the Figure 4.18, it is noted that: 1) when the fatigue induced fracture mode dose not change at both room (reference) temperature and elevated temperature, the

Table 3: Processed data using time-stress superposition.

Temp(C)	Nf	S	Sy	Sf	Sf_ref	1/(S-Sf)	1/(S-Sf)_Tref	log(S_T)	M_Nf
27	3.54	52.6	59.0	14.2	14.2	0.026036	0.0	0	3.535577
	3.59	47.2	59.0	14.2	14.2	0.030281	0.03028089	0	3.592156
	3.66	41.7	59.0	14.2	14.2	0.036262	0.03626193	0	3.661277
	3.83	36.5	59.0	14.2	14.2	0.044679	0.04467872	0	3.828682
	4.03	30.7	59.0	14.2	14.2	0.060397	0.06039672	0	4.030138
60	3.27	36.5	50.0	12	14.2	0.040746	0.04467872	-0.0043255	3.278715
	3.43	33.4	50.0	12	14.2	0.046743	0.05199273	-0.0057744	3.431797
	3.54	29.6	50.0	12	14.2	0.056769	0.06470318	-0.0087274	3.549432
	3.67	26.2	50.0	12	14.2	0.070349	0.08295485	-0.0138659	3.682159
	3.73	23.6	50.0	12	14.2	0.085963	0.10556385	-0.0215612	3.748614
	3.99	22.1	50.0	12	14.2	0.099417	0.12660375	-0.0299056	4.019801
	4.08	20.9	50.0	12	14.2	0.112839	0.14920452	-0.0400024	4.123433
80	3.2	26.4	45.0	10.8	14.2	0.064087	0.08167486	-0.0193461	3.219649
	3.32	23.8	45.0	10.8	14.2	0.077167	0.10417882	-0.0297128	3.352346
	3.48	20.8	45.0	10.8	14.2	0.100008	0.15061965	-0.0556733	3.534816
	3.72	19.2	45.0	10.8	14.2	0.119589	0.19992043	-0.0883648	3.807779
	3.75	18.1	45.0	10.8	14.2	0.137146	0.25435714	-0.1289318	3.883739
	3.86	16.7	45.0	10.8	14.2	0.169316	0.39275601	-0.2457838	4.107856
	4.23	15.4	45.0	10.8	14.2	0.218163	0.8171804	-0.6589187	4.889291
	4.29	15.1	45.0	10.8	14.2	0.230849	1.02898655	-0.877951	5.168742
100	2.85	19.7	36.0	8.64	14.2	0.090697	0.18162797	-0.1000244	2.951282
	3.06	17.8	36.0	8.64	14.2	0.1087	0.27176941	-0.1793758	3.243084
	3.2	17.1	36.0	8.64	14.2	0.117551	0.33479415	-0.2389669	3.441728
	3.38	15.6	36.0	8.64	14.2	0.144245	0.70789945	-0.6200195	3.999687
	3.5	14.4	36.0	8.64	14.2	0.173214	3.9492911	-4.153685	7.650476

application of time-temperature superposition alone is good enough for accelerated fatigue life testing; 2) when the fatigue-induced fracture mode is brittle at room(reference) temperature but is ductile at elevated temperatures, coupling of time-temperature superposition and time-stress superposition need to be considered because

115
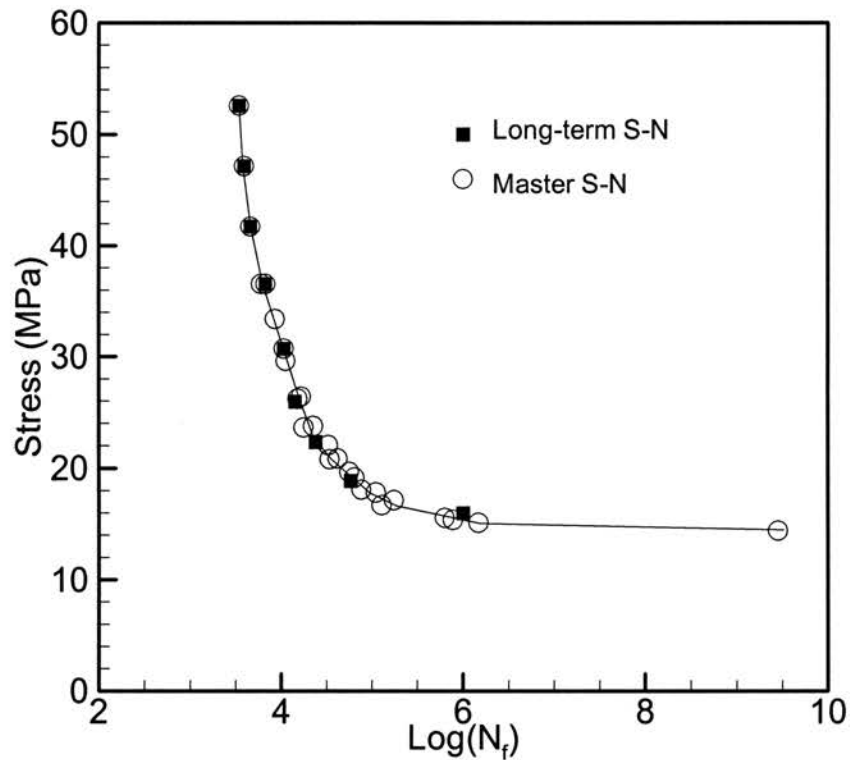
Figure 4.19: Comparison of Master S-N curve and long-term S-N curve.

accelerated short-term fatigue-induced fracture mode is ductile at high temperature, while the actual long-term fatigue-induced fracture mode shows a D-B transition at room temperature. Time-stress shifting behavior allows the accelerated fatigue data at higher temperature associated with ductile fracture mode to predict actual long-term fatigue life. In actual long-term fatigue life, the D-B transition fracture mode is present at lower stress amplitude.

Finally, a master S-N curve generated by employing both time-temperature and time-stress superposition is constructed as shown in Figure 4.19. The master S-N curve is constructed by combined time-temperature shifting and time-stress shifting behavior through the following relation in shift factors

$$\log\left(a(T,\sigma_a)_{T_{ref}} \right) = \log\left(a(T)_{T_{ref}} \right) + \log\left(a(\sigma_a)_{T_{ref}} \right) \tag{4.8}$$

In Equation (4.8), time-temperature shift factor in logarithmic scale, $\log\left(a(T)_{T_{ref}} \right)$, is an empirically determined numerical value by which a short-term S-N curve must shifted to make it smoothly overlap the reference S-N curve. After $\log\left(a(T)_{T_{ref}} \right)$ is determined at each elevated temperature, activation energy barrier, ΔH_{σ_a}, is computed by the Equation (4.3). Time-stress shift factor in logarithmic scale is computed using Equation (4.2). With empirically determined ΔH_{σ_a} and predetermined value of activation volume v_{fs}^*, Equation (4.2) then arranged in to Equation (4.6) for this experiment. To use the Equation to compute time-stress shift factor, fatigue endurance limit σ_{fs} at each elevated temperature needs to be determined. In this experiment, σ_{fs} is assumed to be 0.24 times of by the yield stresses at reference and elevated temperatures. Using the yield stress data at different temperatures and Equation (4. 6), time-stress shift factor in logarithmic scale $\log\left(a(\sigma)_{T_{ref}} \right)$ is then computed so that time-temperature shift behavior can be characterized.

The master S-N curve is then compared with the long-term data. As seen in Figure 4.19, there is a very good agreement between results from accelerated fatigue tests and the actual long-term data under isothermal and constant frequency conditions. This

comparison validates the accelerated lifetime testing methodology for relatively long-term fatigue life prediction for the dog-bone shaped thin and unnotched specimen. Using this accelerated lifetime testing methodology under 0.5Hz, actual testing time can be reduced from more than two months for test to reach 1 million (10^6) cycles to less than one week using ALT. This accelerated lifetime testing methodology can also predict fatigue life over 10^9 cycles.

4.2.2 Result Summary of ALT under Isothermal Conditions

An accelerated lifetime testing (ALT) methodology for the fatigue of carbon filled polycarbonate (PC) with dog-bone shaped thin and unnotched standard specimen under isothermal and constant frequency conditions utilizing both time-temperature and time-stress superposition was developed and verified. Short-term fatigue tests (around 10^4 cycles) at a low frequency under different temperatures were conducted to determine the S-N curves at different temperatures. These curves were shifted horizontally to form a master S-N curve that can be used to predict the long-term fatigue life. The master S-N curve was compared with the actual S-N data obtained at room temperature over a relatively large range of loading cycles. The experimental results show that the proposed methodology using both time-temperature and time-stress superposition for ALT is an effective tool to predict actual long-term fatigue lifetime using S-N curve approach.

This study on fatigue testing on Polycarbonate (PC) also reveals that

- Short-term fatigue test data at different temperatures show that at a given stress amplitude, the fatigue lifetime decreases at elevated temperature. This temperature-

dependent fatigue behavior is consistent with temperature dependence on viscoelastic behavior, such as the relaxation modulus. This fatigue behavior can be used to accelerate fatigue tests.

- Between two neighboring curves, there is a portion for smooth overlapping with each other.

- This behavior allows the construction of a master S-N curve that is formed by horizontal shifting short-term S-N curves using both time-temperature and time-stress superposition for prediction of long-term fatigue life.

- SEM observation of fractographs of samples failed in fatigue has provided phenomenological evidence of the acceleration of the fatigue process through the elevation in temperatures and/or applied stress amplitude. It has been demomstrated that time-temperature and time-stress superposition are applicable for fatigue acceleration in consistent with the acceleration in viscoelastic property as in creep and relaxation functions.

Time-temperature and time-stress superposition can be successfully applied to develop the accelerated fatigue test methodology for amorphous polymers. Using the accelerated lifetime testing (ALT) technique, the fatigue life of Polycarbonate (PC) with 0.5Hz can be determined over 10^9 of cycles by accelerated fatigue in one week.

4.2.3 Accelerated Fatigue Life Testing under Athermal Conditions

In this section, results on short-term fatigue testing under athermal conditions are presented and processed to determine the long-term fatigue behavior. The fatigue testing frequency is now much higher than the reference frequency so viscoelastic hysteresis-induced heating effects may cause an athermal condition where the temperature of the specimen body is higher than that of the surrounding air. As the heated condition during the test causes a thermal fatigue situation, the elevated temperature-induced fatigue process will also be involved. In this test, a high loading frequency is chosen as a main fatigue life acceleration factor. This fatigue acceleration behavior will be quantified through time-frequency superposition as well as through time-temperature and time-stress superpositions. Shifting and processing the short-term fatigue data at high loading frequency should result in a master curve for fatigue life applicable for long-term fatigue life prediction.

Tensile tests at different strain rates and temperatures were conducted to investigate stress-strain responses first. Figure 4.20 shows the tensile stress-strain responses at different strain rates. At a low strain rate, the magnitude of the yield stress is relatively low and shows clear rate dependence. As the strain rate increases, the magnitude of the yield stress increases. In all strain rates, the initial Young's modulus does not change much over the range of strain rates. When the strain rate is above 0.045 s^{-1} and the stress
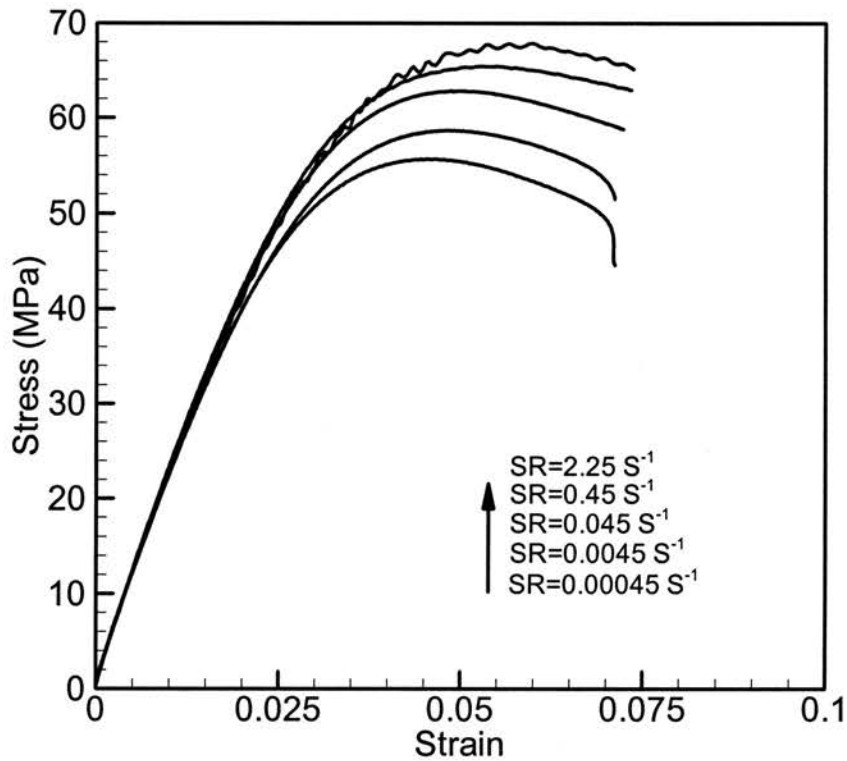
Figure 4.20: Tensile stress-strain response at different strain rates.

amplitude is below 40MPa, there is little rate dependence. This implies that fatigue life under low frequency may be little different from that under high frequency as long as strain rate is kept higher than $0.045s^{-1}$.

Figure 4.21 shows some of the tensile stress-strain responses at different temperatures with a constant strain rate of $0.0045s^{-1}$. It can be observed that the amplitude
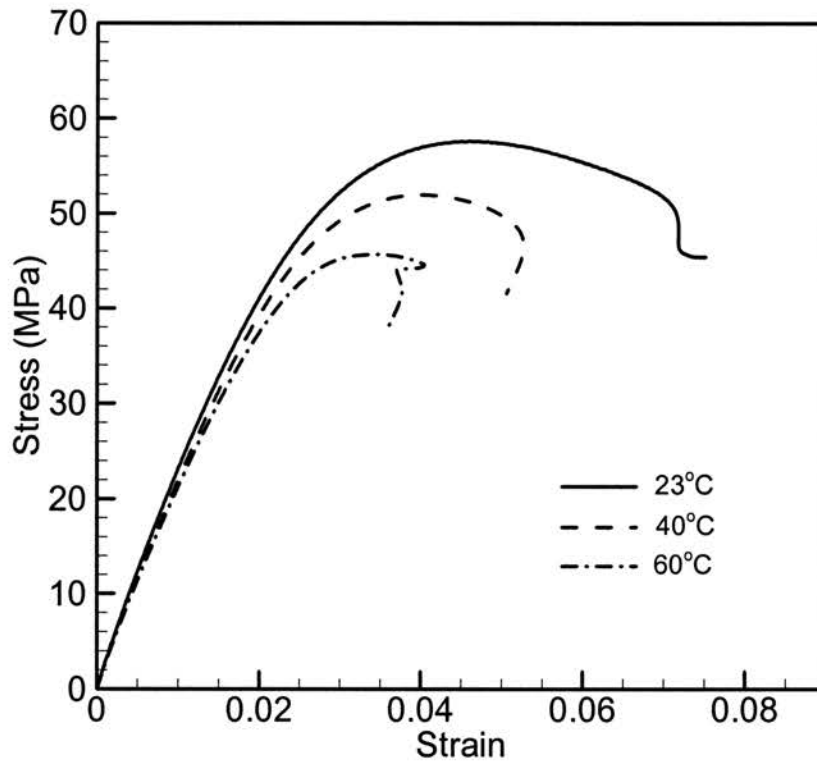
Figure 4.21: Stress-strain response at different temperature with

constant a strain rate of 0.0045 s^{-1}.

of the yield stress and modulus are sensitive to temperature. As temperature increases, the

magnitude of both yield stress and modulus decrease.

The viscoelastic nature of yield behavior with temperature and rate dependence has

been investigated widely using the Eyring theory of viscosity (Eyring, 1958; Argon,

1973; Boyce et al., 1988). In the high stress region where yield occurs, the Eyring theory
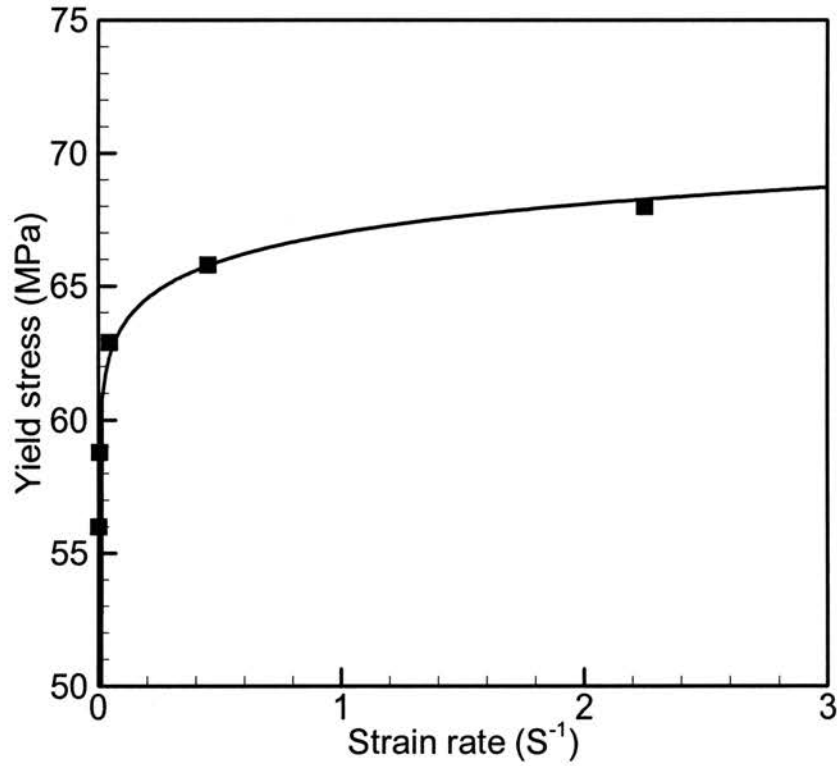
Figure 4.22: Relation between crosshead rate and yield stress at room

temperature ($23\,^{\circ}C$) based upon Eyring theory of viscosity.

gives the relationship between the strain rate and applied shear stress as follows:

$$\dot{\varepsilon} = A\exp\left\{-\frac{\left(\Delta E - v^{*}|\sigma_{s}|\right)}{RT}\right\} \quad (4.9)$$

where A is a constant, R is the gas constant and v^{*} is the activation volume. This

equation can be rearranged as shown in Equation (4.7) to give the yield stress σ_{y} in

123
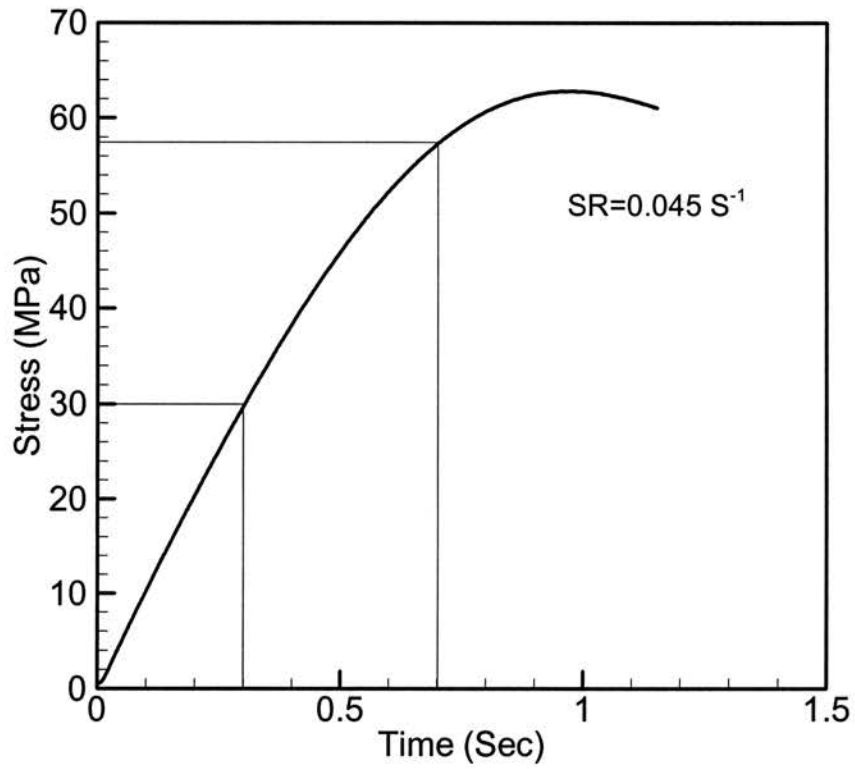
Figure 4.23: Approximation of yield stress during dynamic loading conditions using tension

data (Yield stress is approximated to be 62.6 MPa at 1Hz loading frequency).

terms of the strain rate with a simple yielding criterion such that $2\sigma_s = |\sigma_{xy} - \sigma_{yz}| = \sigma_y$.

Thus, it can be as

$$\frac{|\sigma_y|}{T} = \frac{\Delta E}{v^* T} + \left(\frac{2R}{v^*}\right)\ln\left(\frac{\dot{\varepsilon}}{A}\right) \qquad (4.10)$$

Figure 4.22 shows the relation between yield-stress and strain rates at room temperature ($23\,^{0}C$). In a fatigue test under constant frequency, the strain rate is not constant and changes with stress amplitude. However, a simple relationship can estimate as the yield-stress at a given frequency for a moderate stress amplitude range. When the applied stress is within the applicable range of stress amplitudes, the effect of the strain rate is considered to be the same as the effect of frequency on the specimen (2 inches gauge length) as shown in Figure 4.23. The relationship between the magnitude of yield stress and applied frequency will be

$$\sigma_y = 1.6\ln(f) + 62.6 \qquad (4.11)$$

This simple reference is useful to estimate yield stress of a specimen under a high loading frequency fatigue test if the material follows Eyring's model. If not, it is sometimes difficult to measure the yield stress at very high strain rate. It is noted that the stress-strain response at 2.25 s^{-1} in the Figure 4.20 is similar to the response at 5Hz frequency during the fatigue test. Considerable instability of the strain measurement was observed during high strain rate tensile tests. Using the Equation (4.11), the yield stress at higher strain rate and/or loading frequency can be approximated. For example, the yield stress during the fatigue test at 10Hz frequency is estimated to be ~64MPa when the stress amplitude is above 40MPa.

Next, temperature-dependent and frequency-dependent fatigue behaviors were investigated. The long-term fatigue data is represented first. These data are then compared with a master curve obtained from short-term fatigue data. Figure 4.24 shows

125
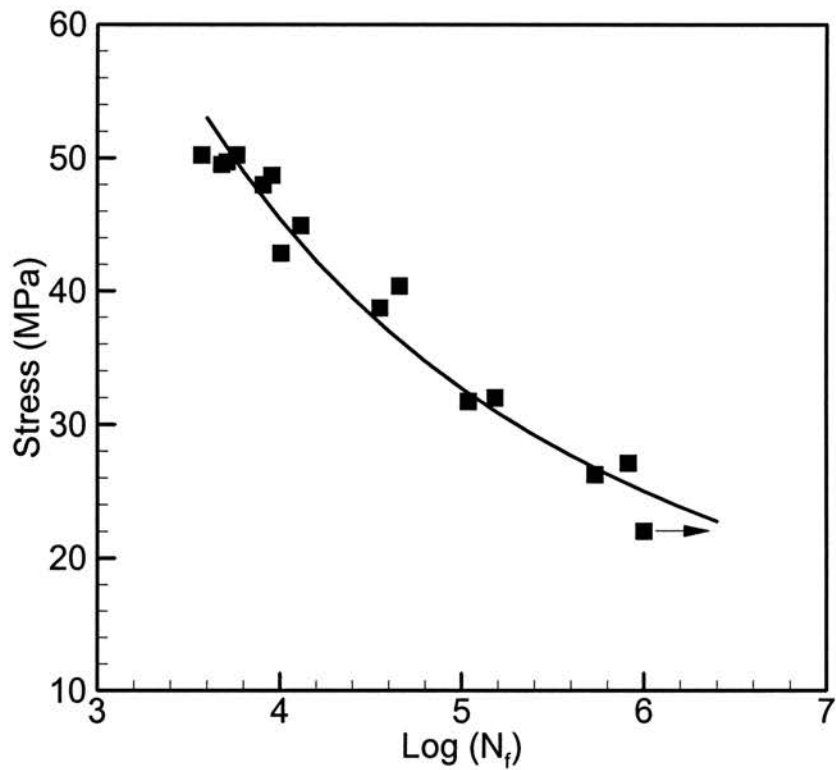
Figure 4.24: S-N data with frequency of 1.0 Hz at $23\,^{0}C$.

the long-term S-N data with a frequency 1.0 Hz at room temperature ($23\,^{0}C$). It shows

that the overall S-N curve shape is different from that obtained from the previous section

for isothermal conditions. It implies that the material (Lexan C1200) used in this test is

more brittle than the material (Lexan 6339R) used under isothermal conditions. This is
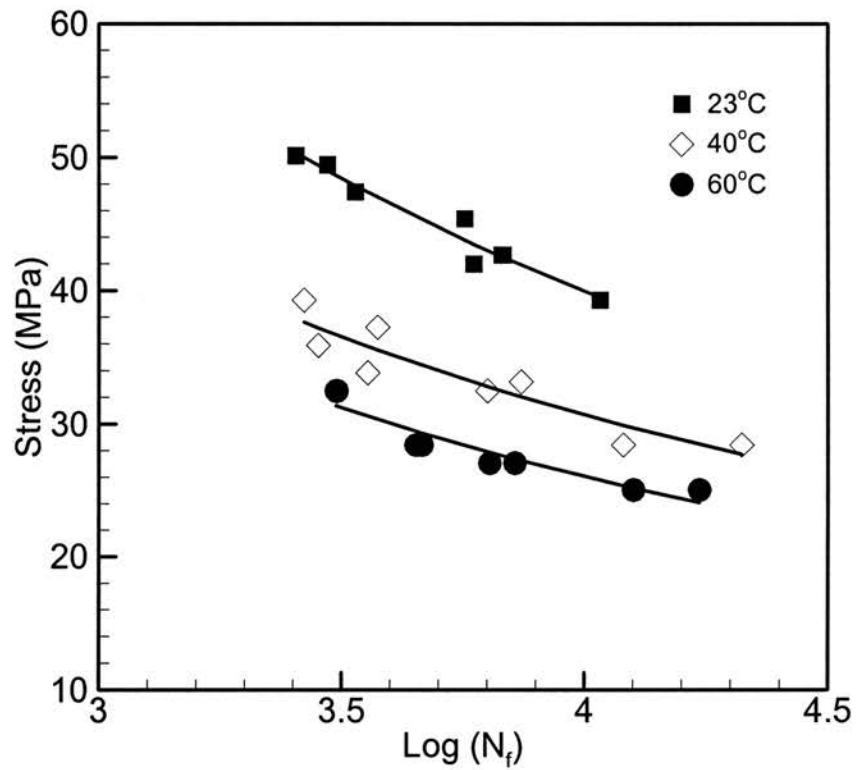
Figure 4.25: Short-term S-N curves at different temperatures with
frequency of 0.3Hz.

most likely due to the increase of concentration in carbon particles in C1200 as compared

with that in 6339R as the carbon particles cause the material to be stiffer but more brittle

(Kurauchi and Ohta, 1984). C1200 grade shows higher yield stress, higher fatigue

strength as well as a longer lifetime at given stress amplitude. There is no information
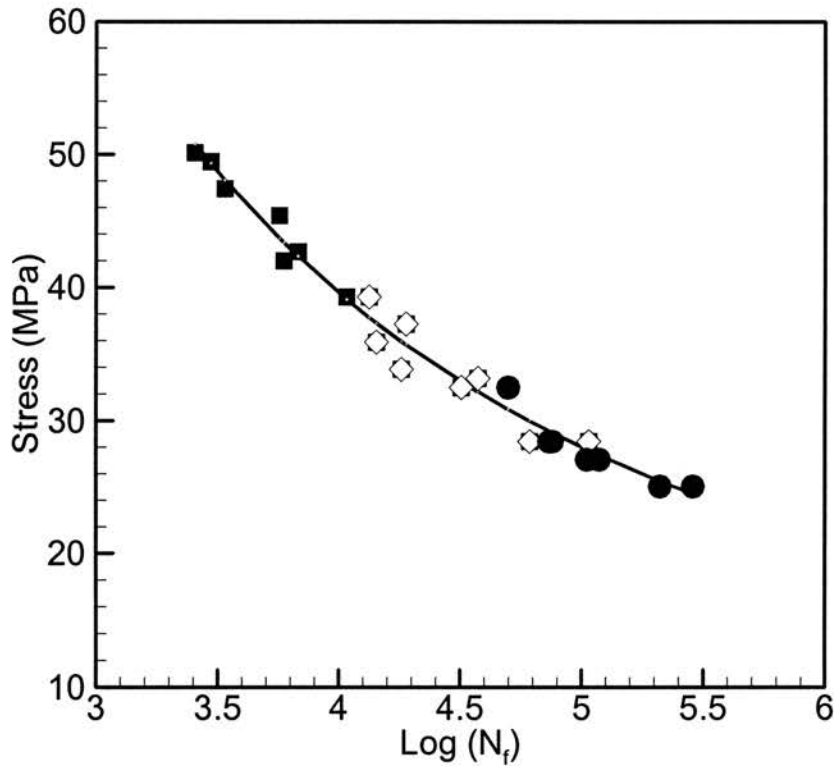
Figure 4.26: Master S-N curve with reference temperature of $23\,^{0}C$

at 0.3Hz frequency.

given about the carbon particle density between them. Below stress amplitude of 23MPa,

the fatigue life exceeds 10^{6} cycles and around this stress amplitude, the fatigue limit is

expected to exist.

Figure 4.25 shows short-term S-N data under different temperatures at a frequency

of 0.3 Hz. The temperature effect on fatigue life in PC has been investigated in detail in
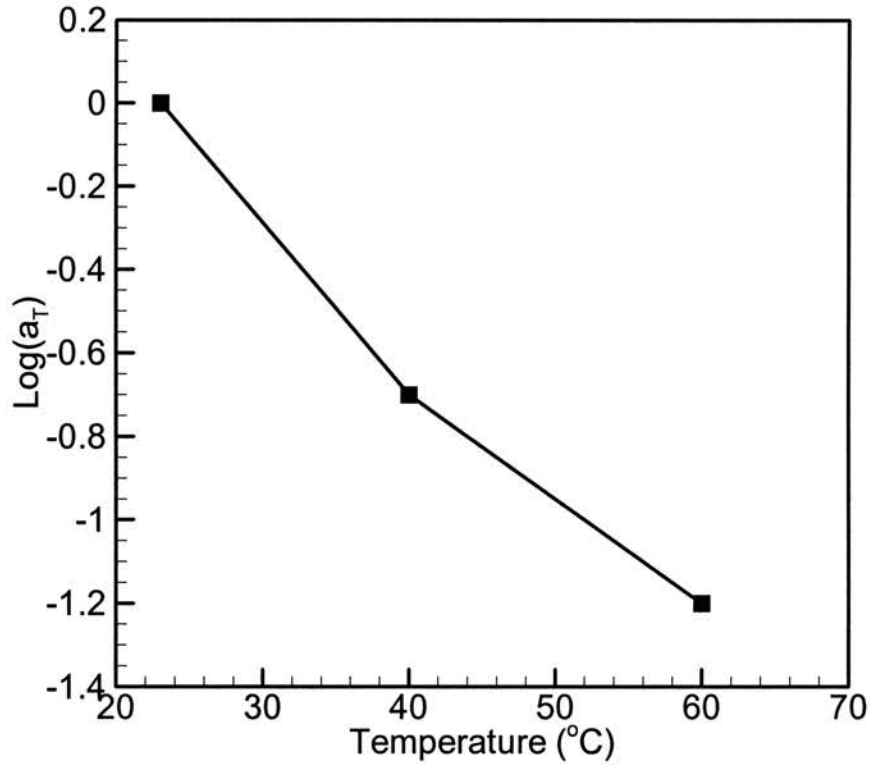
Figure 4.27: Time-temperature shift factors of 1Hz at a reference

temperature of $23 \, ^\circ C$.

the previous section and it was found that temperature could be a fatigue acceleration

factor. Fatigue life decreases as temperature increases at a given stress amplitude. Using

the time-temperature and time-stress superpositions shown in Equation (3.16), a master

S-N curve can be generated as shown in Figure 4.26. The time-temperature shift factor in

Table 4. Processed data using time-temperature and time-stress superpositions

Temp (C)	Nf	S	Sy	Sf	Sf_ref	1/(S-Sf)	1/(S-Sf)_Tref	log(a_S)	log(a_T)	M_Nf
23	3.41	50.1	61.7	14.8	14.8	0.0283	0.02829355	1.153E-05	0	3.404988
	3.47	49.5	61.7	14.8	14.8	0.028854	0.02884696	1.1986E-05	0	3.470688
	3.53	47.4	61.7	14.8	14.8	0.030653	0.03064515	1.3527E-05	0	3.528386
	3.75	45.4	61.7	14.8	14.8	0.032691	0.03268243	1.5385E-05	0	3.753385
	3.77	42	61.7	14.8	14.8	0.036766	0.03675486	1.9459E-05	0	3.772181
	3.83	42.7	61.7	14.8	14.8	0.035871	0.03586116	1.8524E-05	0	3.829881
	3.83	42.7	61.7	14.8	14.8	0.035871	0.03586116	1.8524E-05	0	3.832081
	4.03	39.3	61.7	14.8	14.8	0.040838	0.04082444	2.4007E-05	0	4.032266
40	3.42	39.3	55.7	13.4	14.8	0.03857	0.04082444	-0.0040586	-0.7	4.126559
	3.45	35.9	55.7	13.4	14.8	0.044372	0.04738226	-0.0054192	-0.7	4.157619
	3.55	33.9	55.7	13.4	14.8	0.048774	0.0524361	-0.0065922	-0.7	4.260592
	3.57	37.3	55.7	13.4	14.8	0.041853	0.04452158	-0.004803	-0.7	4.279403
	3.8	32.5	55.7	13.4	14.8	0.052228	0.05645012	-0.0075995	-0.7	4.5081
	3.87	33.2	55.7	13.4	14.8	0.050442	0.05436913	-0.007069	-0.7	4.576969
	4.08	28.4	55.7	13.4	14.8	0.066319	0.07327873	-0.0125266	-0.7	4.792527
	4.32	28.4	55.7	13.4	14.8	0.066319	0.07327873	-0.0125266	-0.7	5.035527
60	3.49	32.5	49.7	11.9	14.8	0.048575	0.05645012	-0.0141754	-1.2	4.703289
	3.49	32.5	49.7	11.9	14.8	0.048575	0.05645012	-0.0141754	-1.2	4.704345
	3.65	28.4	49.7	11.9	14.8	0.060538	0.07327873	-0.0229331	-1.2	4.875943
	3.67	28.4	49.7	11.9	14.8	0.060538	0.07327873	-0.0229331	-1.2	4.888633
	3.81	27.1	49.7	11.9	14.8	0.065952	0.08136399	-0.0277409	-1.2	5.032971
	3.86	27.1	49.7	11.9	14.8	0.065952	0.08136399	-0.0277409	-1.2	5.083941
	4.1	25.1	49.7	11.9	14.8	0.076171	0.09750071	-0.0383933	-1.2	5.338933
	4.24	25.1	49.7	11.9	14.8	0.076171	0.09750071	-0.0383933	-1.2	5.474602

logarithmic scale, $\log\left(a(T)_{T_{ref}}\right)$, is an empirically determined numerical value by which a

short-term S-N curve must shifted to make it smoothly overlap the reference S-N curve.

The reference temperature is $23\,^{0}C$ and the reference frequency is 0.3Hz. In Figure 4.26,

the maximum fatigue life in each short-term S-N curve is around $10^{4.2}$ cycles but, in the

master S-N curve, in Figure 4.26, the maximum fatigue life has been extended over $10^{5.5}$

cycles. The corresponding time-temperature and time-stress shift factors are calculated in Table 4 and depicted in Figure 4.27. The time-stress shift factor calculation is based on the Equations (4.2~5). With the average value of activation energy barrier, 29.15kJ/mol, and activation volume, 0.003854 m^3/mol, the time-stress shift factor can be calculated as

$$\log\left(a(\sigma_a)_{Tref}\right) = (1.8MPa)\left(\left(\frac{1}{\sigma_a - \sigma_{fs}}\right)_T - \left(\frac{1}{\sigma_a - \sigma_{fs}}\right)_{Tref}\right). \tag{4.12}$$

Miyano et al. (1999, 2000) investigated the fatigue behavior of CFRP under different temperatures and frequencies and proposed a methodology to predict fatigue behavior at different temperatures and frequencies. They used a model based on a reduced time to account for time-temperature superposition and time-frequencysuperposition associated with fatigue behavior, under the assumption that the failure process is the same as under creep. It is, however, generally understood that fatigue behavior is different from creep behavior because their failure mechanism is quite different (Kinloch and Young, 1983). It is necessary whether Miyano's assumption can be applied to other materials viscoelastic materials.

In following creep test, time-temperature shifting factors from creep behavior will be quantified and compared with those from fatigue. Time-temperature shift factors comparison between master creep compliance and the master S-N curve is necessary to determine whether the temperature effect is the same on both static and dynamic loading conditions. Creep experiments were conducted at different temperatures. The applied stress is small enough to ensure that all strain are within 0.21 ± 0.02% so that the PC
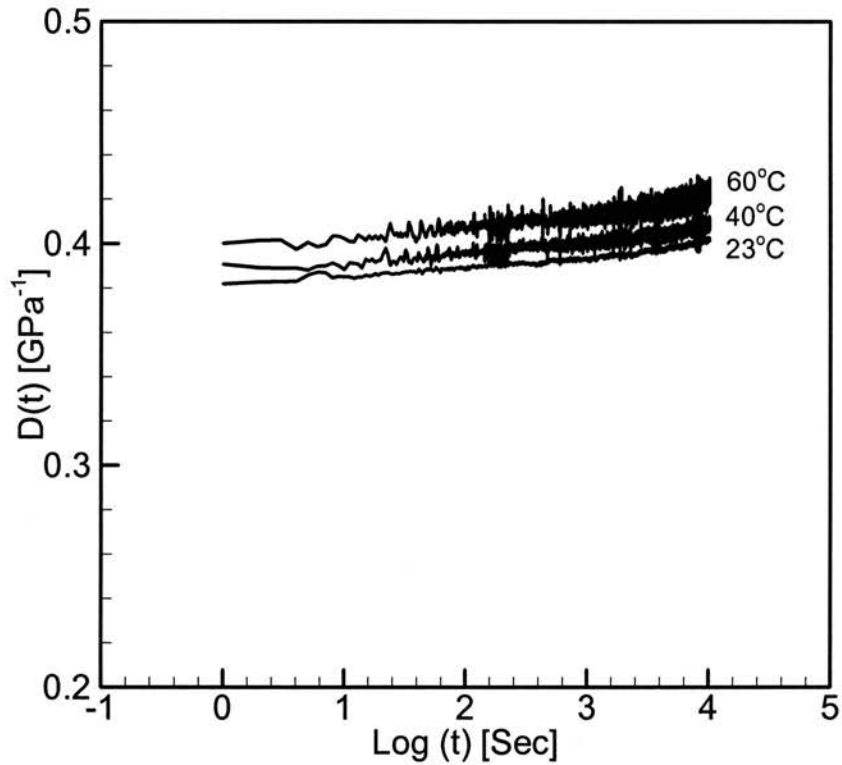
131

Figure 4.28: Creep compliance response of carbon filled Polycarbonate (GE C1200) at

different temperatures with a strain range of $0.21 \pm 2\%$

exhibits linear viscoelastic behavior. Figure 4.28 shows the creep compliance curve at

$23\,^{0}C$, $40\,^{0}C$ and $60\,^{0}C$. Figure 4.29(A) shows the master creep compliance curve

obtained by shifting the creep curve horizontally. The master curve can be used to predict

long-term creep behavior up to 10^{8} seconds. The corresponding time-temperature shift
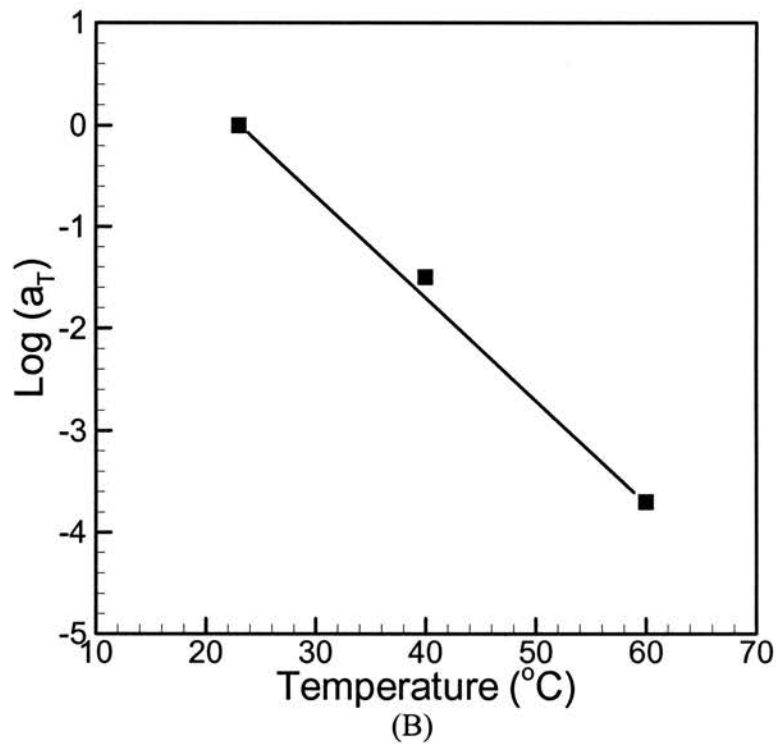
132
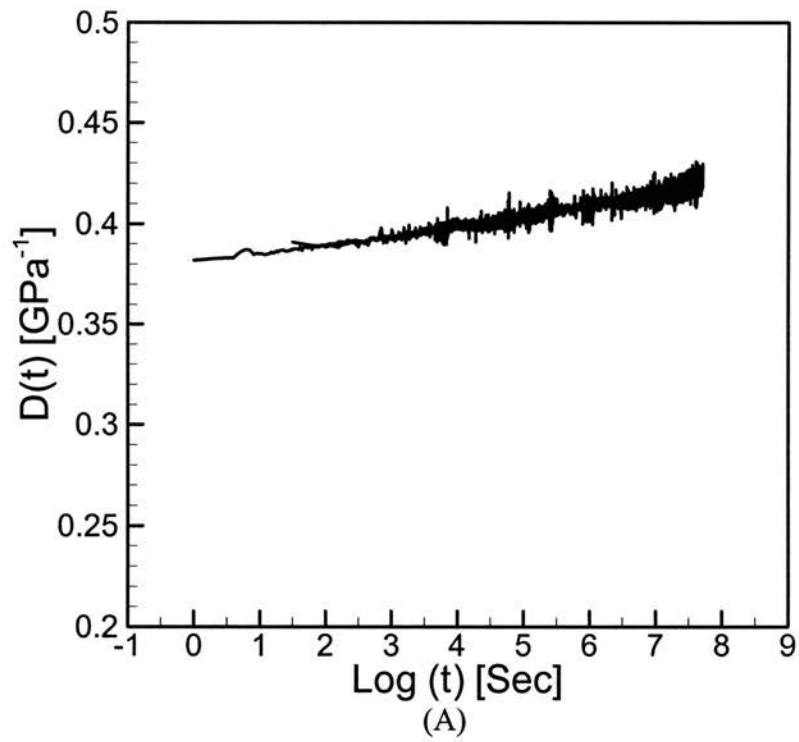
Figure 4.29: (A) Master creep compliance for PC (GE C1200), (B) the

corresponding time-temperature shift factors.
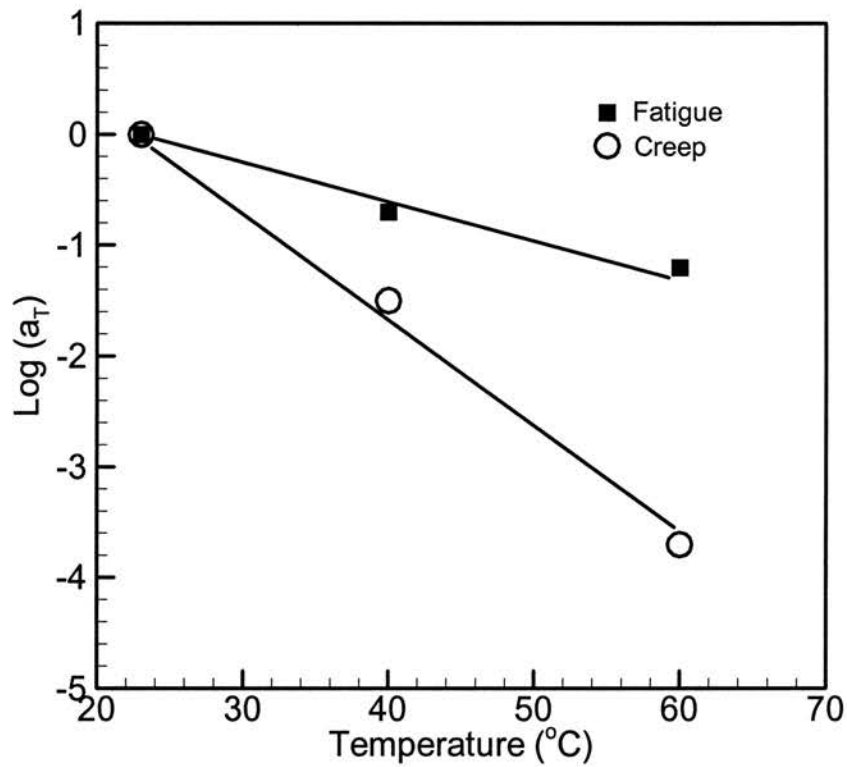
Figure 4.30: Comparison of the time-temperature shift factor between

fatigue and creep compliance.

factors are shown in Figure 5.23(B). Figure 4.30 shows the comparison of shift factors

obtained from the construction of the master creep compliance and from the construction

of the master S-N curve at a frequency of 0.3 Hz. At a given temperature, the shift factor

in fatigue is much less than that in the creep case. Therefore, it can be said that time-

temperature shifting behavior in fatigue may be different from that of creep behavior.
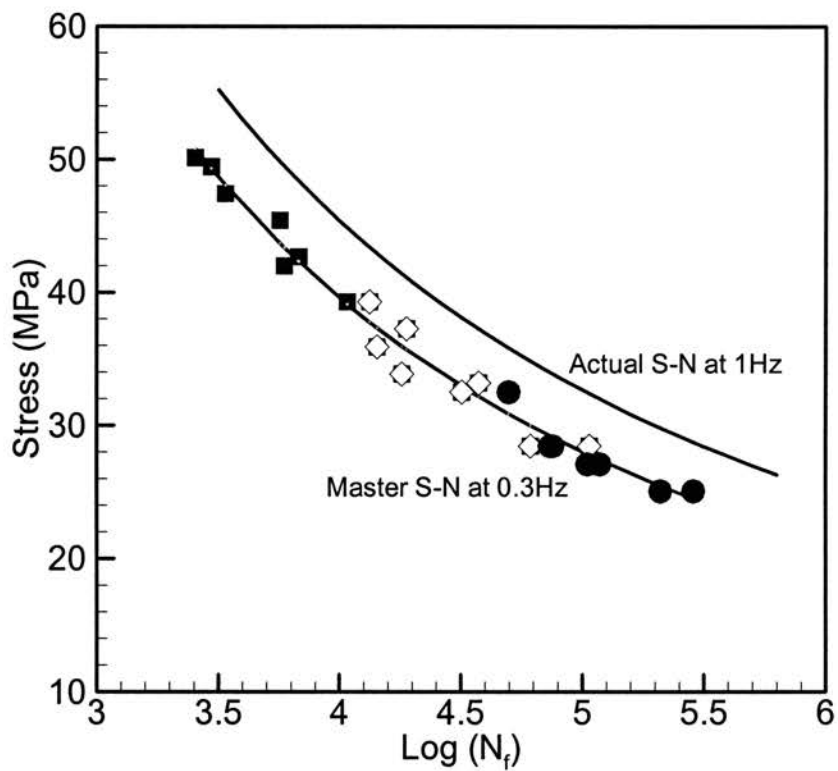
Figure 4.31: S-N curve comparison between frequencies 1Hz and 0.3Hz.

It has been known in fatigue that nonlinear viscoelastic behavior is present in shear yielding and craze formation at localized damage sites, as high stress and strain conditions are involved on the damage sites. A fatigue lifetime model based on the consideration of reduced time for prediction of actual long-term fatigue lifetime has been developed in Chapter 3. The model has been validated under isothermal and low

frequency conditions in section 4.1 using superposition derived from the shifting behavior in time and stress amplitude. In this section, the frequency effect on the fatigue lifetime will be characterized.

Figure 4.31 compares S-N curves of frequencies of 1Hz and 0.3Hz. It is observed that polymer fatigue depends on the frequency. A lower frequency causes a shorter fatigue life at a given stress amplitude. The frequency effect is similar to the inverse of the temperature effect, unless temperature causes a considerable change in yield stress. Horizontal shifting enables characterization of the fatigue lifetime with different frequencies through a simple time-frequency superposition

$$\log\left(a(f)_{f_{ref}}\right) = m\log\left(\frac{f}{f_{ref}}\right) \tag{4.13}$$

where m is a constant. The constant m for carbon filled Polycarbonate (Lexan C1200) used in the study is estimated to be 0.60 from the S-N curves at 1Hz and 0.3Hz.

The frequency effect on the fatigue lifetime in the S-N curve seems to be clear especially under a low frequency. Its effect, however, may be ignored at high frequencies because there is little change in the stress-strain response above the strain rate 0.045 s^{-1} that is the approximated rate under 1Hz of loading frequency (refer Figures 4.20 and 4.23). It implies that if the loading frequency is above 1Hz frequency, the effect may not be the same as that below 1Hz. Instead, thermal energy dissipation due to viscoelastic hysterisis may heat the material during fatigue.
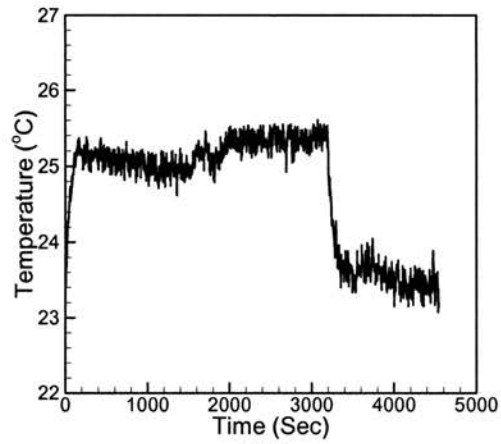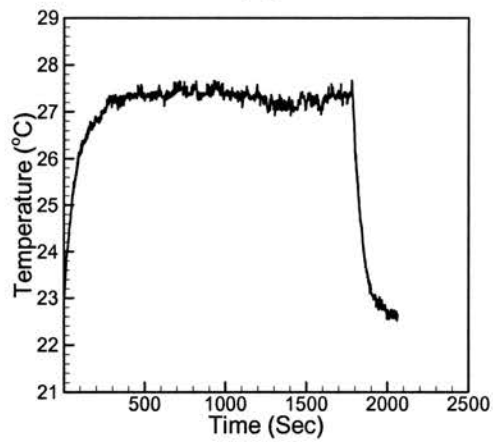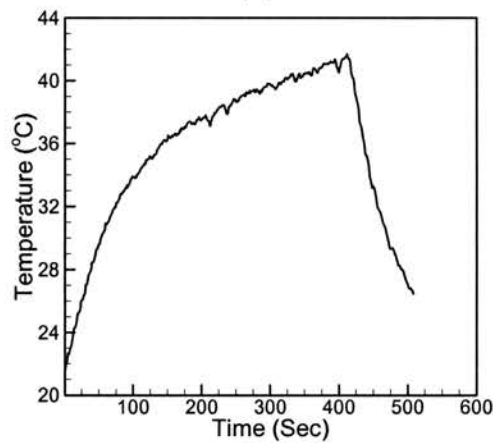
Figure 4.32 Surface temperature increase during fatigue tests at frequency of 10Hz (after failure the temperature decreases sharply).

(A) $\sigma_a = 44.3 MPa$, (B) $\sigma_a = 50 MPa$, (C) $\sigma_a = 52.3 MPa$

137

The material itself changes its stress-strain response of an increased temperature that softens the material. In this case, even though the actual applied frequency is high enough, the corresponding stress-strain response may exhibit frequency dependence as it does at low frequency. It can be noticed that if there is enough temperature increase, due to viscoelastic hysteresis, the material becomes soft and the frequency effect on the polymer lifetime, such as time-frequency shift behavior may still exist at high loading frequency conditions. Furthermore, time-temperature superposition can also be applied to predict the actual long-term fatigue lifetime at a given stress amplitude.

Figure 4.32 shows the surface temperature change during fatigue tests at a frequency of 10Hz, under displacement control. The thermal energy dissipation due to viscoelastic hysteresis heats the material resulting in a surface temperature increase. An observation is that the temperature increases at the initial stage and then reaches a state of thermal equilibrium. The thermal equilibrium state tends to remain stable during the rest of the fatigue lifetime to make the temperature stable when the applied stress amplitude is approximately below 50 MPa. This observation has been predicted (Ferry, 1961; Ratner and Korobov, 1965). Above 50 MPa, there is no thermal equilibrium and the temperature increases continuously until fatigue failure occurs.

A pseudo thermal equilibrium can be considered from the observation of the surface temperature profile. If it is assumed that the frequency-induced thermal heating effect causes a quick temperature change to reach a certain elevated temperature and the temperature does not change through the rest of the fatigue life, the developed time-

138
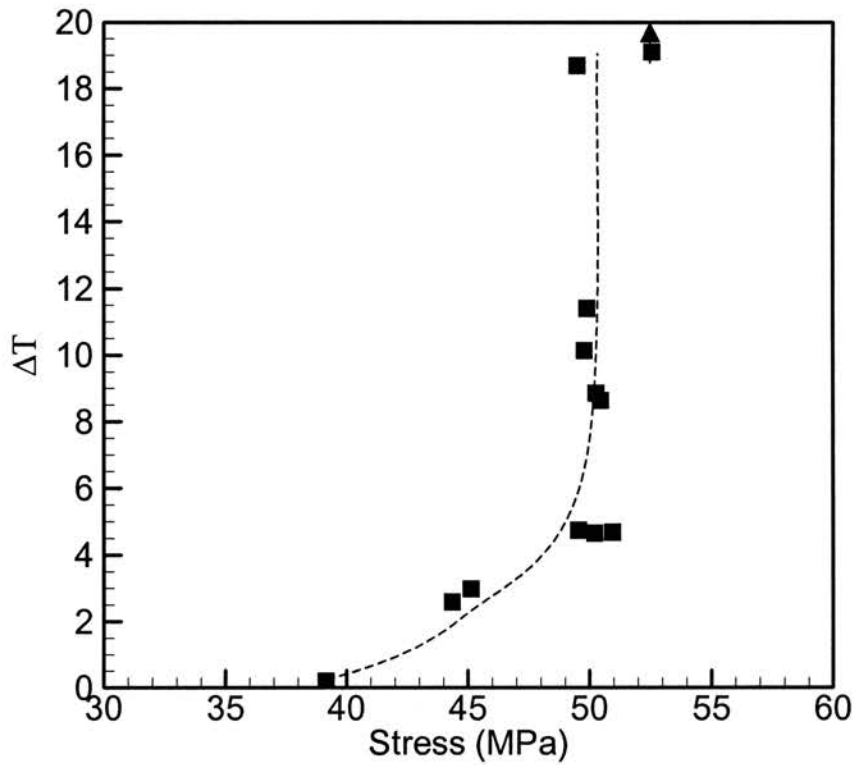
Figure 4.33: Surface temperature rise at different stress amplitudes

during fatigue tests at $23\,^{0}C$ and 10Hz.

temperature superposition for fatigue can be applicable. When there is no thermal

equilibrium state, however, during fatigue tests the temperature will increase

continuously. In this case, it may be very difficult to analyze the hysteresis-induced

thermal fatigue effect quantitatively. Such data was not analyzed, being beyond the scope

of the study.

Figure 4.33 shows the temperature rise during fatigue tests with a frequency of 10Hz. The temperature increases as the applied stress amplitude increases. Below the stress amplitude of 40MPa, the temperature rise is less than $0.5\,^0C$. Thus thermal energy dissipation due to viscoelastic hysteresis can be neglected below 40MPa. This was expected, based on the tensile test data at different strain rates as shown in Figure 4.20, where little rate dependence exists in the stress-strain response below 40 MPa. This implies that the fatigue lifetime may not have any frequency dependence so the fatigue lifetime at high frequencies will be the same as at low frequencies under the same room temperature condition $(23\,^0C)$. When the stress amplitude is above 40MPa, a temperature rise is detectable. When the applied stress is around 50MPa, the corresponding temperature rise varies from $4\,^0C$ to $19\,^0C$.

To keep the tension-tension fatigue test conditions, an initial small tensile stress (or strain) is needed before cycle loading starts. This input loading is expected to avoid a tension-compression situation due to cycle softening. In this experiment, different loading conditions have been used to obtain enough data at different stress amplitudes, but it was hard to get data between 45MPa and 50MPa. It is not clear why a gradual change of the stress amplitude from 45 MPa to 50MPa in the S-N data could not be obtained easily. Several specimens were used but none could induce stress amplitude between 45MPa and 50MPa. Up to 50MPa, a pseudo steady thermal state was observed and the peak temperature was constant until fatigue failure at all set temperatures. Above 52MPa, there
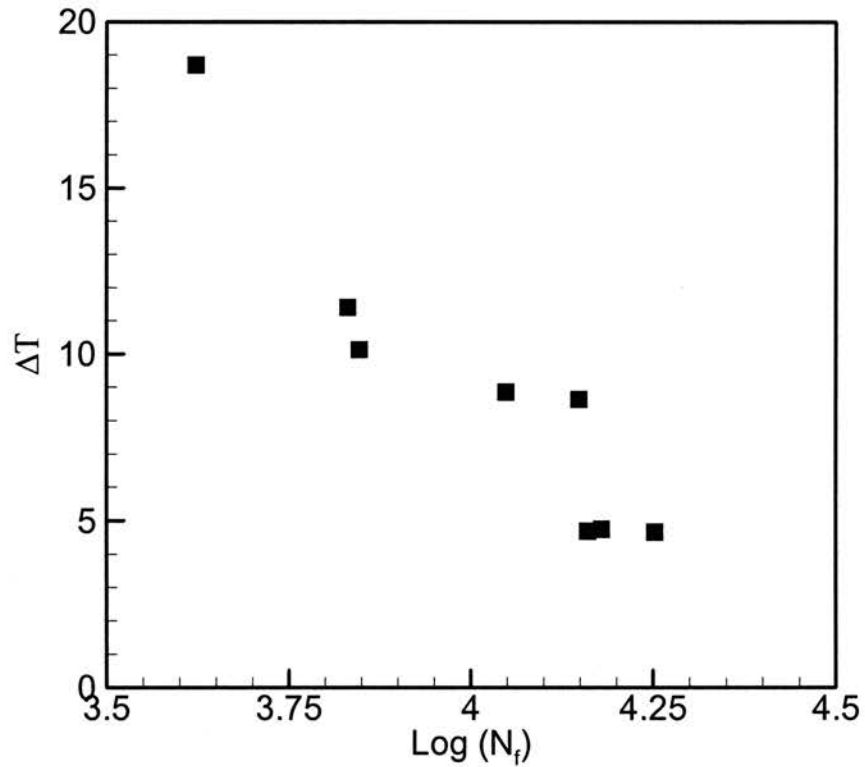
Figure 4.34: Effect of temperature on the fatigue life at the same stress amplitude (50 ± 1MPa) of a frequency of 10Hz.

is not steady thermal state, and the temperature increases continuously until fatigue failure.

Multiple fatigue tests of stress amplitude of 50 ± 1MPa were undertaken. These test data yielded different fatigue live and different temperature changes. Figure 4.34 shows
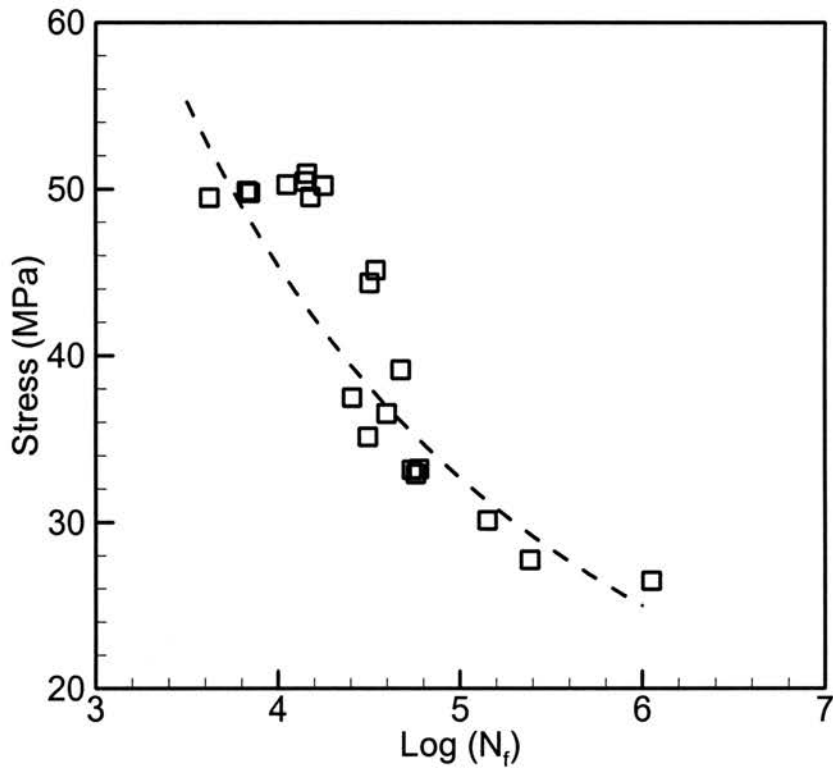
Figure 4.35: S-N data shifting obtained from a 10Hz frequency.

(The dotted line is for 1Hz)

the surface temperature change in these tests plotted against the fatigue life. It is not clear

why temperature changes are different at the same stress amplitude. One clue might rise

from the material's characteristics that lie on the internal friction system of structure. It

indicates that it is the difference in steady state temperature that gives rise a different

fatigue life, even when the applied stress amplitude is the same. Consequently, it shows
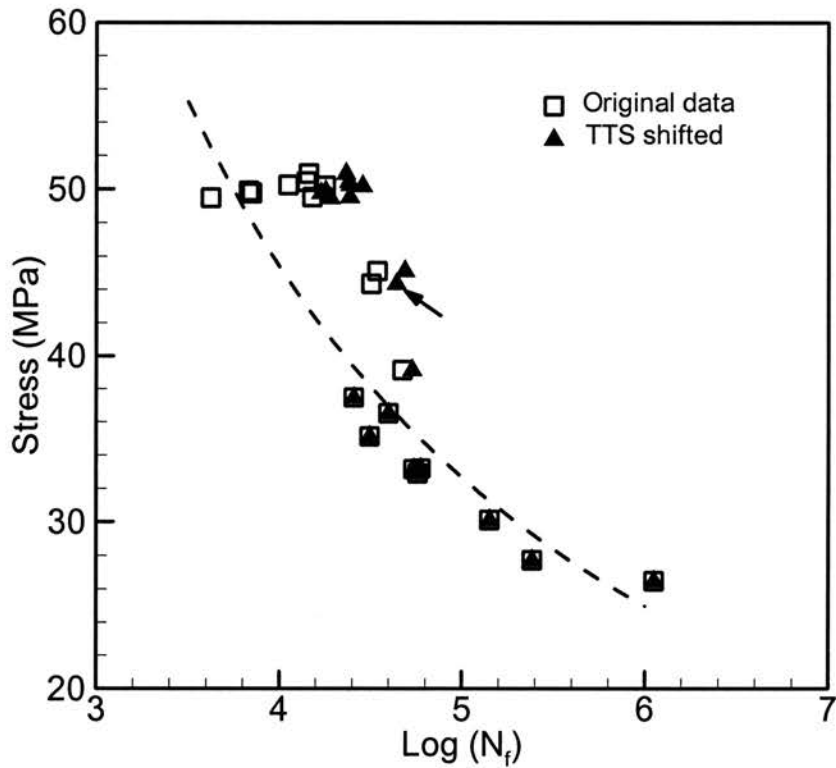
Figure 4.36: S-N data shift obtained from a 10Hz frequency test by time-
temperature and time-stress (TTS) superposition
with respect to a 1Hz of reference frequency.

that the time-temperature superposition can be used to characterize the hysteresis-
induced thermal effect at high frequency fatigue tests if there is a steady temperature rise
during fatigue.

Figure 4.35 shows the actual S-N data at a 10Hz frequency. The dotted line shows
the actual S-N curve at reference frequency 1Hz. It is intended to construct S-N curve to

predict the S-N curve represented in dashed line. As expected from stress-strain response, there is minimal difference in the fatigue lifetime below the stress amplitude 40MPa. Above 40MPa, the data are different from the reference S-N curve of 1Hz. Furthermore; there is a considerable scattering in the data around stress amplitude 50MPa. Figure 4.36 shows only the data without considering the temperature and frequency effects on the fatigue lifetime. The temperature and frequency effects can be considered using time-temperature, time-stress and time- frequency superposition. Employment of time-temperature, time-stress and time-frequency superposition below 40MPa in this study may not cause any corresponding shift behavior because the material has no frequency dependence at room temperature above the reference frequency.

Figure 4.36 shows the S-N data shift using time-temperature and time-stress superpositions (TTS) with respect to a reference frequency of 1Hz. Corresponding time-temperature shift factor at each data above 40MPa are determined using the fitted reference shift factor computed using data Figure 4.27 according to surface temperature data recorded during fatigue tests shown in Figure 4.33 and time-stress shift factor at each data is computed using Equation (4.12). For example, the point with arrow in Figure 4.36 had its original the fatigue life $10^{4.50}$ cycles at 44.3MPa at 10Hz with $2.5\,^{0}C$ temperature rise (blank square symbol). Using the data in Figure 4.27, time-temperature shift factor at $2.5\,^{0}C$ temperature rise is determined as -0.14 in logarithmic scales. Using
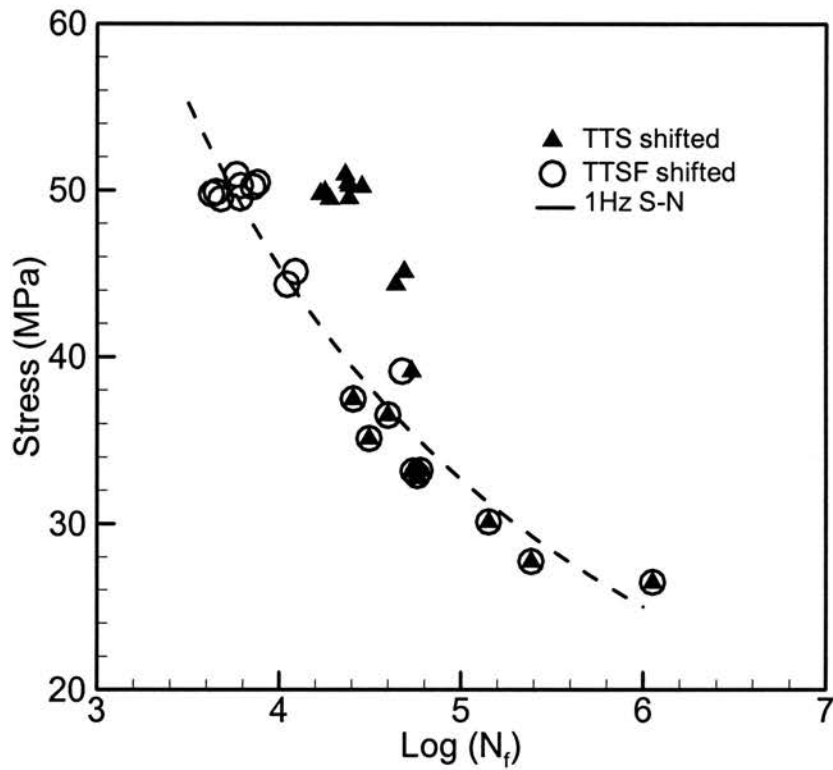
Figure 4.37: S-N data shift obtained from a 10Hz frequency by time-temperature, time-stress and time-frequency (TTSF) superpositions with respect to a 1Hz reference frequency.

Equation (4.12), time- stress shift factor is computed as -0.0007 with σ_a = 44.3MPa, $\left(\sigma_{fs}\right)_{23^0C} = 0.24 \times \left(\sigma_a\right)_{23^0C} 0.42 \times 64.2 = 15.408$MPa, and $\left(\sigma_{fs}\right)_{25.6^0C} = 0.24 \times \left(\sigma_a\right)_{25.6^0C} = 0.24 \times 62.7 = 15.048$MPa. Total shift factor by time-temperature and time-stress superposition becomes $-0.1407 \approx -0.14$ so that shifted fatigue life is $10^{4.64}$ cycles (point with arrow).
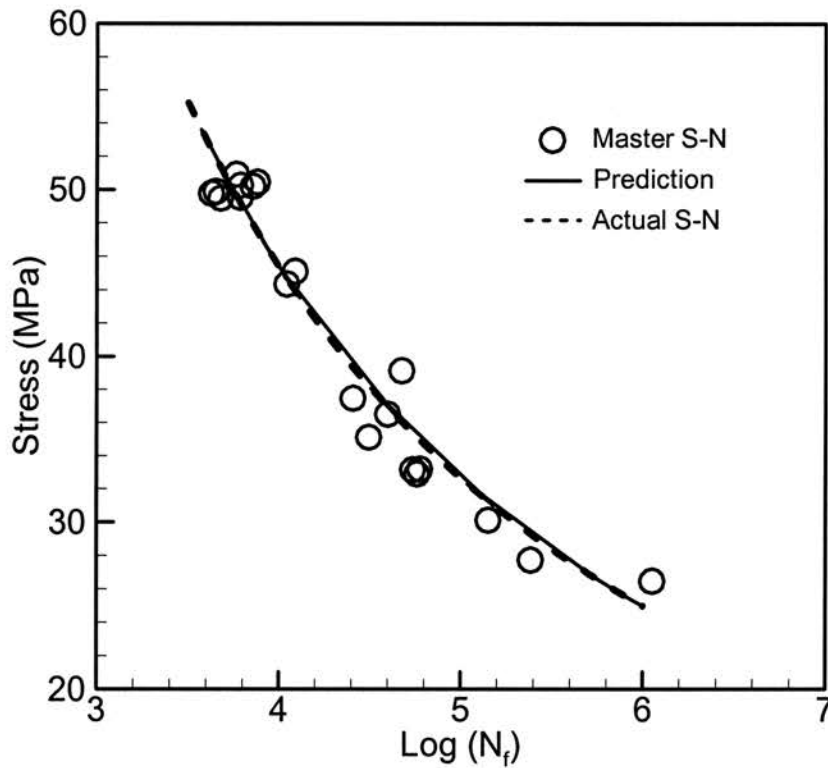
Figure 4.38: Prediction of 1Hz S-N curve using accelerated lifetime

testing (ALT) method at 10Hz data.

Original S-N data were obtained from a 10Hz frequency. The data around 50MPa in stress amplitude were shifted by its own shift factor based upon its temperature rise during the fatigue test. After shifting, the data shows a considerable reduction in scatter. It can be emphasized that if the thermal energy dissipation rate due to viscoelastic

146

hysteresis is stable during the fatigue test resulting in a stabilized value in temperature rise, time-temperature-stress superposition for fatigue has considerable meaning to characterize a correlation between the temperature effect and fatigue lifetime in the S-N curve.

Next, the frequency effect on fatigue lifetime in an S-N curve is considered. Figure 4.37 shows S-N data shift using time-frequency superposition that has been developed by low frequency tests (refer to Figure 4.31 and Equation (4.13)). Finally, a master S-N curve can be obtained from data at the 10Hz frequency and room temperature as shown in Figure 4.37 using time-temperature, time-stress and time-frequency superpositions (TTSF) for fatigue with respect to 1Hz frequency and room temperature. Time-frequency shift factor is simply computed using the Equation (4.9) with m=0.6 for PC (Lexan C1200).

Figure 4.38 shows the comparison between the fitted master S-N curve and actual S-N curve at 1Hz and room temperature. The master S-N curve matches well the actual long-term S-N curve. The figure shows that use of an accelerated lifetime testing technique in the S-N curve is possible for time dependent thermoplastic materials. From the comparison between the fitted master S-N curve and actual S-N curve, it can be said that the application of time-temperature, time-stress and time- frequency superposition developed in this study can be an effective method for the accelerated lifetime testing ALT) technique.

147

4.2.4 Result Summary of ALT under Athermal Conditions

An accelerated lifetime testing (ALT) method for amorphous polymer fatigue under high frequency conditions was developed based on superposition, derived from shifting behavior induced by temperature, stress and frequency superposition. The method is validated through the experiments. Short-term fatigue tests (around 10^4 cycles) at a loading frequency of 10Hz were conducted to generate the S-N curves at different temperatures. At a loading frequency of 10Hz, heating induced by hysteresis was observed.

Two different athermal conditions were observed: One was a steady state condition and the other condition was that a steady state is not obtainable. For accelerated life testing at high loading frequency, the steady state can be always considered. In the case where a steady state was reached on the specimen surface based on the recorded temperature profile, the actual steady temperature on the specimen surface during the fatigue was used to apply time-temperature superposition to determine the long-term fatigue life.

Short-term fatigue data were shifted horizontally to form a master S-N curve using shifting behavior derived from time, temperature, stress and frequency. The master S-N curve referred to $23\,^0C$ obtained from fatigue at frequency 10Hz. The master S-N curve was compared with the actual S-N data obtained at 1Hz under room temperature. Very good agreement has been reached between ALT data and the actual long-term data. The

148

experimental results have thus validated the proposed method for ALT using superposition derived from time, temperature, stress and frequency at high frequency.

CHAPTER FIVE

SUMMARY, RECOMEMDATION AND FUTURE WORK

5.1 Summary

An accelerated fatigue life testing technique was developed for amorphous thermoplastic polymers. Motivated by the shifting behavior of the nonlinear viscoelastic behavior of polymers derived from temperature, frequency and stress amplitude, a theory on the acceleration of fatigue behavior of polymers is proposed and described in Chapter 3. Accelerated lifetime testing (ALT) method originally proposed by Miyano et al. (1999, 2000) is addressed in a different way based on the characterization of fatigue failure mechanism for wide applications on thermoplastic materials.

This research has focused on the fatigue life prediction using the total fatigue life approach, namely S-N curve approach. The accelerated methodology is similar to what was proposed by Miyano et al (1999, 2000) in terms of using temperature-induced fatigue acceleration. This research, however, has addressed the dependence of yiled-stress on temperature and its effect on fatigue acceleration. In addition, failure mode transition, i.e., brittle to ductile transition is considered through time-stress superposition. Also in the case of accelerated fatigue, conducted at a higher frequency than the service frequency, where self-heating is induced by hysteresis, an approach is proposed to shift the short-term data based on the actually measured steady temperature on the specimen surface.

150

With all these considerations, an accelerated fatigue acceleration using shift behavior induced by temperature, frequency and stress has been proposed and validated through comparison between the master S-N curve and the actual long-term S-N curve.

ASTM standard dog-bone shaped specimens made of carbon-filled Polycarbonate PC) were used in all fatigue experiments. Two sets of accelerated fatigue experiments were conducted, they are: (1) fatigue at the low service frequency under isothermal condition, and (2) fatigue at a frequency higher than the service frequency. Under (1), there is no temperature change induced by hysteresis; under (2), there is self-heating induced by hysteresis. Some observations and conclusions are summarized as follows.

5.1.1 Isothermal Conditions

1) To maintain the isothemal condition, relatively low frequency was used such that no temperature change was induced by hysteresis. This study has used frequencies of 0.5 Hz and 1 Hz to maintain the isothermal condition, but did not determine the frequency limit above which isothermal condition can no longer be maintained. It is expected that with the use of appropriate analysis on heat conduction and the energy dissipation from cyclic loading on nonlinear viscoelastic polymers, temperature change could be determined, so that the frequency limit for the isothermal condition could be established. The understanding on temperature change induced by self-heating is expected to be especially useful in developing

151

methods for fatigue acceleration for polymer components with dimensions and geometry complexity causing non-uniform temperature field in accelerated fatigue. Should non-uniform temperature change is induced in polymeric components, the methodology (see 5.1.2) developed under athermal condition might be applicable.

2) It is found that short-term S-N data at different temperatures could be shifted horizontally to form a visibly smooth master curve, indicating that time-temperature superposition, developed for the viscoelastic behavior of thermoplastics such as relaxation and creep under isothermal conditions, is also applicable for fatigue acceleration.

3) It is found that under isothermal condition, ductile failure is observed at a temperature of 100 ^oC, while the actual long-term fatigue failed fracture surface at the same stress level reveals brittle failure, indicating a difference in failure modes. To account for the failure mode difference, a model based on the Eying energy activation theory is proposed to make correction on the ductile (at 100^oC) to brittle (at room temperature, also the service temperature) transition via time-stress superposition.

5) The combined time-temperature and time-stress superpositions allow the short-term S-N curves at low frequency and isothermal condition at different temperatures to form a master S-N curve that can be used to predict relatively long-term fatigue life (S-N curve). Time-temperature shift factor is determined empirically and time-

152

stress shift factor is computed by an equation (4.6) with parameters determined from time-temperature shift factors.

6) The master S-N curve is then compared with actual long-term S-N curve with good agreement as shown in Figure 4.19. This provides conclusive proof that this ALT method works for PC samples under isothermal conditions.

5.1.2 Athermal Conditions

1) At a frequency of 10 Hz, i.e., a frequency higher than the reference frequency (1Hz), self-heating occurs.

2) At stress levels near the yield stress, temperature continuously increases until final fatigue failure, preventing the use of time-temperature superposition for fatigue acceleration analysis, as a steady temperature history does not exist.

3) At stress amplitudes much lower than the yield stress, temperatures increase quickly to stable values. Under this situation, the actual temperature measured during fatigue must be used in applying time-temperature superposition. In addition, time-frequency superposition must be applied to convert S-N curve at a higher frequency to a lower frequency.

4) To generate a master S-N curve, time-temperature and time-frequency shift factors are determined empirically. The Equation (4.13) with a parameter determined from S-N curves at two frequencies can be used for time-frequency shifting at other frequencies.

153

Time-stress shift factor is computed using Equation (4.12) with parameters of energy activation barrier, ΔH, determined from time-temperature superposition and predetermined free volume for fatigue, v_{fs}^*. After superpositions derived from temperature, frequency and stress are all considered, a master S-N curve is determined and is compared very well with the actual long-term S-N curve at reference temperature and frequency as shown in Figure 4.38.

5.2 Recommendation

In the application involving thick polymer components, it is a challenge to measure the temperature profile around fatigue crack initiation zone especially when fatigue crack initiation zone cannot be visually detectable. In this case, if the analysis and computation of stress field, normalization of geometry effect and other considerations allows experimental fatigue tests to represent actual fatigue situation for practical application, ALT methodology under low frequency, corresponding to isothermal conditions, rather than high frequency possibly involving athermal conditions, is recommended because there is no need to consider the complicated temperature profile around fatigue crack initiation zone.

To create isothermal conditions, a temperature bath can be used. In this case, moisture or solvent effect on the change of viscoelasic behavior of the polymeric materials must be characterized because moisture or solvent content in the soaked

154

polymer will change the free volume, resulting in change of fatigue behavior. Therefore, Using a heat chamber would create isothermal conditions easily and does not need to consider moisture or solvent content effect on mechanical property change of the polymeric materials

5.3 Future Work

For more practical use of ALT methodology under isothermal condition, it is necessary to determine the fatigue endurance limit. It is expected that the fatigue lifetime around fatigue endurance limit does not depend on frequency, thus relatively high loading frequency can be used to find fatigue endurance limit. In some cases, however, actual fatigue tests to find fatigue endurance limit can be a time consuming work. Instead, an alternative approach using the ALT under isothermal condition can be used to determine the fatigue endurance limit in short time.

The ALT methods can also be developed to consider physical aging effect on viscoelastic materials because physical aging causes an important time-dependent change in mechanical properties.

It is also recommended, in the future work, to extend this method for long-term fatigue life prediction for polymer matrix composite materials and semi-crystalline polymers material. The wide applications of the proposed ALT methodology on complicated polymer components can also be recommended.

REFERENCES

Adam, G., Gibbs, J.H., 1965. On the temperature dependence of cooperative relaxation properties in glass forming liquids. Journal of Chemical Physics 43, p139

Argon, A.S., 1996a. Mechanical properties of single phase crystalline media: Deformation at low temperatures. Physical Metallurgy 3, 4th Eds.

Argon, A.S., 1996b. Mechanical properties of single phase crystalline media: Deformation at high temperatures. Physical Metallurgy 3, 4th Eds.

Argon, A.S., Bulatov, V.V., Mott, P.H., Suter, U.W., 1994. Plastic deformation in glassy polymers by atomistic and mesoscopic simulation. Journal of Rheology 39(2), p377

Argon, A.S., Hannoosh, J.G., 1977. Initiation of crazes in polystyrene. Philosophical Magazine 36, p1195

Argon, A.S., Salama, M.M., 1977. Philosophical Magazine 35, p1217

Argon, A.S., 1975. Roll of heterogeneities in the crazing of glassy polymer. Pure and Applied Chemistry 43, p247

Argon, A.S., 1973. Low-temperature plastic deformation of glassy polymers. The Philosophical Magazine 28, p839

American Society for Metals. 1975. Polymeric Materials.

Attermo, R., Ostberg, G., 1971. Measurement of temperature rise ahead of a fatigue crack. International Journal of Fracture Mechanics 7, p122

Bauwens-Crowet, C., Bauwens, J.C., Homes, G., 1969. Tensile yield-stress behavior of glassy polymers. Journal of Polymer Science A2, 7, p735

Beardmore, P., Rabinowitz, S. 1974. Cyclic Deformation And Fracture in Polymer. Applied Polymer Symposium No. 24, p25

Berger, L.L., Sauer, B.B., 1991. Enhanced segmental mobility at polymer surfaces: thermally simulated current studies of crazed films. Macromolecules 24, p2096

Boyer, R.F., 1976. General reflections on the symposium on physical structure of amorphous state. Journal of Macromolecular Science and Physics B 12(2), p253

Boyce, M.C., Parks, D.M., Argon, A.S. 1988. Large inelastic deformation of plassy polymers. Mechanics of Materials 7, p15

Boyce, M.C., Arruda, E.M., 1989. Mechanics of Plastics and Plastic Composites, 104. ASME Winter Annual Meeting.

Bucknall, C.B., Stevens, W.W., 1980. Rubber toughening of plastics. Journal of Materials Science 15, p2950

Chau, C.C., Li, J.C.M., 1981. Fracture of shear bands in atatic polystyrene. Journal of materials science 16, p1858

Chen, T.J., Chudnovsky, A., Bosnyak, C.P., 1994. Observation of the mocro-mechanisms of fatigue-crack initiation in polycarbonate: A fatigue crack initiation map for polycarbonate. Journal of Material Science 29, p5903

Chen, T.J., Bosnyak, C.P., Kao, C.I., Chudnovsky, A. 1993. A fatigue crack initiation map for polycarbonate. Journal of Applied Polymer Science 49, p1909

Chou, Y.F., Sun, C.T., 1983. Modeling of the frequency effect on fatigue crack propagation in PMMA. Engineering Fracture Mechanics 17, p17

Crawford, R.J., Benham, P.P., 1974. Cyclic stress fatigue and thermal softening failure of a thermoplastic. Joournal of Materials Science 9, p18

Crawford, R.J., Benham, P.P., 1975. Some fatigue characteristics of thermoplastics. Polymer 16, p908

Doolittle, A.K., 1951. Studies in Newtonian flow. II. The dependence of the viscosity of liquids on free-space. Journal of Applied Physics 22, p1471

Dyre, J.C., 1999. Solidity of viscous liquids. Physics Rev. E 59, p2458

Dyre, J.C., 1987. Master-equation approach to the glass transition. Physics Rev. Lett 58, p792

Engel, L., Klingele, H., Ehrenstein, G.W., Schaper, H. 1981. An Atlas of polymer damage. Prentice-Hall, Inc.

Estevez, R., Tijssens, M.G.A., Van der Giessen. E., 2000. Modeling of the competition between shear yielding and crazing in glassy polymers. Journal of the Mechanics and Physics of Solids 48, p2585

Eyring, H., Ree, T., 1958. In: Rheology, Ed. By F.R. Eirich, Vol. II, Academic Press, New York.

Ezrin, M. 1996. Plastic Failure Guide: Cause and Prevention. Hanser Publishers, Munich Vienna New York.

Ferry, J.D. 1961. Viscoelastic properties of polymers. Wiley, New York.

Findley, W.N., 1981. 26-year creep and recovery of poly (vinyl chloride) and polyethylene. Polymer Engineering and Science 27(8), p583

Findley, W.N., Lai, J.S.Y., 1966. Brown University Report. EMRL-27.

Friedrich, K., Schafer, K., 1979. Coarse shear bands and fracture in polystyrene. Journal of Materials Science 14, p480

Fung, Y.C. 1993. Biomechanics, Mechanical Properties of Living Tissues, 2nd. Springer-Verlag, New York.

Furue, H., Shimamura, S., 1980. Fatigue behavior of rigid polymeric materials and composites at room and elevated temperature. International Journal of Fracture 16(6), p553

Martin, G.C., Gerberich, W.W., 1976a. Journal of Materials Science 11, p231.

Ha, K., Schapery, R.A., 1998. A three-dimensional viscoelastic constitutive model for particulate composite with growing damage and its experimental validation. International Journal of Solids and Structures 35, p3497

Hasan, O.A., Boyce, M.C., 1995. A Constitutive Model for the Nonlinear Viscoelstic Viscoplastic Behavior of Glassy Polymers. Polymer Engineering and Science 35(4), p331

Haward, R.N. 1993. Strain hardening of thermoplastics. Macromolecules 26, p5860

Haward, R.N. 1972. Amorphous Materials, Ed. by Douglas, R.W. & Ellis, B. Wiley, London.

Haward, R.N., Thackray, G., 1968. Proc. Roy. Soc. A 302, p453

Hertzberg, R.W., Manson, J.A. 1980. Fatigue of Engineering Plastics. New York Academic.

Hertzberg, R.W., Manson, J.A., Skibo, M., 1975. Frequency sensitivity of fatigue process in polymeric solids. Polymer Engineering And Science 15(4) April, p252

Hope, P.S., Duckett, R.A., Ward, I.M., 1980. Effect of free monomer content on the drawing behavior of poly(methyl methacrylate). Journal of applied Polymer Sciences 25, p1373.

Hope, P.S., Ward, I.M., Gibson, A.G., 1980. The hydrostatic extrusion of polymethylmethacrylate. Journal of Materials Science 15 p2207.

Hopkins, I.M., 1958. Journal of Polymer Sciences 30, p631.

Ishikawa, M., 1995. Stability of plastic deformation and toughness of polycarbonate blended with poly (acrylonitride-butadien-styrene) copolymer. Polymer 36, p2203

Jeong, C.Y., Nam, S.W., Ginsztler, J., 1999. Activation process of stress relaxation during hold time in 1Cr-Mo-V steel. Materials Science and Engineering A264, p188

Johnson, A.T., 1971. Fatigue-crack growth in polymetyl/methacrylate. Experimental Mechanics 11, p433

Kausch, H.H., 1978. Polymer fracture. Springer-Verag, Berlin.

Kinloch, A.J., Young, R.J., 1983. Fracture behavior of polymers. Applied Science Publishers. London and New York.

Kitagawa, M., 1982. Plastic deformation and fracture of notched specimens due to bending in glassy polymers, Journal of materials science 17, p2514

Knauss, W.G., 1970. Delayed failure - The Griffith pProblem for linearly viscoelatic materials. International Journal of Fracture Mechanics 6(1), p7

Knauss, W.G., Emri, I.J., 1981. Journal of Comput. Structures 13, p123

Kobayashi, A.S., 1993. Experimental Mechanics 2nd Edition. Society for Experimental Mechanics

Kozlov, G.V., Novikov, V.U. 2001. A Cluster Model for the Polymer Amorphous State. Physics-Uspekhi. 44(7) p681

Kramer, E.J., 1975. Journal of Polymer Science and Polymer Physics 11, p434

Kramer, E.J., 1983. Microscopic and molecular fundamentals of crazing, Advanced Polymer Sciences 52-53, p1

Kramer, E.J., Berger, L.L., 1990. Fundamental processes of craze growth and fracture. Advanced Polymer Sciences 91-92, p1

Kurauchi, T., Ohta, T., 1984. Energy absorption in blends of polycarbonate with ABS and SAN. Journal of Materials Science 19, p1699

Kurobe, T., Wakashima, H., 1970. Japan Congr. Materials Resource – Non-Metal Materials 13 (March), p192

Kurobe, T., Wakashima, H., 1972. Japan Congr. Materials Resource – Non-Metal Materials 15 (March), p137

Lai, J., Bakker, A., 1995. An integral constitutive equation for nonlinear plasto-viscoelastic behavior of high-density polyethylene. Polymer Engineering and Science 35, p1339

Leadermann, H., 1943. Elastic and creep properties of filamentous materials. Textile Foundation, Washington D.C.

Lemaitre, J. 1990. Micro-mechanism of crack initiation. International Journal of Fracture 42, p87

Loi, G.U, Knauss, W.G, 1992 April. Free volume theory and nonlinear thermoviscoelasticity. Polymer Engineering and Science 32(8), p542

Lu, H., Cary, P.D., 2000. Deformation measurements by digital image correlation: implementation of second order displacement gradient. Experimental Mechanics 40(4), p393

Lu, H., Tan, G., Chen, W., 2001. Modeling of Constitutive Behavior for Epon 828/T-403 at High Strain Rates. Mechanics of Time-Dependent Materials 5, p119-130.

Mai, Y.W., Williams, J.C., 1979. Temperature and environmental effects on the fatigue fracture in polystyrene. Journal of Materials Science 14(8), p1933

Martin, G.C., Gerberich, W.W., 1976. Temperature effects on fatigue crack growth in polycarbonate. Journal of Materials Science 11, p231

McKenna, G.B., Penn, R.W. 1980. Time-dependent failure in poly(methylmethacrylate) and polyethylene. Polymer 21, p213

Miller, D.A., Priest, R.H., 1987. Materials response to thermal-mechanical strain cycling: high temperature fatigue, properties and prediction. P.R. Skelton, Ed., Elsevier Applied Science Publishers Ltd. London, New York, p113

Min, S.S., Lee, S.-S., Jho, J.Y. 2001. Effect of chain structure on ductile-brittle transition in some Polycarbonates. Polymer Testing 20, p855

Miner, L.H., Wolffe, R.A., Zweben, C.H., 1974. Fatigue, creep and impact resistance of aramid fiber reinforced composites. Composites Reliability, ASTM STP 580, p549.

Miyano, Y., Nakada, M., Kudoh, H., Muki, R. 1999. Prediction of tensile fatigue life under temperature environment for unidirection CFRP. Advanced Composite Materials. Vol.8(3) p235.

Miyano, Y., Nakada, M., Kudoh, H., Muki, R. 2000. Determination of tensile fatigue life of unidirectional CFRP specimens by strand testing. Mechanics of Time-dependent Materials. Vol. 4 p127.

Mukherjee, B., Burns, D.J., 1971. Fatigue-crack growth in polymethy/methacrylate. Experimental Mechanics 11, p433.

Nisitani, H. and Hyakutake, H., 1985. Condition for Determining the static yield and fracture of a polycarbonate plate specimen with notches. Engineering fracture mechanics 22, p359

Odian, H. 1991. 1991. Principle of Polymeration. 3rd Ed., Wiley, New York.

Painter, P.C., Colemen, M.M. 1997. Fundamentals of Polymer Science. Technomic Publishing Company, Inc. Pennsylvania.

Parks, D.M., Argon, A.S., Bagepalli, B. 1984. Large elastic-plastic deformation of glassy polymers. MIT program in Polymer Science and Technology Report, MIT.

Peters, W.H., Ranson, W.F., 1982. Digital Imaging Techniques in Experimental Stress Analysis. Opt. Eng. 21(3), p427-432

Quinson, R., Perez, J., Germain, Y., Murraciole, M., 1995. β- and α-relaxation in poly(methyl methactylate) and polycarbonate: non-linear anelasticity studies by antistress relaxation. Polymer 36(4), p743

Rabinowitz, S., Krause, A.R., Beardmore, P., 1873. Failure of polystyrene in tensile and cyclic deformation. Journal of Materials Science 8, p11

Radon, J.C., 1980. Fatigue Crack Growth in Polymers. International Journal of Fracture. Vol.16 p533

Radon, J.C., Culver, L.E., 1975. Fatigue crack growth in polymers I. Effect of frequency and temperature. Polymer Engineering and Science 15(7), p500

Ramsteiner, F., Armburst, T. 2001. Fatigue crack growth in polymers, Test method. Polymer Testing 20, p321

Ratner, S.B., Korobov, V.I., 1965. Self-heating plastics at cyclical deformation. Mekhanika Polimerov 1(3), p93

Ree,T., Eyring, H., 1958. In rheology, Ed. By F.R. Eirich, Vol. II, Academic Press, New York, p83

Reifsnider, K.L., Stinchcomb, W.W., O'Brich, T.K., 1977. Frequency effects on a stiffen-based fatigue failure criterion. ASTM STP 636, p171

Richardson, T.L. 1989. Industrial Plastics. Delmar.

Riddell, M.N., Koo, G.P., O'Toole, J.L. 1966. Fatigue mechanisms of thermoplastics. Polymer Engineering and Science 6, p363

Rizos, A.K., Ngai, K.L., 1999. Experimental determination of the cooperative length scale of a glass-forming liquid near the glass transition temperature. Phsyics Rev. E 59, p612

Sauer, J.A., Richardson, G.C. 1980. Fatigue of polymers. International Journal of Fracture 16, p499-532

Schapery, R.A., 1997. Thermoviscoelastic constitutive equations for polycrystalline ice. Journal of Cold Regions Engineering, ASCE 11, p146

Schapery, R.A., 1984. Correspondence principle and a generalized J integral for large deformation and fracture analysis of viscoelastic media. International Journal of Fracture 25, p195

Schapery, R.A., 1975a. A theory of crack initiation and growth in viscoelastic media (I. Theoretical development). International Journal of Fracture 11(1), p141

Schapery, R.A., 1975b. A theory of crack initiation and growth in viscoelastic media (II. Approximate methods of analysis). International Journal of Fracture 11(3), p369

Schapery, R.A., 1969. Polymer Engineering and Science 9, p4

Schmidt, A.X., Marlies, C.A., 1948. Principle of high-polymer theory and practice. McGraw-Hill, New York, p578.

Sehitoglu, H., Maier, H.J., 2001. Thermo-mechanical Behavior of Materials, 3rd vol. ASTM (STP1371).

Sternstein, S.S., Ongchin, L., 1964. Polymers Pre-prints, American Chemistry Society 5, p422

Sun, C.T., Chan, W.S., 1979. Frequency effect on fatigue life of a laminated composites. ASTM STP 674, p418

Suresh, S., 1991. Fatigue of Materials. Cambridge University Press

Sutton, M.A., Wolters, W.J., Peters, W.H., Ranson, W.F., McNeil, S.R., 1983. Determination of Displacements Using an Improved Digital Image Correlation Method. Image Vision Computing 1(3), p133-139

Takemori, M. T. and Matsumoto, D. S., 1982. An unusual fatigue crack-tip plastic zone: The epsilon plastic zone of polycarbonate. Journal of Polymer Science and Polymer Physics Edition 20, p2027

Takemori, M., 1984. Polymer fatigue. Annual Review Materials Science 14, p171

Trantina, G.G. & Ysseldyke, D.A. 1987. An Engineering Design Database for Plastics. Materials Engineering. Vol.104(October) p35.

Tsuji, K., Iwase, K., Ando, K., 1999. An investigation into the location of crack initiation sites in alumina, polycarbonate and mild steel. Fatigue Fracture Engineering Materials Structure 22, p509

Tuttle, M.E., Pasricha, A., Emery, A.F., 1995. The nonlinear viscoelastic-viscoplastic behavior of IM7/5360 composites subjected to cyclic loading. Journal of Composite Materials 29, p2025

Uzan, J., 1996. Asphalt concrete characterization for pavement performance prediction. Journal of the Association of Asphalt Paving Technologists 65, p573

Vincent, P.I. 1960. The tough-brittle transition in thermoplastics. Polymer 1, p425

Wang, B., Lu, H., Kim, G., 2002. A damage model for the fatigue life of elastomeric materials. Journal of Mechanics of Materials 34 (8), p475

Wang, B., Lu, H., Tan, G., Chen, W., 2003. Strength of damaged polycarbonate after fatigue. Theoretical and Applied Fracture Mechanics, 39(2), p163-169

Wang, M.C., Guth, E., 1952. Statistical theory of networks of non-Gaussian flexible chains. Journal of Chemical Physics 20, p1144-1157

Wann, R.J., Martin, G.C., Gerberich, W.W., 1976a. The mechanical behavior of polyarylsulfone. Polymer Engineering and Science 16(9), p645

Wann, R.J., Martin, G.C., Gerberich, W.W., 1976b. Polymer Engineering and Science 16(9), p897

Ward, D.J., Mitchell, G.R. 1995. Modeling the structure of polymer glass poly (methyl methacrylate) through neutron-scattering experiments. Physica T57, p153

Ward, I. M. 1983. Mechanical properties of solid polymers 2nd Edition. John Wiley and Sons, Ltd. P377

Williams, M. L., Landel, R. F., Ferry, J. D. 1955. The temperature dependence of relaxation mechanics in amorphous polymers. Journal American Chemical Society. Vol.77 p3701.

Wnuk, M.P., 1971. Progressive Report NASA Grant NGR 42-003-006 (May)

Wu, J.B.C., Li, J.C.M., 1976. Slip process in the deformation of polystyrene. Journal of Materials and Science 11, p434

Xiao, C., Jho, J.Y., Yee, A.F., 1994. Correlation between the shear yielding behavior and secondary relaxation of Bisphenol A Polycarbonate and related Copolymers. Marcromolecules 27, p2761

Yamamoto, T., Furukawa, H., 1995. Relationship between molecular structure and deformation-fracture mechanism of amorphous polymers; 2. Crazing stress. Polymer 36, p2393

Yokobori, T., Sato, K., 1976. The effect of frequency on crack propagation rate and striation spacing in 2034-T3 aluminum alloy and SM-50 steel. Engineering Fracture Mechanics 8, p81

VITA (2)

GYU-HO KIM

Candidates for the Degree of

Doctor of Philosophy

Thesis: ACCELERATED LIFETIME TESTING OF CARBON FILLED
POLYCARBONATE UNDER CYCLIC LOADING CONDITIONS

Major Field: Mechanical Engineering

Biographical:

Personal Data: Born in Dae-Gu, Korea, On February 20, 1964, the son of
Ki-Yong and Wol-Kae Kim.

Education: Graduated from Kyeong-Sinn High School, Dae-Gu, Korea in
February 1982; received Bachelor of Science degree in Mechanical
Engineering from Korea Air Force Academy, Seoul, Korea in April
1986; received Master of Science degree in Mechanical Engineering
from Oklahoma State University, Stillwater, Oklahoma in December
1994. Completed requirements for the Doctor of Philosophy with a
major in Mechanical Engineering at Oklahoma State University in
December, 2003.

Experience: Raised in Dae-Gu City, Korea; employed as a Korea Air Force
officer, 1986 to present.